

①

AD 721742

DEVELOPMENT OF A GRADIOMETER FOR MEASURING GRAVITY GRADIENTS UNDER DYNAMIC CONDITIONS

by

Charles B. Ames, Curtis C. Bell, Robert L. Forward,
Glenn F. Kloiber, Robert W. Peterson, David W. Rouse

HUGHES RESEARCH LABORATORIES

3011 Malibu Canyon Road
Malibu, California

Contract No. F19628-69-C-0219

Project No. 7600, 8607

Task No. 760007, 860703

Work Unit No. 76000701, 86070301

FINAL REPORT

PERIOD COVERED: 15 APRIL 1969 through 14 AUGUST 1970

NOVEMBER 1970

Contract Monitor: David Anthony
TERRESTRIAL SCIENCES LABORATORY

DDC
RECEIVED
APR 20 1971
REGISTERED

THIS DOCUMENT HAS BEEN APPROVED FOR PUBLIC
RELEASE AND SALE; ITS DISTRIBUTION IS UNLIMITED.

Prepared for

AIR FORCE CAMBRIDGE RESEARCH LABORATORIES
AIR FORCE SYSTEMS COMMAND
L. G. HANSCOM FIELD
Bedford, Massachusetts 01730

Reproduced by
NATIONAL TECHNICAL
INFORMATION SERVICE
Springfield, Va. 22151

173

BLANK PAGE

ACCESSION FOR		
CFTW	WHITE SECTION	<input checked="" type="checkbox"/>
DDG	DIFF SECTION	<input type="checkbox"/>
UNANNOUNCED		<input type="checkbox"/>
JUSTIFICATION		
BY		
DISTRIBUTION/AVAILABILITY CODES		
DIST.	AVAIL. and or	SPECIAL
A		

Qualified requestors may obtain additional copies from the Defense Documentation Center. All others should apply to the Clearinghouse for Federal Scientific and Technical Information.

AFCRL-71-0003

DEVELOPMENT OF A GRADIOMETER
FOR MEASURING GRAVITY GRADIENTS
UNDER DYNAMIC CONDITIONS

by

Charles B. Ames, Curtis C. Bell, Robert L. Forward,
Glenn F. Kloiber, Robert W. Peterson, David W. Rouse

Hughes Research Laboratories
3011 Malibu Canyon Road
Malibu, California 90265

Contract No. F19628-69-C-0219

Project No. 7600, 8607
Tasks 760007, 860703
Work Unit No. 76000701, 86070301

FINAL REPORT

Period Covered: 15 April 1969 through 14 August 1970

November 1970

Contract Monitor: David Anthony
Terrestrial Sciences Laboratory

This document has been approved for public
release and sale; its distribution is unlimited.

Prepared for

AIR FORCE CAMBRIDGE RESEARCH LABORATORIES
AIR FORCE SYSTEMS COMMAND
L. G. HANSCOM FIELD
BEDFORD, MASSACHUSETTS 01730

ABSTRACT

Design and development of a portable rotating gravitational gradiometer has been continued. A breadboard laboratory model of the gradiometer was constructed and tested. Testing has indicated that angular rate isolation and spin speed control represent major factors in maintaining noise free sensor operation.

Analysis has been performed on the sensor's susceptibility to angular rate and a feasible rate isolation method is outlined.

Preliminary design studies for an isoelastic servo-balanced arm have been completed and are discussed.

A preliminary design specification for an appropriate inertial platform for use in an airborne application was generated, and vendor liaison was established to obtain initial response to this specification.

Studies were also performed on sensor angular position errors, noise and clutter due to proximate masses, and first stage vibration isolation methods.

TABLE OF CONTENTS

I.	INTRODUCTION	I-1
II.	(This Section Deleted)	
III.	BACKGROUND.	III-1
	A. Introduction	III-1
	B. Theory of Sensor Operation	III-1
	C. Soft Mounted Sensor Project	III-3
IV.	SENSOR DESIGN CONSIDERATIONS	IV-1
	A. Gradiometer Model	IV-1
	B. Angular Position Errors	IV-8
	C. Angular Rate Errors.	IV-22
	D. Arm Balancing and Bending	IV-29
V.	EXPERIMENTAL PROGRAM	V-1
	A. Hard Mounted Sensor Project.	V-1
	B. Noise Sources	V-9
VI.	APPLICATION CONSIDERATIONS	VI-1
	A. Airborne Motion Isolation System	VI-1
	B. Mass Noise Effects	VI-4
VII.	SUMMARY AND CONCLUSIONS	VII-1
	A. Sensor Error Sources	VII-2
	B. Laboratory Development Summary	VII-4
	C. Operational System Considerations	VII-9
	D. Conclusions	VII-13
	APPENDIX A - Gravity Gradiometer Broadband Isolation System	A-1
	APPENDIX B - Preliminary Procurement Speci- fication for a Gravity Gradiometer Three-Axis Motion Isolation Platform	B-1

I. INTRODUCTION

The following were the overall objectives of the work performed under this contract.

1. Design, construct and test a laboratory breadboard model of a gradiometer to be used for the measurement of the second order gradient of the earth's gravity potential.
2. Conduct theoretical studies to determine stabilization and vibration isolation requirements for a flyable prototype gradiometer and to determine the effect of masses in the aircraft and attitude of aircraft on gradiometer performance.
3. Provide motion isolation studies and analysis leading to the establishment of a preliminary specification for a sensor motion isolation system.

This Report is intended to present a review of the laboratory and analytical work performed under AFCRL Contract No. F19628-69-C-0219 and Supplemental Agreement No. 2.

Sections III through VI provide the reader with: 1) background information pertaining to the torsionally resonant rotating gradiometer; 2) design considerations concerning the sensor sub-system; 3) a description of the steps taken in the experimental program, and 4) a brief review of a preliminary airborne motion isolation system for gravity surveying.

Section VII provides the reader with a relatively concise overview of the work performed for AFCRL and a set of specific conclusions.

The Appendices contain supplementary material relevant to gradiometer system applications.

II. This Section Deleted.

BLANK PAGE

III. BACKGROUND

A. Introduction

This section provides a discussion of the theory of operation and development of the Hughes rotating gravity gradiometer.

B. Theory of Sensor Operation

The rotating gravity gradient sensor that has been developed and demonstrated is a device for measurement of the second order gradient of the gravity potential. In general, the gravity potential field consists not only of the gravitational field due to masses, but also the inertial fields due to rotation that exist because the sensor is usually not operated in a inertial reference frame.

1. General Gravitational and Inertial Gradient Field

The general form for the gradient tensor, which includes all combinations of gravitational and inertial force gradients, is given by

$$\bar{G}_{ij} = \begin{pmatrix} \Gamma_{xx} + \Omega_y^2 + \Omega_z^2 & \Gamma_{xy} - \dot{\Omega}_z - \Omega_x \Omega_y & \Gamma_{xz} + \dot{\Omega}_y - \Omega_x \Omega_z \\ \Gamma_{yx} + \dot{\Omega}_z - \Omega_y \Omega_x & \Gamma_{yy} + \Omega_z^2 + \Omega_x^2 & \Gamma_{yz} - \dot{\Omega}_x - \Omega_y \Omega_z \\ \Gamma_{zx} - \dot{\Omega}_y - \Omega_z \Omega_x & \Gamma_{zy} + \dot{\Omega}_x - \Omega_z \Omega_y & \Gamma_{zz} + \Omega_x^2 + \Omega_y^2 \end{pmatrix}$$

where Γ_{ij} is the gravitational force gradient that causes a force in the i direction on an object displaced in the j direction, Ω_k is the inertial rate of rotation about the k axis, and $\dot{\Omega}_i$ is the inertial angular acceleration about the i axis.

This equation for the general form of the gradient tensor indicates that although there are no gradients resulting from linear acceleration, the gradients caused by angular velocity and angular acceleration can interfere with the measurement of the gravitational

gradients. For the proposed application it is desirable to be able to measure gravitational gradients down to 10^{-9} sec^{-2} . The angular velocity that would cause this equivalent gradient is $3 \times 10^{-5} \text{ rad/sec}$ ($6^\circ/\text{hour}$) and the angular acceleration is $10^{-9} \text{ rad/sec}^2$ ($0.7^\circ/\text{hour}$ change per hour). Both of these rotational gradients involve very small angular quantities.

The rotational gradient resulting from angular velocity is seen to enter into every term in the G_{ij} gradient tensor and it is not possible to separate the effects completely. Thus, any instrument designed to measure gravitational gradients will have to be inertially stabilized in some way or compensated for the instantaneous inertial angular rate.

The rotational gradient caused by inertial angular acceleration is relatively easy to circumvent, since it does not enter in all the terms of the gradient tensor. A well designed in-line gradiometer that measures either G_{xx} , G_{yy} , G_{zz} will not experience interference from angular acceleration (although it will sense any angular velocity). The rotating sensor which Hughes is developing does not have a first order susceptibility to angular acceleration because of its double-quadrupole design. However, angular acceleration due to inertia imbalance of the sensor arms is of significance to the sensor design. This problem is discussed in more detail in Section IV-D.

In operation, the sensor is rotated about its torsionally resonant axis at an angular rate ω that is exactly one-half the torsional resonant frequency. Only the differential torque, ΔT , between the sensor arms at the double frequency is coupled into the sensor output. This differential torque in an inertially stable sensor is given by

$$\Delta T = \frac{m\ell^2}{2} [(\Gamma_{yy} - \Gamma_{xx}) \sin 2\omega t + 2\Gamma_{xy} \cos 2\omega t]$$

where ℓ is the characteristic length of the sensor, and m is the mass at the end of the sensor arms.

From the above equation it can be seen that measurement of the in-phase and quadrature components of the sensor response with respect to the sensor rotational phase reference will provide a measure of certain components of the gravity gradient tensor. The particular components measured will depend upon the orientations of the sensor spin axis and the phase reference direction. An orthogonal triad of measurements at a point is sufficient to obtain all the components of the gravity gradient tensor. The differential torque induced by a point or spherical mass M at a distance R from the sensor is

$$\Delta T = \frac{3}{2} \frac{GM m \ell^2}{R^3} \sin 2\omega t.$$

The angular resonant deflection between the two quadrupoles of the sensor rotating at one-half its torsional resonant frequency $\omega_n = 2\omega$ with an associated quality factor Q is, therefore,

$$\delta = \frac{\Delta T Q}{I \omega_n^2} = \frac{3 G M Q}{R^3 \omega_n^2} \sin \omega_n t$$

where $I = m \ell^2 / 2$ is the quadrupole inertia.

The angle δ is extremely small. Surface gradients produced by the earth (3000 E.U.) will produce angular deflections of $\approx 5 \times 10^{-8}$ rad in typical torsional sensor designs ($Q = 300$, $\omega = 100$ rad/sec), while useful threshold signals of 1 E.U. produce angular responses of $\approx 10^{-11}$ rad.

It is now necessary to transduce this mechanical motion into an electrical signal for processing and transmission. This is accomplished by using a flexural pivot as the torsional spring and affixing a barium titanate stain transducer to one of the flexural spring leaves. These transducers have been found to be more than adequate for sensing these small strains.

C. Soft Mounted Sensor Project

1. Project History

The ultimate object in the development of rotating gravitational gradient sensors is a class of small, lightweight, rugged sensors of high sensitivity and precision that may be used to measure accurately and rapidly the details of mass distribution in making rapid gravitational field surveys and as a component in an inertial guidance system to remove the effects of gravitational anomalies on the system performance.

The objectives of the preliminary research programs were to investigate the physical feasibility of the basic concept, to develop sensor structures which would operate at a high sensitivity level both in free fall and in a 1g environment, to measure the sensor's sensitivity to gravitational fields, and to investigate the sources of noise produced by the rotation of the sensor structure. A torsionally resonant rotating gradiometer configuration utilizing piezoelectric readout was found to be a suitable design and offers a significant

improvement over other possible gradiometer designs because of its ability to be operated in an earth-bound laboratory environment while still maintaining the high sensitivity and signal-to-noise ratio required to measure gravitational gradients as low as 10^{-9} sec^{-2} (1 Eötvös unit (E. U.)).

Four years ago a project was initiated at Hughes to design, fabricate and test a "soft mounted" gradiometer configuration. After some experimental work and hardware modifications, the sensor detected the gradients of stationary masses. The first successful test occurred in August 1967. The noise level of these tests was over ± 100 E.U. Since that time the soft mounted system has been completely reworked until the noise level has been reduced to ± 1 E.U. (1 σ standard deviation at an integration time of 10 seconds). These tests fully verified the gradiometer theory. It should be noted that development of the soft mounted system was accomplished almost entirely on Internal Research and Development funding before 1969. Minor changes in the system were accomplished under NASA contract NAS 8-24788, Lunar Orbiter Selenodesy Feasibility Demonstration.

2. Noise and Drift in the Soft Mounted Test Set Up

One of the tests run on the sensor was to simply measure the sensor output for approximately 1000 seconds. Care was exercised to prevent any variations in the gravity field of the room (a person passing 3 feet away would add significantly to the sensor output). The average slope of the curve is 1.4 E.U./min, which represents the general drift rate of the system. The drift is known to be caused by temperature variations in the magnetic levitation system, which cause the sensor to be raised or lowered slightly in the background gradient field of the room, and by changes in stiffness of the elastic suspension.

The standard deviation of the random noise superimposed on the linear drift was measured as

$$\sigma = 4 \text{ E.U. for } \tau = 3 \text{ sec}$$

or

$$\sigma = 1.2 \text{ E.U. for } \tau = 10 \text{ sec.}$$

In addition, Flyby Simulation tests were run that simulated a spin stabilized lunar orbiting satellite with a gradiometer mounted inside passing over typical lunar masscons. These tests fully demonstrated the sensor's dynamic response capability.

IV. SENSOR DESIGN CONSIDERATIONS

An ideal second order gravity gradiometer operating in an inertially fixed frame of reference will produce output signals proportional to the second order gradient of the gravity field only. The output of a non-ideal sensor operating in a non-inertial frame of reference will contain, among other noises, errors due to acceleration and rotation of the sensor frame of reference. This section presents a dynamic analysis of this latter class of errors by using a simple model of the second order gradiometer.

A. Gradiometer Model

A simple mechanical model, consisting of three torsional springs and dampers and two inertia arms, will serve as the basis for this analysis. As shown in Figure 4-1, the inertia arms are individually coupled to the case of the instrument through the supporting springs (K_1 , K_2) and are mutually coupled by the common torsional spring (K_0). Each spring is assumed to contain viscous damping defined by the coefficients (D_0 , D_1 , D_2) and is assumed to be infinitely rigid in all directions other than about the common torsional axis (\bar{k}).

The inertial tensors of the arms are defined in terms of the principal axes of the arms as Equations (4-1) and (4-2).

$$\bar{\Phi}_1 \triangleq I_1 [\bar{i}_1 \bar{i}_1 + \bar{k} \bar{k}] \quad (4-1)$$

$$\bar{\Phi}_2 \triangleq I_2 [\bar{j}_2 \bar{j}_2 + \bar{k} \bar{k}] \quad (4-2)$$

The unit vectors (\bar{i}_1 , \bar{j}_2) are nominally orthogonal, but they become nonorthogonal due to differential motion of the arms. In this analysis, the inertial tensors of Equations (4-1) and (4-2) will be approximated by Equations (4-3) and (4-4) wherein the tensors are described in a sensor case-fixed frame ($\bar{i} \bar{j} \bar{k}$) and the products of inertia are neglected.

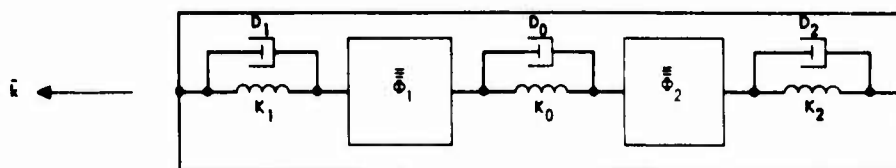


Figure 4-1. Gradiometer model.

$$\bar{\Phi}_1 \cong I_1 [\bar{ii} + \bar{kk}] \quad (4-3)$$

$$\bar{\Phi}_2 \cong I_2 [\bar{jj} + \bar{kk}] \quad (4-4)$$

The common torsional spring (K_0) also includes a strain transducer to sense the differential angular deflection of the inertia arms. The electrical output of this strain transducer is amplified, phase-sensitive demodulated, and filtered to produce the ultimate output of the gradiometer.

1. Equations of Motion

Since the ultimate output of the gradiometer is a function of the differential angular deflection of the inertia arms about the common torsional axis, it is of interest to derive the dynamic equations of motion that relate this parameter to the sensible inputs to the instrument. This derivation will be accomplished on the basis of the classical equivalence of torque to the time rate of change of the angular momentum of each arm.

The angular momenta of the arms are defined in terms of their inertial tensors and angular velocities as Equations (4-5) and (4-6), where ($\bar{\omega}$) is the inertial angular velocity of the sensor case, and the scalars ($\dot{\theta}_1$, $\dot{\theta}_2$) are the velocities of the arms relative to the sensor case.

$$\bar{H}_1 \triangleq \bar{\Phi}_1 \cdot [\bar{\omega} + \bar{k}\dot{\theta}_1] \quad (4-5)$$

$$\bar{H}_2 \triangleq \bar{\Phi}_2 \cdot [\bar{\omega} + \bar{k}\dot{\theta}_2] \quad (4-6)$$

The time rates of change of these momenta are produced by external torques acting on the arms as the result of the gravity gradient, arm mass unbalance, and the elastic and viscous coupling between the arms and between the arms and the case as shown in Equations (4-7) and (4-8).

$$\dot{\bar{H}}_1 = \bar{M}_{g1} + \bar{M}_{\mu 1} + \bar{M}_{21} + \bar{M}_{c1} \quad (4-7)$$

$$\dot{\bar{H}}_2 = \bar{M}_{g2} + \bar{M}_{\mu 2} + \bar{M}_{12} + \bar{M}_{c2} \quad (4-8)$$

For the present objectives, only the components of these momental rates about the sensor output axis (\bar{k}) are required; from Equations (4-5) and (4-6) these scalars may be expressed as Equations (4-9) and (4-10).

$$\bar{k} \cdot \dot{\bar{H}}_1 = I_1 \ddot{\theta}_1 + \bar{k} \cdot \left[\bar{\Phi}_1 \cdot \dot{\bar{\omega}} + \bar{\omega} \times (\bar{\Phi}_1 \cdot \bar{\omega}) \right] \quad (4-9)$$

$$\bar{k} \cdot \dot{\bar{H}}_2 = I_2 \ddot{\theta}_2 + \bar{k} \cdot \left[\bar{\Phi}_2 \cdot \dot{\bar{\omega}} + \bar{\omega} \times (\bar{\Phi}_2 \cdot \bar{\omega}) \right] \quad (4-10)$$

The elastic and viscous coupling torques acting on the arms may be expressed as Equations (4-11) and (4-12).

$$\bar{k} \cdot \left[\bar{M}_{c1} + \bar{M}_{12} \right] = - \left[A_1 + A_o \right] \theta_1 + A_o \theta_2 \quad (4-11)$$

$$\bar{k} \cdot \left[M_{c2} + M_{21} \right] = - \left[A_2 + A_o \right] \theta_2 + A_o \theta_1 \quad (4-12)$$

where, by definition:

$$\left. \begin{aligned} A_o &\triangleq D_o S + K_o \\ A_1 &\triangleq D_1 S + K_1 \\ A_2 &\triangleq D_2 S + K_2 \end{aligned} \right\} \quad (4-13)$$

The dynamic equations of arm motion may be stated in the matrix form Equation (4-14) by combining Equations (4-7) through (4-12).

$$\begin{bmatrix} (I_1 S^2 + A_1 + A_o) & (-A_o) \\ (-A_o) & (I_2 S^2 + A_2 + A_o) \end{bmatrix} \begin{bmatrix} \theta_1 \\ \theta_2 \end{bmatrix} = \begin{bmatrix} M_1 \\ M_2 \end{bmatrix} \quad (4-14)$$

where, by definition:

$$\left. \begin{aligned} M_1 &\triangleq \bar{k} \cdot \left[\bar{M}_{g1} + \bar{M}_{\mu 1} - \left(\bar{\Phi}_1 \cdot \dot{\bar{\omega}} + \bar{\omega} \times (\bar{\Phi}_1 \cdot \bar{\omega}) \right) \right] \\ M_2 &\triangleq \bar{k} \cdot \left[\bar{M}_{g2} + \bar{M}_{\mu 2} - \left(\bar{\Phi}_2 \cdot \dot{\bar{\omega}} + \bar{\omega} \times (\bar{\Phi}_2 \cdot \bar{\omega}) \right) \right] \end{aligned} \right\} \quad (4-15)$$

The solution of Equation (4-14) for the differential angular deflection of the arms is stated as Equation (4-16).

$$(\theta_1 - \theta_2) = \frac{(I_2 S^2 + A_2)M_1 - (I_1 S^2 + A_1)M_2}{I_1 I_2 S^4 + [I_1(A_2 + A_o) + I_2(A_1 + A_o)]S^2 + A_1 A_2 + A_o(A_1 + A_2)} \quad (4-16)$$

A normalized form of Equation (4-16) is presented as Equation (4-17) wherein the denominator is factored into two quadratics representing the "sum mode" and the "difference mode" characteristic frequencies (β_{12} and ω_o).

$$(\theta_1 - \theta_2) = \frac{\left[S^2 + a_2 S + \beta_2^2 \right] \left[\frac{M_1}{I_1} \right] - \left[S^2 + a_1 S + \beta_1^2 \right] \left[\frac{M_2}{I_2} \right]}{\left[S^2 + a_{12} S + \beta_{12}^2 \right] \left[S^2 + \frac{\omega_o}{Q} S + \omega_o^2 \right]} \quad (4-17)$$

where

$$a_1 = D_1 / I_1$$

$$a_2 = D_2 / I_2$$

$$a_{12} \cong \frac{D_1 + D_2}{I_1 + I_2}$$

$$\beta_1^2 = K_1/I_1$$

$$\beta_2^2 = K_2/I_2$$

$$\beta_{12}^2 \cong \frac{K_1 + K_2}{I_1 + I_2}$$

$$\frac{\omega_o}{Q} \cong D_o \left[\frac{I_1 + I_2}{I_1 I_2} \right] + \left[\frac{D_1 + D_2}{I_1 + I_2} \right]$$

$$\omega_o^2 = K_o \left[\frac{I_1 + I_2}{I_1 I_2} \right] + \left[\frac{K_1 + K_2}{I_1 + I_2} \right]$$

The "sum mode" parameters (α_{12} , β_{12}) are approximately equal to their counterparts in the numerator of Equation (4-17) and become exactly equal to them when the spring rates (K_1 , K_2), damping (D_1 , D_2) and inertias (I_1 , I_2) are matched. Under these "ideal" conditions, the "difference mode" frequency (ω_o) may be expressed as Equation (4-18).

$$\omega_o^2 = (2K_o + K)/I \quad (4-18)$$

where

$$K \triangleq K_1 = K_2 \text{ and } I \triangleq I_1 = I_2.$$

The differential angular deflection ($\theta_1 - \theta_2$) may be scaled by (ω_o^2/Q) to yield an expression for an "equivalent" gradient signal as shown in Equation (4-19).

$$\Gamma_e \triangleq (\omega_o^2/Q) [\theta_1 - \theta_2] \quad (4-19)$$

Combining Equations (4-17) and (4-19) yields Equation (4-20).

$$\Gamma_e = \left[\frac{\omega_o^2}{Q} \right] \frac{\left(s^2 + a_2 s + \beta_2^2 \right) \left(\frac{M_1}{I_1} \right) - \left(s^2 + a_1 s + \beta_1^2 \right) \left(\frac{M_2}{I_2} \right)}{\left(s^2 + a_{12} s + \beta_{12}^2 \right) \left(s^2 + \frac{\omega_o}{Q} s + \omega_o^2 \right)} \quad (4-20)$$

At this point it is instructive to expand and normalize Equation (4-15) to obtain the forcing functions of Equation (4-20). The result of this expansion is Equation (4-21).

$$\left. \begin{aligned} \frac{M_1}{I_1} &= -\Gamma_{ij} - \dot{\omega}_k + \omega_i \omega_j + \Gamma_{\mu 1} \\ \frac{M_2}{I_2} &= \Gamma_{ij} - \dot{\omega}_k - \omega_i \omega_j + \Gamma_{\mu 2} \end{aligned} \right\} \quad (4-21)$$

where

$$\Gamma_{\mu 1} = (\bar{k} \cdot \bar{M}_{\mu 1})/I_1$$

$$\Gamma_{\mu 2} = (\bar{k} \cdot \bar{M}_{\mu 2})/I_2.$$

The largest gradient error due to arm mass unbalance occurs when the individual unbalances are of opposite sign. Therefore, in this analysis, the largest mass unbalance error will be assumed to be as defined by Equation (4-22).

$$\Gamma_{\mu 1} \triangleq -\Gamma_{\mu 2} \triangleq \Gamma_{\mu \max} \quad (4-22)$$

The resulting "equivalent" gradient is obtained by combining Equations (4-20), (4-21) and (4-22) and is presented as Equation (4-23).

$$\Gamma_e = \left[\frac{\epsilon_o^2}{Q_o^2} \right] \left[\frac{\left[s^2 + \left(\frac{a_1 + a_2}{2} \right) s + \frac{\beta_1^2 + \beta_2^2}{2} \right] \left[-2\Gamma_{ij} + 2\omega_i \omega_j + 2\Gamma_{\mu \max} \right]}{\left[s^2 + a_{12}s + \beta_{12}^2 \right] \left[s^2 + \frac{\omega_o}{Q} s + \omega_o^2 \right]} \right] \\ + \left[\frac{\epsilon_o^2}{Q_o^2} \right] \left[\frac{\left[(a_1 - a_2) s + (\beta_1^2 - \beta_2^2) \right] \dot{\omega}_k}{\left[s^2 + a_{12}s + \beta_{12}^2 \right] \left[s^2 + \frac{\omega_o}{Q} s + \omega_o^2 \right]} \right] \quad (4-23)$$

Equation (4-23) illustrates the following three basic gradient error sources:

1. Rotational field
2. Arm Mass unbalance
3. "Sum Mode" mismatch

An interesting property of Eq. (4-23) is that errors due to "sum mode" mismatch are attenuated as the square of frequency above the "sum mode" frequency up to the "difference mode" frequency (ω_o). Above the "difference mode" frequency these errors are attenuated as the fourth power of frequency until the "lead" of the numerator becomes effective. For light damping of the "sum mode," the "lead" becomes effective at $\omega \approx 2Q_{12}\beta_{12}$. This latter frequency is usually above the "difference mode" frequency by two orders of magnitude or better; beyond that frequency, the error is attenuated further as the third power of frequency.

Equation (4-23) can now be used to determine equivalent gradient outputs when angular rate and acceleration inputs, arm mass unbalance parameters, and sensor sum and difference frequencies have been established.

B. Angular Position Errors

1. Introduction

A general technique is described for calculating the output of any second order gravity gradient sensor interacting with a generalized gravity gradient field as a function of the relative angular orientation of the sensor and the field. The various gradiometer sensor structures (Eötvös torsion balance, quartz microbalance, vibrating string, floated dumbbell, accelerometer pair, rotated cruciform, rotated starburst) can be represented by a symmetric tensor. The output of a given sensor in a given angular orientation in a given gravity gradient field is then obtained by taking the scalar product of the sensor tensor and the gravity gradient tensor.

2. The Gravity Gradient Tensor

The gravity gradient tensor to be sensed is the entire gravitational-inertial tensor that contains not only the gravitational gradient tensor field due to nearby masses, but also the inertial gradients due to angular rotation and angular acceleration of the inertial reference frame that we are in. The generalized gravity gradient tensor G_{ij} has three components

$$G_{ij} = \Gamma_{ij} + \Omega_{ij}^2 + \dot{\Omega}_{ij} . \quad (4-24)$$

The first component of the gravity gradient tensor is the gravitational gradient field which is always symmetric and whose trace is zero if the center of reference has no mass (or mass difference with respect to its surroundings).

$$\Gamma_{ij} = \begin{pmatrix} \Gamma_{xx} & \Gamma_{xy} & \Gamma_{zx} \\ \Gamma_{xy} & \Gamma_{yy} & \Gamma_{yz} \\ \Gamma_{zx} & \Gamma_{yz} & \Gamma_{zz} \end{pmatrix}$$

$$\Gamma_{xx} + \Gamma_{yy} + \Gamma_{zz} = -\text{div } \rho \approx 0 \quad (4-25)$$

$$\Gamma_{ij} = \Gamma_{ji} .$$

For a spherical mass M oriented in the $\pm x$ direction at a distance R , the gravitational gradient field takes the form

$$\Gamma_{ij}(\pm x) = \frac{GM}{R^3} \begin{pmatrix} +2 & 0 & 0 \\ 0 & -1 & 0 \\ 0 & 0 & -1 \end{pmatrix} \quad (4-26)$$

The gravitational gradient field is not uniform and there exist higher order gradient derivatives of this field.

The second component of the gravity gradient tensor is the angular velocity gradient field. This tensor is symmetric with a positive trace that is twice the square of the total rotation about the reference point

$$\Omega_{ij}^2 = \begin{pmatrix} \Omega_x^2 + \Omega_z^2 & -\Omega_x \Omega_y & -\Omega_z \Omega_x \\ -\Omega_x \Omega_y & \Omega_z^2 + \Omega_z^2 & -\Omega_y \Omega_z \\ -\Omega_z \Omega_x & -\Omega_y \Omega_z & \Omega_x^2 + \Omega_y^2 \end{pmatrix} \quad (4-27)$$

$$\Omega_{ii}^2 = 2(\Omega_x^2 + \Omega_y^2 + \Omega_z^2) . \quad (4-28)$$

This gradient field only exists, of course, if the sensor was operated in a non-inertial frame of reference.

The third component of the gravity gradient tensor is the angular acceleration gradient field. This tensor is antisymmetric with zero trace.

$$\dot{\Omega}_{ij} = \begin{pmatrix} 0 & -\dot{\Omega}_z & +\dot{\Omega}_y \\ +\dot{\Omega}_z & 0 & -\dot{\Omega}_x \\ -\dot{\Omega}_y & +\dot{\Omega}_x & 0 \end{pmatrix} \quad (4-29)$$

Again, this field only exists as part of the gravity gradient tensor for convenience (or lack of knowledge). The calculations or operation of the sensor has been carried out in a non-inertial reference frame.

Notice that both the angular velocity and the angular acceleration gradient fields are uniform — they have no dependence upon radius. Thus unlike the gravitational gradient field, there are no higher order gradients to these fields.

Since the angular velocity and angular acceleration fields can enter into a specific problem because of lack of knowledge or deliberate choice of coordinates, care must be used in the choice of coordinates. For calculational simplicity it is assumed that an earth oriented coordinate system was chosen rather than an inertial coordinate system so that the gradient of the sensor orbital motion drops out. Now only the gravitational gradient field is considered which is symmetric and usually traceless

$$G_{ij} = \Gamma_{ij} \quad (4-30)$$

3. Rotation Matrices

The effect of relative sensor-field angular orientation and rotation on the response of the sensor to the field will now be studied. The rotation matrices to be used as a rotation about the x axis are defined

$$\Psi_{ij} = \begin{pmatrix} 1 & 0 & 0 \\ 0 & \cos \psi & \sin \psi \\ 0 & -\sin \psi & \cos \psi \end{pmatrix} \quad (4-31)$$

a rotation about the y axis

$$\Theta_{ij} = \begin{pmatrix} \cos \theta & 0 & \sin \theta \\ 0 & 1 & 0 \\ -\sin \theta & 0 & \cos \theta \end{pmatrix} \quad (4-32)$$

and a rotation about the z axis

$$\Phi_{ij} = \begin{pmatrix} \cos \psi & \sin \psi & 0 \\ -\sin \psi & \cos \psi & 0 \\ 0 & 0 & 1 \end{pmatrix} \quad (4-33)$$

These three rotation matrices have been chosen because of their simplicity in physical interpretation. The reader should be warned, however, that these three rotations are not independent of each other and, therefore, are not suitable as generalized coordinates for the Lagrangian formulation of mechanics. They are adequate for these purposes, however, where the effects of small angular errors about a nominal orientation are to be studied.

4. Tensor Sensors

To measure the gravitational gradient field, gradiometers are used that respond to the differential forces and torques induced in the sensor by the field. All gradiometers have roughly the same type of structure. They consist of sets of two or more masses in which interact with the field, spaced at a characteristic distance \bar{r} from the center of mass of the sensor system. They also have force or displacement measuring transducer(s) which together with the sensor structure decide the sensitive direction(s) of the sensor.

The properties of any sensor can be written as a tensor matrix for each transducer output, written in a coordinate system that is sensor fixed. The scalar product of the sensor matrix with the gravity gradient field then gives the scalar quantity that is the amplitude of the voltage output of the transducer in the sensor

$$a = S_{ij} \Gamma_{ij} .$$

Note that since the information obtained in the form of a voltage output from the transducer is only a scalar magnitude, no intrinsic direction is associated with it. The directional information has to be obtained from previous knowledge of the orientation of the sensor coordinate system with respect to inertial space or the gravity gradient reference system.

Radial Gradiometer. The simplest gradiometer is the radially sensitive gradiometer consisting of two masses m connected by a spring of length $2r$. Examples of this type of system are the vibrating string gradiometer, the freely falling mass gradiometer and back-to-back accelerometers on the end of a stick. (It should be noted that some versions of the freely falling mass and back-to-back accelerometer gradiometers have used only one sensing mass, the mass of the vehicle supplies the reference mass. In this case, one uses only the differential moments of the system in the calculations.)

The simple radial gradiometer can be represented by

$$R_{ij} = mr \begin{pmatrix} 1 & 0 & 0 \\ 0 & 0 & 0 \\ 0 & 0 & 0 \end{pmatrix}. \quad (4-34)$$

If this interacts with the gravity gradient field of a mass M a distance R in the X direction

$$\Gamma_{ij} = \frac{GM}{R^3} \begin{pmatrix} 2 & 0 & 0 \\ 0 & -1 & 0 \\ 0 & 0 & -1 \end{pmatrix}. \quad (4-35)$$

The output of the sensor will be

$$a = R_{ij} \Gamma_{ij} = mr \Gamma_{xx} = \frac{2GM}{R^3} mr. \quad (4-36)$$

To study the effect on the sensor output of relative orientation of the sensor with respect to the gradient field, the rotation matrix can be applied to either the sensor or the gradient field. If the sensor is rotated an angle θ about the y axis

$$\begin{aligned} R'_{kl} &= \Theta_{ki} R_{ij} \Theta_{jl}^{-1} \\ &= mr \begin{pmatrix} \cos^2 \theta & 0 & -\sin \theta \cos \theta \\ 0 & 0 & 0 \\ -\sin \theta \cos \theta & 0 & \sin^2 \theta \end{pmatrix} \end{aligned} \quad (4-37)$$

The response of the sensor in this new orientation to the original gravitational gradient flow is now

$$\begin{aligned}
 a(\theta) &= R_{kl}^i \Gamma_{kl} = (2 \cos^2 \theta - \sin^2 \theta) \frac{GM}{R^3} mr \\
 &= (3 \cos^2 \theta - 1) \frac{GM}{R^3} mr .
 \end{aligned}
 \tag{4-38}$$

This directional sensitivity pattern is fundamental to the mathematics of the gradient field - tensor sensor interaction and can be assumed to apply in one form or another to all sensors. The one for the radial sensor is plotted in Fig. 4-2.

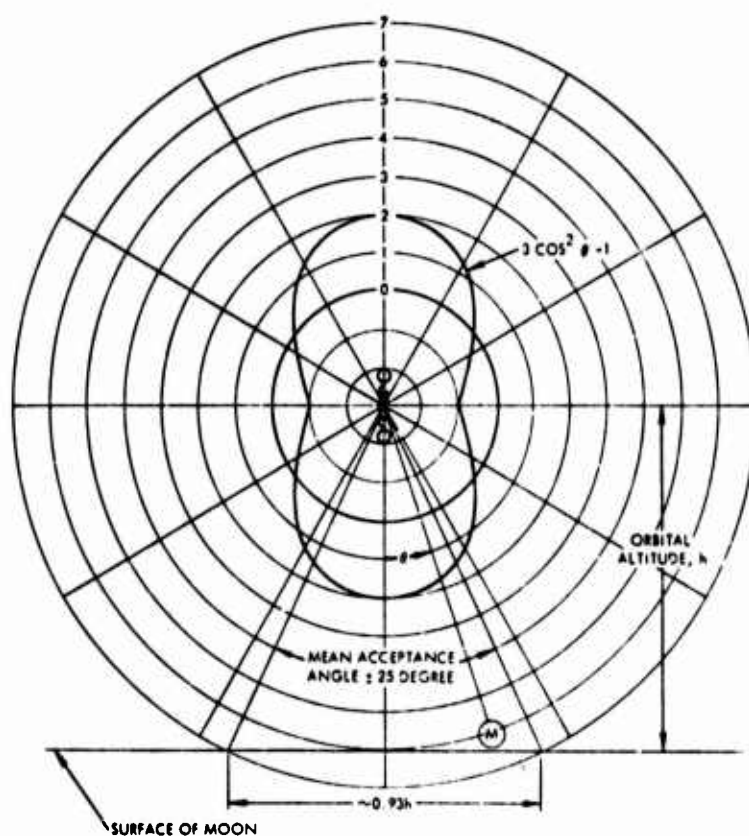


Figure 4-2. Directional sensitivity of a radial gravitational gradient sensor.

Because of this relatively broad $\cos^2 \theta$ angular response of gradiometers, their angular resolution is not high. Typically (depending upon the assumptions as to the 3 dB point and the target distance as a function of angle) the acceptance angle of the sensor is ± 25 to ± 40 degrees. Thus, as a practical rule of thumb, the spatial resolution of the sensor for two masses is approximately the distance of the sensor to the mass pair.

Rotating Torsional Gradiometer. Although the radial gradiometer is conceptually easy to visualize and was used in the previous section for clarity, the only gradiometer that has demonstrated the sensitivity required for practical applications along with an instrument time constant compatible with typical aircraft velocities is the rotating torsional gradiometer. The interaction of this sensor will be studied with gravitational gradient field as a function of the relative angular orientation of the sensor and field to determine how small errors in the sensor angular attitude couple into the background gradient of the earth to give erroneous indications of small variations in the gradient field due to local anomalies.

A torsional sensor with arm radius r and arm mass m with its spin axis along the z direction and its arms at 45° with respect to the x, y axes can be represented by the tensor matrix

$$C_{ij} = mr \begin{pmatrix} 0 & 1 & 0 \\ 1 & 0 & 0 \\ 0 & 0 & 0 \end{pmatrix} \quad (4-39)$$

If the sensor is rotated about the z axis (its usual spin axis), the tensor representing the sensor becomes

$$\begin{aligned} C'_{kl} &= \Phi_{ki} C_{ij} \Phi_{jl}^{-1} = \\ &= mr \begin{pmatrix} \sin 2\phi & \cos 2\phi & 0 \\ \cos 2\phi & -\sin 2\phi & 0 \\ 0 & 0 & 0 \end{pmatrix} \end{aligned} \quad (4-40)$$

If this sensor then interacts with the gravity gradient tensor Γ_{kl} , the amplitude of angular acceleration on one arm of the sensor is

$$a = C_{kl}' \Gamma_{kl} = mr [(\Gamma_{xx} - \Gamma_{yy}) \sin 2\phi + 2\Gamma_{xy} \cos 2\phi]. \quad (4-41)$$

If the rotation is continuous, so that $\phi = \omega t + \alpha$ where ω is the rotation frequency and α is the phase angle, the formula for the differential torque between the two arms of the sensor is obtained

$$\begin{aligned} \Delta T = 2ar = 2mr^2 [(\Gamma_{xx} - \Gamma_{yy}) \sin (2\omega t + 2\alpha) \\ + 2\Gamma_{xy} \cos (2\omega t + 2\alpha)]. \end{aligned} \quad (4-42)$$

This formula is the same as that derived directly from Newtonian force calculations either the sine and cosine components of the signal or the amplitude and (bi)phase of the signal can be read out. It is assumed that the amplitude and (bi)phase will usually be read out.

The amplitude of the signal is

$$A = \frac{\Delta T}{2mr^2} = \left[(\Gamma_{xx} - \Gamma_{yy})^2 + 4\Gamma_{xy}^2 \right]^{1/2} \quad (4-43)$$

and the (bi)phase that gives the (bi)direction of the gradient field components is given by

$$2\alpha = \tan^{-1} \frac{2\Gamma_{xy}}{\Gamma_{xx} - \Gamma_{yy}} \quad (4-44)$$

Now the errors are calculated that are introduced into response of the sensor as a function of the errors in attitude of the sensor coordinate system with respect to the local surface coordinate system.

If the sensor is above the earth (see Fig. 4-3) with its spin axis aligned horizontally perpendicular to the flight path ($\psi \approx 0$) and the phase reference direction chosen near the principal axis of the Γ_{xx}

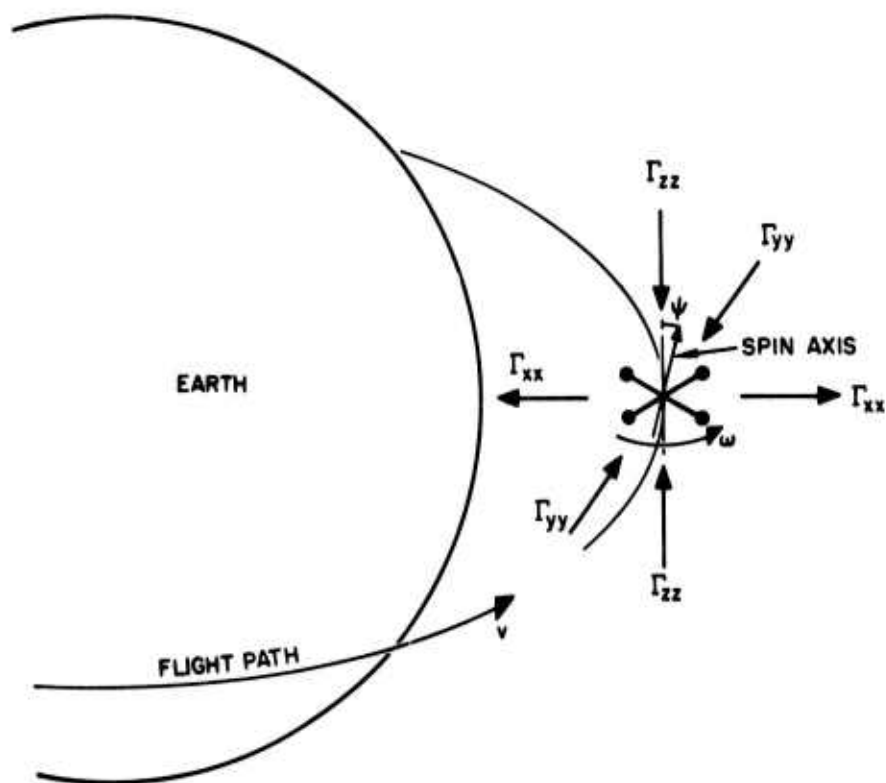


Figure 4-3. Sensor and gravitational field relative orientation schematic.

component (near the local vertical), then the components of the gravitational field measured by the sensor will be approximately

$$\begin{aligned}
 \Gamma_{xx} &\approx 2\Gamma \pm 2\gamma \approx 3000 \pm 40 \text{ E. U.} \\
 \Gamma_{yy} &\approx \Gamma_{zz} \approx -\Gamma \pm \gamma \approx -1500 \pm 20 \text{ E. U.} \\
 \Gamma_{xx} - \Gamma_{yy} &\approx 3\Gamma \pm 3\gamma \approx 4500 \pm 60 \text{ E. U.} \\
 \Gamma_{xy} &\approx \Gamma_{yz} \approx \Gamma_{zx} \approx \pm \gamma \approx \pm 20 \text{ E. U.}
 \end{aligned}
 \tag{4-45}$$

where the background gradient signal $\Gamma = GM/R^3 = 1500$ E. U. of the earth has been separated out

$$\Gamma_{ij} = \frac{GM}{R^3} \begin{pmatrix} 2 & 0 & 0 \\ 0 & -1 & 0 \\ 0 & 0 & -1 \end{pmatrix} \quad (4-46)$$

from an assumed fluctuation (± 20 E. U.) due to the local mass anomalies

$$\gamma_{ij} = \begin{pmatrix} \pm 2\gamma & \pm\gamma & \pm\gamma \\ \pm\gamma & \pm\gamma & \pm\gamma \\ \pm\gamma & \pm\gamma & \pm\gamma \end{pmatrix} \quad (4-47)$$

and where it is assumed that the gravitational gradient cross components of the local anomalies can be as large as the in-line components.

5. Pitch or Phase Error

It is obvious without resort to tensor manipulations that if there is an error in the orientation of the phase reference axis of the sensor with respect to the vertical to the surface (pitch error) that this will not cause an error in the measurement of the amplitude of the signal but only an error in the measured phase. A 1 degree error in orientation produces a 2 degree error in signal (bi)phase which is equivalent to a 1 degree error in the calculation of the direction of the center of the moon. Thus, if the principal axes of the gradient as measured by the sensor were chosen to calculate the position of the local anomaly signals, the map would be offset by the error in phase angle. Since the angular resolution (± 30 degrees) is much larger than this, the phase angle errors are negligible.

In addition to being small, a phase reference error is primarily a direction error rather than an amplitude error. To get a feel for the amplitude errors, it is assumed that there is an angular error ϕ

in the angular orientation of the phase reference to the vertical. The total gravity gradient field of the earth at the new angle is now:

$$\Gamma'_{kl} = \Phi_{ki} \Gamma_{ij} \Phi_{jl}^{-1} =$$

$$\begin{pmatrix} \left[\begin{array}{c} \Gamma_{xx} \cos^2 \phi + 2\Gamma_{xy} \sin \phi \cos \phi + \Gamma_{yy} \sin^2 \phi \\ (\Gamma_{yy} - \Gamma_{xx}) \sin \phi \cos \phi + \Gamma_{xy} (\cos^2 \phi - \sin^2 \phi) \\ \Gamma_{xz} \cos \phi + \Gamma_{yz} \sin \phi \end{array} \right] & \left[\begin{array}{c} \Gamma'_{xy} \\ \Gamma_{xx} \sin^2 \phi - 2\Gamma_{xy} \sin \phi \cos \phi + \Gamma_{yy} \cos^2 \phi \\ -\Gamma_{xz} \sin \phi + \Gamma_{yz} \cos \phi \end{array} \right] & \left[\begin{array}{c} \Gamma'_{xz} \\ \Gamma'_{yz} \\ \Gamma_{zz} \end{array} \right] \end{pmatrix}$$

(4-48)

The output of the inphase component is

$$A_I = (\Gamma'_{xx} - \Gamma'_{yy}) = (\Gamma_{xx} - \Gamma_{yy}) \cos 2\phi \quad (4-49)$$

(note that the Γ_{xy} cross product term drops out for the rotating torsional sensor).

The output of the quadrature component is

$$A_Q = 2\Gamma'_{xy} = 2\Gamma_{xy} \cos 2\phi - (\Gamma_{xx} - \Gamma_{yy}) \sin 2\phi. \quad (4-50)$$

The presence of the large $\sin 2\phi$ error signal in the quadrature component causes concern since an error ϕ in the phase of the signal would cause a substantial increase in the quadrature output due to the coupling to the background gradient.

$$\begin{aligned} \Delta A_Q &= -3\Gamma \sin 2\phi \\ &\approx -6\Gamma\phi \approx 9000 \phi \text{ (E.U.)} \end{aligned} \quad (4-51)$$

To keep this output below 1 E.U. would require knowing the phase to $1.1 \times 10^{-4} \text{ rad} = 0.0060 = 0.36 \text{ arc min} = 21 \text{ arc sec}$. This phase accuracy establishes a combined requirement on platform vertical and signal phase readout repeatability of 21 arc sec error rms. The platform should provide the required isolation (see Appendix B, para. 3.1.5). The phase readout repeatability should also meet this requirement, but detailed analysis has yet to be performed to corroborate this conclusion.

6. Effect of Tilts Out of Orbital Plane

If there is a relative angular misorientation between the sensor centered coordinates and the mass centered coordinates about the other two axes then the rotation matrix has to be applied to one or the other of the tensors before their scalar interaction can be determined.

If the sensor is tilted about the x axis (yaw) an angle $-\psi$ then the gravity gradient field has been tilted by the angle ψ .

$$\Gamma'_{kl} = \Psi_{ki} \Gamma_{ij} \Psi_{jk}^{-1}$$

$$= \begin{pmatrix} \begin{bmatrix} \Gamma_{xx} & \Gamma_{xy} \cos \psi + \Gamma_{xz} \sin \psi \\ \Gamma'_{xy} & \Gamma_{yy} \cos^2 \psi + 2\Gamma_{yz} \sin \psi \cos \psi + \Gamma_{zz} \sin^2 \psi \end{bmatrix} & \begin{bmatrix} -\Gamma_{xy} \sin \psi + \Gamma_{xz} \cos \psi \\ \Gamma'_{yz} \end{bmatrix} \\ \begin{bmatrix} \Gamma'_{xz} & (\Gamma_{zz} - \Gamma_{yy}) \sin \psi \cos \psi + \Gamma_{yz} (\cos^2 \psi - \sin^2 \psi) \end{bmatrix} & \begin{bmatrix} \Gamma_{zz} \cos^2 \psi - 2\Gamma_{yz} \sin \psi \cos \psi + \Gamma_{yy} \sin^2 \psi \end{bmatrix} \end{pmatrix}$$

(4-52)

Thus, in the output of the sensor

$$\begin{aligned} \frac{\Delta T}{2mr^2} &= (\Gamma'_{xx} - \Gamma'_{yy}) \sin 2(\omega t + a) + 2\Gamma'_{xy} \cos 2(\omega t + a) \\ &= \left[\frac{3}{2} \Gamma_{xx} + \frac{1}{2} (\Gamma_{zz} - \Gamma_{yy}) \cos 2\psi - \Gamma_{yz} \sin 2\psi \right] \sin 2(\omega t + a) \\ &\quad + \left[2\Gamma_{xy} \cos \psi + \Gamma_{xz} \sin \psi \right] \cos 2(\omega t + a). \end{aligned}$$

(4-53)

The amplitude is now

$$\begin{aligned} A = \frac{|\Delta T|}{2mr^2} &= \left\{ \left[\frac{3}{2} \Gamma_{xx} + \frac{1}{2} (\Gamma_{zz} - \Gamma_{yy}) \cos 2\psi - \Gamma_{yz} \sin 2\psi \right]^2 \right. \\ &\quad \left. + 4 \left[\Gamma_{xy} \cos \psi + \Gamma_{xz} \sin \psi \right]^2 \right\}^{1/2} \end{aligned}$$

(4-54)

and the (bi)phase

$$2\alpha = \tan^{-1} \frac{2(\Gamma_{xy} \cos \psi + \Gamma_{xz} \sin \psi)}{\frac{3}{2}\Gamma_{xx} + \frac{1}{2}(\Gamma_{zz} - \Gamma_{yy}) \cos 2\psi - \Gamma_{yz} \sin 2\psi}. \quad (4-55)$$

To determine the effect of an error in knowledge of the angle ψ in converting the background gradient of the earth into a signal, the fact is used that only the three principal gradients of the earth are important, so that

$$\begin{aligned} \Gamma_{xx} &\approx 2\Gamma \approx +3000 \text{ E. U.} \\ \Gamma_{yy} &\approx \Gamma_{zz} \approx -\Gamma = -1500 \text{ E. U.} \\ \Gamma_{xy} &\approx \Gamma_{xz} \approx \Gamma_{yz} = 0. \end{aligned} \quad (4-56)$$

Then the amplitude and (bi)phase reduce to

$$A = 3\Gamma \quad (4-57)$$

$$2\alpha = 0. \quad (4-58)$$

Thus to first order the amplitude and phase of the signal does not change with a rotation (yaw) of the sensor about the x (vertical) axis.

If the sensor is tilted (rolled) about the y axis (direction of flight) by an angle θ , then the gravity gradient in the new sensor coordinate system looks like

$$\Gamma'_{kl}(\theta) = \otimes_{ki} \Gamma_{ij} \otimes_{jl}^{-1}$$

$$\begin{pmatrix} \left[\Gamma_{xx} \cos^2 \theta + 2\Gamma_{xz} \sin \theta \cos \theta + \Gamma_{zz} \sin^2 \theta \right] & \left[\Gamma'_{xy} \right] & \left[\Gamma'_{xz} \right] \\ \left[\Gamma_{xy} \cos \theta + \Gamma_{yz} \sin \theta \right] & \left[\Gamma_{yy} \right] & \left[\Gamma'_{yz} \right] \\ \left[\Gamma_{xz} \right] & \left[\Gamma'_{yz} \right] & \left[\Gamma_{zz} \cos^2 \theta - 2\Gamma_{xz} \sin \theta \cos \theta + \Gamma_{xx} \sin^2 \theta \right] \end{pmatrix} \quad (4-59)$$

Thus the amplitude and (bi)phase that the sensor reads is

$$A = \left\{ \left[\Gamma_{xx} \cos^2 \theta + 2\Gamma_{xz} \sin \theta \cos \theta + \Gamma_{zz} \sin^2 \theta - \Gamma_{yy} \right]^2 + 4 \left[\Gamma_{xy} \cos \theta + \Gamma_{yz} \sin \theta \right]^2 \right\}^{1/2} \quad (4-60)$$

$$2\alpha = \tan^{-1} \frac{2 (\Gamma_{xy} \cos \theta + \Gamma_{yz} \sin \theta)}{\Gamma_{xx} \cos^2 \theta + 2\Gamma_{xz} \sin \theta \cos \theta + \Gamma_{zz} \sin^2 \theta - \Gamma_{yy}} . \quad (4-61)$$

To determine the effect of an error in knowledge of the roll angle θ in converting the background gradient of the earth into a false anomaly signal it can be assumed again that only the three principal gradients of the earth are important, so that

$$\Gamma_{xx} \sim 2\Gamma \approx 3000 \text{ E. U.}$$

$$\Gamma_{yy} \approx \Gamma_{zz} \approx -\Gamma \approx -1500 \text{ E. U.} \quad (4-62)$$

$$\Gamma_{xy} \approx \Gamma_{xz} \approx \Gamma_{yz} \approx 0 .$$

and the amplitude and phase of the rolled sensor become

$$A = 3\Gamma \cos^2 \theta \quad (4-63)$$

$$2\alpha = 0 . \quad (4-64)$$

There is no phase shift, but a change in amplitude.

For small angles

$$A \approx 3\Gamma (1 - \theta^2) . \quad (4-65)$$

Thus, an unknown error of θ in the attitude of the sensor about $\theta = 0$ would give an equivalent error of

Error ($3\Gamma\theta^2$)		
($^\circ$)	(rad)	E. U.
3	0.05	11.3
1	0.017	1.3
0.6	0.01	0.45

C. Angular Rate Errors

1. Introduction

Detailed analysis is performed in this section developing a statistical treatment of the response of the sensor to angular rate inputs. Preliminary analysis of the isolation of a "knuckle air bearing" is described and one approach of servo control for such a bearing is discussed.

2. Sensor Response

As has been shown in Section III-B the ideal rotating gradiometer responds to a gradient tensor of the form

$$\bar{G}_{ij} = \begin{pmatrix} \Gamma_{xx} + \Omega_y^2 + \Omega_z^2 & \Gamma_{xy} - \dot{\Omega}_z - \Omega_x\Omega_y & \Gamma_{xz} + \dot{\Omega}_y - \Omega_x\Omega_z \\ \Gamma_{yx} + \dot{\Omega}_z - \Omega_y\Omega_x & \Gamma_{yy} + \Omega_z^2 + \Omega_x^2 & \Gamma_{yz} - \dot{\Omega}_x - \Omega_y\Omega_z \\ \Gamma_{zx} - \dot{\Omega}_y - \Omega_z\Omega_x & \Gamma_{zy} + \dot{\Omega}_x - \Omega_z\Omega_y & \Gamma_{zz} + \Omega_x^2 + \Omega_y^2 \end{pmatrix} \quad (4-66)$$

the equivalent gradient output of the sensor (including angular rate) is therefore (z axis spin)

$$\left[(\Gamma_{yy} - \Gamma_{xx}) + (\omega_x^2 - \omega_y^2) \right] \sin 2 \omega t + 2(\Gamma_{xy} - \omega_x \omega_y) \cos 2 \omega t \quad (4-67)$$

or

$$\underbrace{(\Gamma_{yy} - \Gamma_{xx}) \sin 2\omega t + 2\Gamma_{xy} \cos 2\omega t}_{\Gamma_g} + \underbrace{(\omega_x^2 - \omega_y^2) \sin 2\omega t - 2\omega_x \omega_y \cos 2\omega t}_{\Gamma_e} \quad (4-68)$$

the magnitude of the error term is therefore

$$\left. \begin{aligned} \Gamma_e &= \left[(\omega_x^2 - \omega_y^2)^2 + (-2\omega_x \omega_y)^2 \right]^{1/2} \\ \text{or} \\ \Gamma_e &= \left[\omega_x^4 + 2\omega_x^2 \omega_y^2 + \omega_y^4 \right]^{1/2} \\ \Gamma_e &= \omega_x^2 + \omega_y^2 \end{aligned} \right\} \quad (4-69)$$

These angular velocities (ω_x , ω_y) are defined to be the orthogonal components of the total angular velocity normal to the spin axis of the gradiometer, and the reference axes (\bar{x} , \bar{y}) are defined to be fixed to the gradiometer case. The output gradient error due to transverse angular velocities is defined by Equation (4-70) where $H(s)$ represents the equivalent gradiometer filter process.

$$\Gamma_{eo} = H(s) \Gamma_e \quad (4-70)$$

To establish requirements for angular rate isolation, some estimate of the relation between the power spectra of the angular rates and the output gradient error is necessary. This objective may be accomplished through an estimate of the autocorrelation function of the prefiltered gradient error. In Equation (4-69) the rate components (ω_x, ω_y) are defined as the sums of a zero-mean stationary gaussian random variable (x, y) and an average value (Ω_x, Ω_y) as in Equation (4-71).

$$\begin{aligned}\omega_x &\triangleq x + \Omega_x \\ \omega_y &\triangleq y + \Omega_y\end{aligned}\tag{4-71}$$

The resultant autocorrelation function of the pre-filtered gradient error is shown in Equation (4-72).

$$\begin{aligned}R_{\Gamma_e}(\tau) &= \left[\sigma_x^2 + \sigma_y^2 + \Omega_x^2 + \Omega_y^2 \right]^2 \\ &\quad + 2 \left[R_x^2(\tau) + R_y^2(\tau) + R_{xy}^2(\tau) + R_{yx}^2(\tau) \right] \\ &\quad + 4 \left[\Omega_x^2 R_x(\tau) + \Omega_y^2 R_y(\tau) + \Omega_x \Omega_y \{ R_{xy}(\tau) + R_{yx}(\tau) \} \right]\end{aligned}\tag{4-72}$$

Equation (4-72) may be simplified for the spectral estimation by assuming that the normal random variables (x, y) are uncorrelated and that their autocorrelation functions are approximately equal. These assumptions are defined in (4-73).

$$\begin{aligned}R_{xy}(\tau) &\triangleq 0 \triangleq R_{yx}(\tau) \\ R_x(\tau) &\triangleq R_\omega(\tau) \triangleq R_y(\tau) \\ R_\omega(0) &\triangleq \sigma_\omega^2 \\ \Omega_x^2 + \Omega_y^2 &\triangleq \Omega^2\end{aligned}\tag{4-73}$$

Substitution of Equation (4-73) into Equation (4-72) yields the following simplified estimate of the autocorrelation function of the pre-filtered gradient error.

$$R_{\Gamma_e}(\tau) \cong \left[2\sigma_\omega^2 + \Omega^2 \right]^2 + 4R_\omega^2(\tau) + 4\Omega^2 R_\omega(\tau) \quad (4-74)$$

The corresponding pre-filtered gradient error power spectrum is obtained directly as the Fourier Transform of Equations (4-74) as shown in (4-75).

$$S_{\Gamma_e}(f) = \left[2\sigma_\omega^2 + \Omega^2 \right]^2 \delta(f) + 4S_\omega(f) * S_\omega(f) + 4\Omega^2 S_\omega(f) \quad (4-75)$$

The equivalent filter process of the gradiometer, $H(s)$, passes low frequencies with unity gain such that the power spectrum of the output gradient error may be written as Equation (4-76).

$$S_{\Gamma_{eo}}(f) = \left[2\sigma_\omega^2 + \Omega^2 \right]^2 \delta(f) + 4 \left| H(j2\pi f) \right|^2 \left[S_\omega(f) * S_\omega(f) + \Omega^2 S_\omega(f) \right] \quad (4-76)$$

The significant result of Equation (4-76) is that most of the power is contained in the d-c terms, and the variance of the output gradient error may be approximated as (4-77),

$$\sigma_{\Gamma_{eo}}^2 \cong \left[2\sigma_\omega^2 + \Omega^2 \right]^2 \quad (4-77)$$

$$\sigma_{\Gamma_{eo}} \cong 2\sigma_\omega^2 + \Omega^2 \quad (4-78)$$

If the random rate contribution to the gradient error standard deviation is required to be less than (1/3) EU, then the allowable rate variance per axis is approximately $1.7 \times 10^{-10} \text{ sec}^{-2}$. Thus, the allowable standard deviation per axis is approximately $1.3 \times 10^{-5} \text{ rad/sec}$.

It is doubtful that a conventional ball-bearing supported stable platform can achieve this requirement in the presence of aircraft motion and vibration. Therefore, isolation in addition to that of the stable platform is required.

3. Control System

The baseline configuration of the motion isolation system includes additional isolation in the form of a gyro stabilized "knuckle air bearing servo." This servo acts as a low pass filter between platform angular motions and the angular motions of the gradiometer stable element. An estimate of the power spectrum and variance of gradiometer angular velocity can be made based on the filter properties of the "knuckle bearing" servo and an estimate of the platform power spectrum of angular velocity.

Figure 4-4 shows one side of the estimated two-sided power spectrum of the stable platform angular velocity, and the dotted asymptotes show the filtering effects of the "knuckle bearing" servo. The frequency (f_0) is the outer loop bandwidth of the "knuckle bearing" servo, the frequency (f_2) is the bandwidth of the platform stabilization loops, and the frequency (f_1) relates to platform servo compensation networks. The maximum level of the platform power spectrum is designated as

$$\Phi_0 \frac{(\text{rad/sec})^2}{\text{Hz}} .$$

The variance of platform angular velocity may be estimated by an integration under the asymptotes of Figure 4-4. This estimate is shown as Equation (4-79).

$$\begin{aligned} \sigma_{\omega_p}^2 &\cong 2\Phi_0 \left[\int_0^{f_1} \left(\frac{f}{f_1} \right)^2 df + f_2 - f_1 + \int_{f_2}^{\infty} \left(\frac{f_2}{f} \right)^2 df \right] \quad (4-79) \\ &\cong 4\Phi_0 f_2 \quad ; \quad f_2 > f_1 \end{aligned}$$

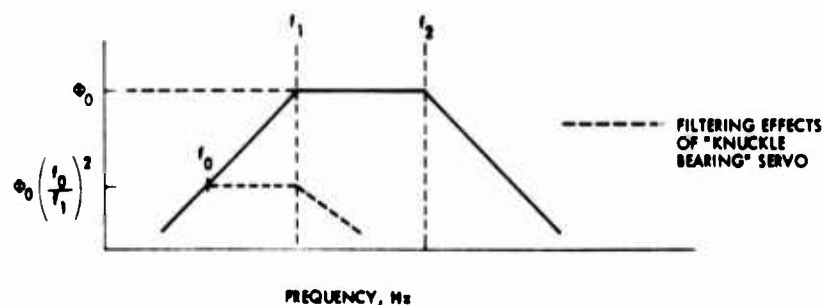


Figure 4-4. Estimated two-sided power spectrum, one side.

Similarly, asymptotic integration under the filtered function yields the following estimated variance of gradiometer angular velocity.

$$\sigma_{\omega}^2 \approx 2\Phi_0 \left[\int_0^{f_0} \left(\frac{f}{f_1} \right)^2 df + \left(\frac{f_0}{f_1} \right)^2 (f_1 - f_0) + \int_{f_1}^{\infty} \left(\frac{f_0}{f} \right)^2 df \right] \quad (4-80)$$

$$\approx 4\Phi_0 \left(\frac{f_0^2}{f_1} \right) ; \quad f_1 > f_0$$

From Equations (4-79) and (4-80) the standard deviation of gradiometer rate (σ_{ω}) has been reduced from that of the platform ($\sigma_{\omega p}$) by the factor $\sqrt{f_1 f_2 / f_0}$ due to the filter action of the "knuckle bearing" servo. It is estimated that this attenuating factor could be of the order of 500 to 1000 using an outer loop band width of 0.01 Hz in the "knuckle bearing" servo. This implies that to achieve $\sigma_{\omega} \approx 1.3 \times 10^{-5}$ rad/sec, comparable to $3\sigma_{\Gamma_e} = 1$ EU, the platform rate standard deviation must be less than approximately 10^{-2} rad/sec for the assumed power spectrum shape. If in addition to the assumed platform rate power spectrum, discrete frequencies are present due to platform limit cycles, pick-up, etc.; the variance of gradiometer angular velocity will be increased accordingly. The increase may be described as the weighted-sum* of the individual variances. Platform rates at discrete frequencies below the bandwidth of the "knuckle bearing" servo (f_0) will come through directly; however, those rates at frequencies above this bandwidth will be attenuated in direct proportion to their frequency. Thus, the weighted-sum of the rate variances for frequencies above (f_0) is directly proportional to the sum of the angular variances as shown in Equation (4-81).

$$\sum_i \frac{f_0^2 \sigma_{\omega}^2 p_i}{f_i^2} = (2\pi f_0)^2 \sum_i \frac{\sigma_{\theta}^2 p_i}{f_i} ; \quad f_i > f_0 \quad (4-81)$$

To keep this contribution to the gradiometer rate standard deviation less than 1.3×10^{-5} (rad/sec), the total standard deviation of platform angular motion at discrete frequencies (σ_{θ}) must be less than Equation (4-82).

$$\sigma_{\theta} < \frac{1.3 \times 10^{-5}}{2\pi f_0} \text{ rad} \quad (4-82)$$

*Weighted by the "knuckle-servo" filter process.

A selection of $f_0 = 0.01$ Hz yields approximately 2×10^{-4} rad (40 sec) for σ_0 from (14). This seems to be a practical figure, but it does indicate that the platform and its stabilization system must be carefully designed to avoid low amplitude motions that might result from such things as platform limit cycling, gyro spin motor interaction through a common power supply, electrical pick-up, etc. Of course, equal care must be exercised in the design of the "knuckle-bearing" servo as well.

4. Knuckle-Bearing Servo

Single loop control of the air knuckle bearing servo is not practical because of conflicting control bandwidth requirements. To provide the required isolation from platform angular velocity, the servo bandwidth must be low; however, to provide the required isolation from disturbance torques due to mass-unbalance in the presence of linear acceleration, the servo bandwidth must be high. Practical considerations of the rate disturbances to be expected from a conventional ball-bearing supported stable platform and of the mass-unbalance torques to be expected with state-of-the-art balancing techniques indicate these servo control bandwidth requirements to be more than a decade apart. For these reasons, a multiple loop control of the knuckle bearing servo is required.

A logical approach to a multiple loop design for this application is to provide a high bandwidth inner loop for disturbance-torque isolation and a low bandwidth outer loop for platform angular velocity isolation. In addition, there is the obvious requirement that the implementation of these control loops must not introduce added unacceptable disturbances. To meet this latter requirement, the high bandwidth inner control loop must be implemented without direct coupling to the stable platform motions. This objective may be accomplished by using an "inertial quality" rate integrating gyro to implement the inner control loop. The term "inertial quality" as used here means that the rate disturbances introduced by the gyro above the bandwidth of the outer control loop must be "acceptably small." Because of the presence of the outer control loop, there are no severe requirements on long term gyro drift rate comparable to the requirements of an inertial navigation system.

A simplified, single-axis block diagram of a multiplex loop design is shown in Figure 4-5. This model has four disturbance inputs:

1. Platform rate, ω_p
2. Outer loop position sensing noise, η_e
3. Integrating rate gyro drift, Ω_d
4. Disturbance torque, T_d

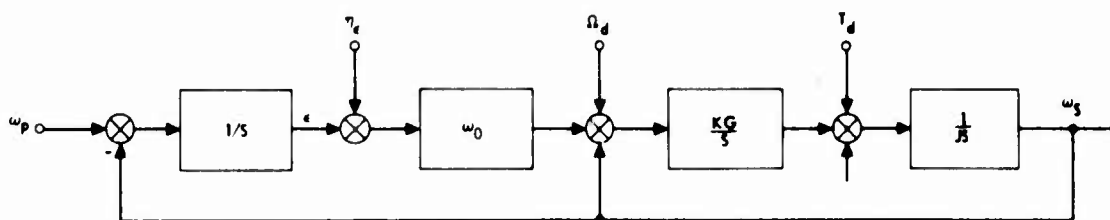


Figure 4-5. Single-axis multiple loop design, simplified block diagram

The objective of the design is to maintain the stable element inertial velocity, ω_s , below the "acceptable level" in the presence of the stated disturbances. Obviously, achievement of this objective depends on the amplitude and spectral properties of the disturbance inputs. Practical considerations indicate that it is entirely feasible to meet the design objective of platform rate, ω_p , and disturbance torque, T_d , isolation with this multiple loop design; however, two new disturbances have been introduced (η_e , Ω_d) by the implementation. It is anticipated that these added disturbances can be held within acceptable limits using state of the art hardware and design techniques.

D. Arm Balancing and Bending

The major problem in designing a portable gravity gradiometer is in isolating the sensor from vibrationally generated noise. By its nature the sensor is not sensitive to vibrational accelerations to first order. However, due to unavoidable mass imbalances and arm flexing, vibrational acceleration can cause differential torques which will generate spurious signals. Towards minimizing this disturbance, two approaches are necessary.

- (1) It is necessary to mass balance the arms to an extent finer than conventional methods allow. This balancing may be accomplished by the null-seeking servo-arm balance system to be discussed.
- (2) It is necessary to maintain the geometrical balance of the sensor against the distorting forces of gravity on an instantaneous basis as the sensor is rotated horizontally. An "isoelastic" arm design will be used and is discussed next. A few practical realizations of these principles will be illustrated, and a practical design concept embodying both servo arm balancing and isoelastic construction will be illustrated.

1. Anisoelastic Torques

Anisoelastic " g^2 " torques are a familiar gyro design problem. These torques occur whenever an initially balanced structure deflects under acceleration in a manner that causes the C.G. to move in a line not coincident with the acceleration vector. This results in an acceleration induced imbalance and spurious torque whose amplitude is proportional to the square of the acceleration.

In general the anisoelastic torque about the spin-axis (z) can be shown to be

$$T = m_a^2 \left(\frac{1}{k_x} - \frac{1}{k_y} \right) a_x a_y \quad (4-83)$$

where

m_a = mass of arm

k_i = spring constant along i axis

a_i = acceleration along i axis

Only if the compliances in both directions are equal can this torque be reduced to zero.

In the sensor arm design it was initially realized that the generation of undesirable torques by bending of the sensor arms when operated with a horizontal spin axis could be at least partially compensated for by stretching of the sensor arms.

Since the two sensor arms are located at right angles to one another, coincidence of C.G. 's can remain under acceleration only if both arms deflect isoelastically, so that both C.G. 's move along the line of the applied acceleration. Thus, for example, if we assume that the C.G. of each arm was originally located at the spin axis, the application of a one g acceleration field will depress the C.G. 's below their original position. Under the conditions of isoelasticity, both C.G. 's will be depressed an equal amount in the direction of the acceleration. Thus, the steady state condition will be for the arms to spin with their C.G. 's located at a steady, coincident position below the spin axis.

The arm designs used up to the present time have approximately 10 times the compliance in bending as in stretching. The aim of an isoelastic arm design then, is to increase an arm's compliance to stretch. Schematically, three concepts are shown in Figure 4-6. Each of these offers high stiffness to bending while allowing increased lateral compliance. An analysis of the elastic properties of the arm and truss configurations indicate that both configurations can be made isoelastic while maintaining practical dimensions.

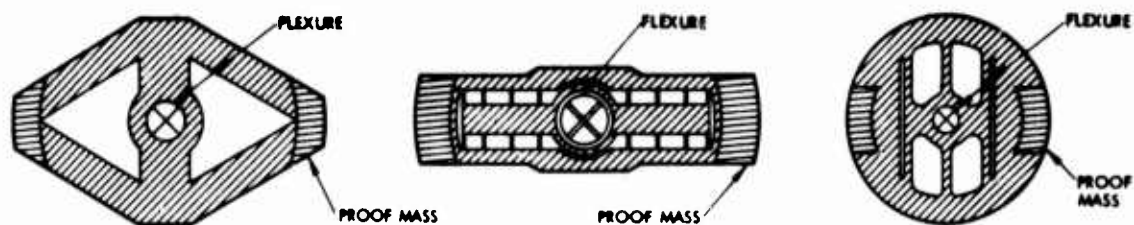


Figure 4-6. Arm designs

Of these, the truss arrangement has been selected to incorporate a servo-arm balancing device whose function is to correctly position the masses so that the c.m. of each arm lies upon the torsional axis and, in addition, position the radius of the masses so that proper torsional isolation is achieved. The correct adjustment of the c.m. and the arm inertias will improve the insensitivity of the device to lateral acceleration and torsional acceleration about the spin axis respectively. Naturally, hand balancing will be initially used to bring the components within the adjustment range of the servo balancer. In addition to initial requirements for proper mass and inertia balance, elasticity balance may also require adjustment. Isoelasticity, or its lack, can be determined by methods such as comparing the bending mode vibrational frequency of the arm with its lateral mode frequency.

2. Servo Arm Balance

The required position accuracy of the arm c.m.s to give sufficient noise isolation from various aircraft 1 and 3 ω vibrations is approximately 10^{-9} inch. To overcome the dimensional instabilities of materials in this range, and to facilitate achieving this balance, a set of four piezoelectric linear positioning devices per arm would be used, arranged as in Fig. 4-7, with each device forming an arm of the diamond shaped structure. Each unit individually consists of a stack of two-hundred 0.001 inch thick PZT discs. The discs are polarized to give expansion along their axis for the correctly applied voltage. The voltage is applied in parallel across each of the discs, while the discs are stacked with their polarities alternating so as to give addition of expansion movements for voltages applied as shown. A thin aluminum tube of 0.04 thickness encases the discs and preloads them, giving the transducer structural integrity. Since the elastic modulus of PZT is about 7.8×10^6 , it differs little from that of Al.; thus the small total area of the Al tube does little to inhibit the expansion or contraction of the stack as a whole. Movement of the c.m. of the arm with this arrangement can be affected in two dimensions, by changing the voltages on the proper transducer sets. Overall inertia can be raised or lowered by changing the voltage on all four transducer sets simultaneously. Thus, in theory, only one of the two arms need be active, and the other arm can be a non-servoed isoelastic arm.

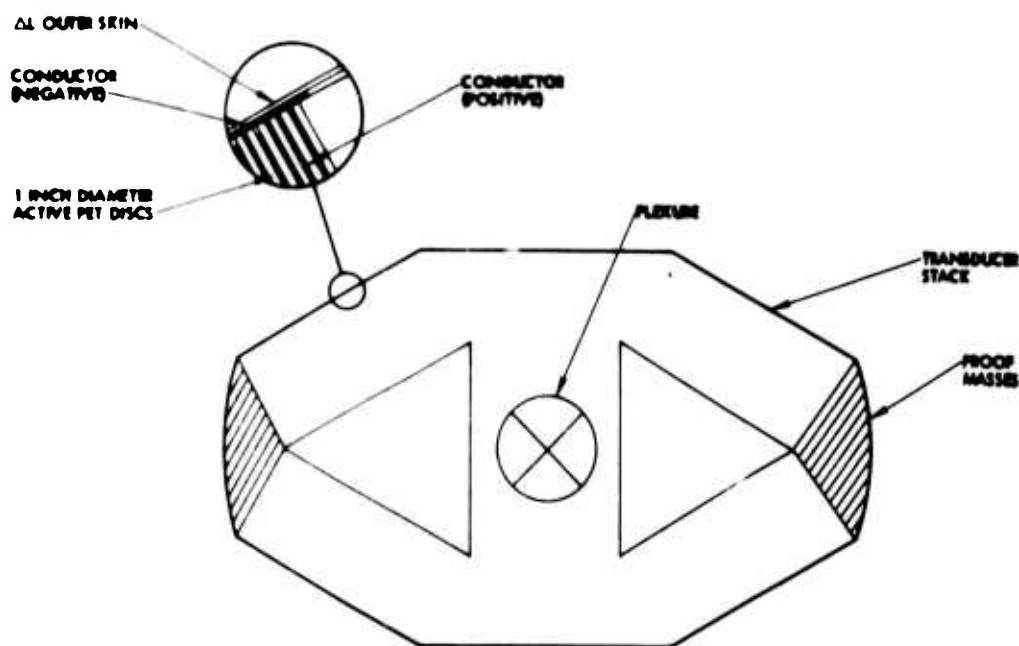


Figure 4-7. Iscelastic servo-balanced arm.

The method whereby the position of the arm c.m.s. are located is to apply a specific frequency of translational vibration (say, 1 KHz) to the entire sensor, or possibly to the entire platform. This acceleration is sensed by the gradient sensor if the arms are unbalanced. The output signal of the sensor is passed through a 1 KHz filter which separates out this unbalance signal from the gravitationally induced gradient signal. The 1 KHz signal is phase-detected and the output used to servo position the transducers for a null. An angular input can be added to achieve a balance signal for arm inertia balance. Finally, for horizontally oriented sensors, the "d-c" gravitational field can also be used to generate a signal proportional to arm imbalance at the frequency of rotation.

3. Transducer Design

Piezoelectric materials characteristically show a small change of dimensions for an applied voltage. It can be easily shown that

$$\Delta X = nVd_{33} \quad (4-84)$$

where

ΔX = total movement of a stack of piezoelectrics

V = applied voltage

d_{33} = piezoelectric charge coefficient

n = no. of piezoelectric elements

It is seen that the displacement is proportional to the number of elements whereas the thickness of the elements is related to the total length available to house a given number. For a 2-inch transducer, a standard thickness 1-inch diameter disc of 0.010 will allow 200 elements. For a lead zirconate titanate material such as Gulton Glennite G1512, the value of the charge coefficient is 500×10^{-12} meters/volt. An applied voltage of ± 15 volts results in an excursion of $\pm 0.59 \times 10^{-4}$ inches. If more excursion is required a higher voltage up to 150V can be accommodated or a greater number of thinner discs can be used. The thin aluminum tube encasing the transducer stack preloads the transducer stack giving it mechanical integrity despite the presence of tension due to centrifugal forces. The Young's Modulus of aluminum is similar to that of the piezoelectric material and it can be shown that the relatively small cross-sectional area of the aluminum tube does little to inhibit the expansion of the piezoelectric discs.

4. Isoelastic Arm Design

To design a truss structure having suitable properties, the approach will be to compute the deflection of the end masses in the bending mode e_1 and in the lateral stretch-compression mode e_2 . Naturally these deflections can be expressed as a function of the applied forces W and Q in the respective directions of deflection e_1 and e_2 . In other words, the spring constants of the structure in the e_1 and e_2 directions can be calculated. These are then equated and the remaining variables available may be chosen.

The structure will be approximated as a pin-ended truss (Fig. 4-8) here for simplicity of these initial feasibility calculations.

At point C:

$$(F_1 + F_2) \sin \theta = W \quad (4-85)$$

$$(F_1 - F_2) \cos \theta = Q \quad (4-86)$$

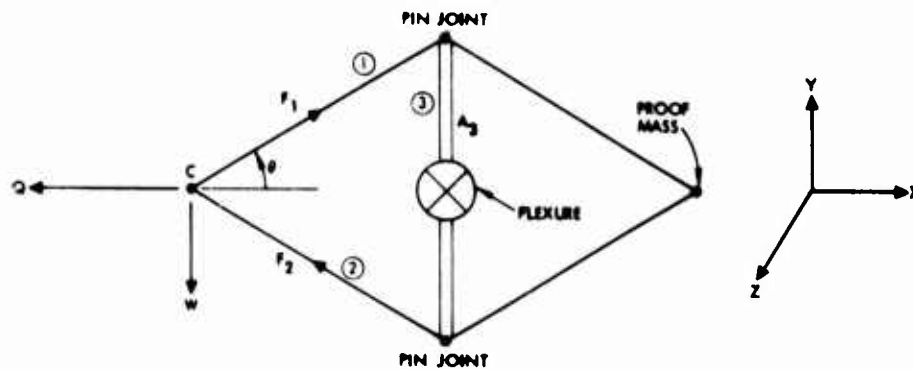


Figure 4-8. Pin-ended truss

solving for F_1 and F_2

$$F_1 = \frac{1}{2} \left(\frac{W}{\sin \theta} + \frac{Q}{\cos \theta} \right) \quad (4-87)$$

$$F_2 = \frac{1}{2} \left(\frac{W}{\sin \theta} - \frac{Q}{\cos \theta} \right) \quad (4-88)$$

By the principle of Virtual Work (Castigliano's Theorem), the total energy is

$$V = \sum_{i=1}^n \frac{F_i^2 \ell_i}{2A_i E_i} ; n = 3 . \quad (4-89)$$

The displacement in the W direction is

$$e_1 = \frac{\partial V}{\partial W} \quad (4-90)$$

and the displacement in the Q direction is

$$e_2 = \frac{\partial V}{\partial Q} . \quad (4-91)$$

in other words

$$\begin{aligned}
 e_1 &= \frac{\partial}{\partial W} \left[\left(\frac{W}{2 \sin \theta} + \frac{Q}{2 \cos \theta} \right)^2 \frac{\ell_1}{2A_1 E_1} + \left(\frac{W}{2 \sin \theta} - \frac{Q}{2 \cos \theta} \right) \frac{2\ell_1}{2A_1 E_1} \right. \\
 &\quad \left. + \frac{W^2 \ell_2}{2A_3 E_3} \right] (*) \\
 e_1 &= \frac{\partial}{\partial W} \left[\frac{1}{4} \left(\frac{W^2}{\sin^2 \theta} + \frac{Q^2}{\cos^2 \theta} + \frac{2 W Q}{\sin \theta \cos \theta} \right) \frac{\ell_1}{2A_1 E_1} \right. \\
 &\quad \left. + \frac{1}{4} \left(\frac{W^2}{\sin^2 \theta} + \frac{Q^2}{\cos^2 \theta} - \frac{2 W Q}{\sin \theta \cos \theta} \right) \frac{\ell_1}{2A_1 E_1} + \frac{W^2 \ell_3}{2A_3 E_3} \right] \\
 &= \frac{1}{2} \left(\frac{W}{\sin^2 \theta} + \frac{W}{\sin^2 \theta} \right) \frac{\ell_1}{2A_1 E_1} + \frac{W \ell_3}{A_3 E_3} \\
 e_1 &= \frac{W \ell_1}{2A_1 E_1 \sin^2 \theta} + \frac{W \ell_3}{A_3 E_3} \tag{4-92}
 \end{aligned}$$

*The forces in only one of the two vertical arms is included because the actual load on the center section is $2W$ applied to both arms. After differentiation it will be seen that this is equivalent to force W applied to the arm.

similarly, in Q direction

$$\begin{aligned}
 e_2' &= \frac{\partial V}{\partial Q} = \frac{\partial}{\partial Q} \left[\frac{1}{4} \left(\frac{W^2}{\sin^2 \theta} + \frac{Q^2}{\cos^2 \theta} \right) \frac{\ell_1}{2A_1 E_1} \right. \\
 &\quad \left. + \frac{1}{4} \left(\frac{W^2}{\sin^2 \theta} + \frac{Q^2}{\cos^2 \theta} \right) \frac{\ell_1}{2A_1 E_1} + \frac{W^2 \ell_3}{2A_3 E_3} \right] \\
 &= \frac{1}{4} \frac{Q}{\cos^2 \theta} \left(\frac{\ell_1}{A_1 E_1} \right) + \frac{1}{4} \frac{Q}{\cos^2 \theta} \left(\frac{\ell_1}{A_1 E_1} \right) \\
 e_2' &= \frac{Q \ell_1}{2A_1 E_1 \cos^2 \theta}
 \end{aligned}$$

In the Q direction, the additional displacement of the masses due to bending of beam 3 must be included

$$e_2'' = \frac{Q \ell_3^3}{3E_3 I_3}$$

for the slender beam approximation

where

$$I_3 = \frac{1}{12} b h^3 \quad (4-93)$$

b = thickness of beam along z-axis

h = width of beam

$A_3 = bh$

Thus, the total deflection in the Q direction is $e_2' + e_2''$ or

$$e_2 = Q \frac{\ell_1}{2A_1E_1 \cos^2 \theta} + \frac{\ell_3^3}{3E_3I_3}. \quad (4-94)$$

By equating the reciprocals of the spring constant

$$\frac{e_2}{Q} = \frac{e_1}{W} \quad (4-95)$$

the condition of isoelasticity may be satisfied.

Thus, from Equations (4-92) and (4-94), using (4-95)

$$\begin{aligned} \left[\frac{\ell_1}{2A_1E \sin^2 \theta} + \frac{\ell_3}{2A_3I_3} \right] &= \left[\frac{\ell_1}{2A_1E_1 \cos^2 \theta} + \frac{\ell_3^3}{3E_3I_3} \right] \\ \frac{\ell_1}{2A_1E_1 \sin^2 \theta} - \frac{\ell_1}{2A_1E_1 \cos^2 \theta} &= \frac{\ell_3^3}{2E_3I_3} - \frac{\ell_3}{A_3E_3} \\ \frac{\ell_1}{2A_1E_1} \left(\frac{1}{\sin^2 \theta} - \frac{1}{\cos^2 \theta} \right) &= \frac{\ell_3}{E_3} \left(\frac{\ell_3^3}{2I_3} - \frac{1}{A_3} \right) \end{aligned} \quad (4-96)$$

To satisfy this equation, the variables available are θ , E_1 , E_3 , A_1 , A_2 , A_3 , l_1 , l_2 , l_3 . Since an infinite number of solutions are available, practical values will be arbitrarily assigned to most of the variables. Aluminum will be chosen for the center strut so

$$E_3 = 10 \times 10^6 \text{ psi}$$

The equivalent Young's Modulus of the piezoelectric is

$$E_1 = 7.8 \times 10^6 \text{ psi}$$

The radius of the masses from the center is related to the theoretical signal to noise ratio desired apart from considerations of mechanical noise. Calculations indicate that sufficient output is obtainable with

$$r = 3 \text{ inches}$$

or

$$\left(l_1^2 - l_3^2 \right)^{1/2} = 3 \text{ inches } (l_1 = l_2)$$

The angle θ will be arbitrarily chosen for the purposes of this demonstration to be

$$\theta = 30^\circ$$

Also, the area A_1 will be arbitrarily chosen to be based on the previously described transducer stack which consists of 1 inch diameter discs. This diameter could easily be made smaller if some additional considerations were to arise,

$$A_1 = A_2 = \frac{\pi}{4} (1 \text{ inch})^2$$

Finally, the central truss thickness b_3 will be chosen arbitrarily = 1 inch.

Substituting these values into Equation (4-96)), and expressing I_3 and A_3 in terms of the thickness and width (Equation (4-93)), the equation reduces to

$$h_3^3 + 0.355 h_3^2 - 4.1 = 0$$

A few trials suggest a solution of the width

$$h_3 \approx 1.5 \text{ inches}$$

This solution can be rapidly checked by substitution into Equations (4-92) and (4-94).

The deflections expressed on a per lb. of load basis are

$$\begin{aligned} \frac{e_1}{W} &= \frac{\ell_1}{2A_1 E \sin^2 \theta} + \frac{\ell_3}{A_3 E_3} \\ &= (1.13 + 0.115) \times 10^{-6} \end{aligned}$$

$$\frac{e_1}{W} = 1.24 \times 10^{-6} \text{ inches/lb}$$

and

$$\begin{aligned} \frac{e_2}{Q} &= \frac{\ell_1}{2A_1 E_1 \cos^2 \theta} + \frac{\ell_3^3}{3E_3 I_3} \\ &= (0.377 + 0.830) \times 10^{-6} \\ &= 1.21 \times 10^{-6} \text{ inches} \end{aligned}$$

Thus, it is seen that an arm of these dimensions will deflect approximately 1 millionth of an inch per pound load in any direction. The more exact matching of these spring constants can be done by grinding the width of the central truss beam.

It should be noted that these calculations refer to the static case only. Under rapid rotation, consideration might have to be given to matching the damping of the two arms and perhaps to equalizing the damping in a manner similar to the matching of spring constants in two directions.

The degree to which these compliances must be matched can be computed from the equation previously stated

$$T = m_a^2 \left(\frac{1}{k_x} - \frac{1}{k_y} \right) a_x a_y$$

substituting

$$a_x = g \cos \theta$$

$$a_y = g \sin \theta$$

$$T = \frac{m_a^2 g^2}{2} \left(\frac{1}{k_x} - \frac{1}{k_y} \right) \cos 2\theta \quad (4-97)$$

The torque generated by a gravitational gradient is

$$T = \frac{3}{2} (I_y - I_x) \left(\frac{GM}{R^3} \right) \cos 2\theta \quad (4-98)$$

If the gradient is defined as

$$\Gamma = 2 \frac{GM}{R^3}$$

the equivalent gradient signal in E. U. generated by an anisoelasticity can be solved by equating (4-97) and (4-98).

$$\frac{m_a^2 g^2}{2} \left(\frac{1}{k_x} - \frac{1}{k_y} \right) = \frac{3}{4} (I_y - I_x) \Gamma$$

At this point, further simplifications can be made as this calculation is meant to be merely illustrative. I_x will be assumed zero and $I_y = mr^2$ where m is the proof mass on the end of the arm. Further, the arm weight will be neglected and m_a set equal to $2m$. Then

$$2m^2 g^2 \left(\frac{1}{k_x} - \frac{1}{k_y} \right) = \frac{3}{4} mr^2 \Gamma$$

or

$$\Gamma = \frac{8}{3} \frac{mg^2}{r^2} \left(\frac{1}{k_x} - \frac{1}{k_y} \right) \quad (4-99)$$

Substitution of typical values indicates that an uncompensated anisoelastic arm will generate a 125,000 E. U. signal. To ease the requirement for isoeleastic arm matching, the platform acceleration will be monitored by an accelerometer and this quantity used to calibrate out any remaining arm bending signals. If we assume an accelerometer with a resolution of 10^{-2} in/sec² and assume an allowable error of 0.1 E. U. we can calculate the required tolerance on stiffness matching of the arm by a simple error analysis from Equation (4-99).

$$(\Gamma + \Delta \Gamma) = \frac{8}{3} \frac{m(g + \Delta g)^2}{r^2} \left(\frac{1}{k_x} - \frac{1}{k_y} \right)$$

thus

$$\begin{aligned}\Delta\Gamma = 0.1 &= \frac{16}{3} \frac{m(g\Delta g)}{r^2} \left(\frac{1}{k_x} - \frac{1}{k_y} \right) \times 10^9 \\ &= \frac{16 (0.55) (10^{-2})}{9} \left(\frac{1}{k_x} - \frac{1}{k_y} \right) \times 10^9\end{aligned}$$

or

$$\left(\frac{1}{k_x} - \frac{1}{k_y} \right) = 0.307 \times 10^{-7}$$

$$\text{let } k_y = \delta k_x \text{ and } k_x = 0.82 \times 10^6$$

$$\frac{1}{k_x} \left(1 - \frac{1}{\delta} \right) = 0.307 \times 10^{-7}$$

and

$$\delta = 1.025 \text{ or a matching accuracy of 2.5 percent}$$

If resonant frequencies in bending and lateral modes are measured to determine isoelasticity, 2.5 percent accuracy is roughly equivalent to a 50 Hz difference in frequency ($f_0 = 3820$ Hz).

V. EXPERIMENTAL PROGRAM

A. Hard Mounted Sensor Project

The initial effort in development of the "hardmounted" gravity gradiometer during this contract was concentrated in design, fabrication and testing a breadboard gradiometer model. The sensor was the subject of several design changes that were directed toward obtaining improved sensor sensitivity. This approach has been effective in obtaining information which increases our understanding of sensor noise problems and led to improvements at a minimum design and development expense.

1. Original Design

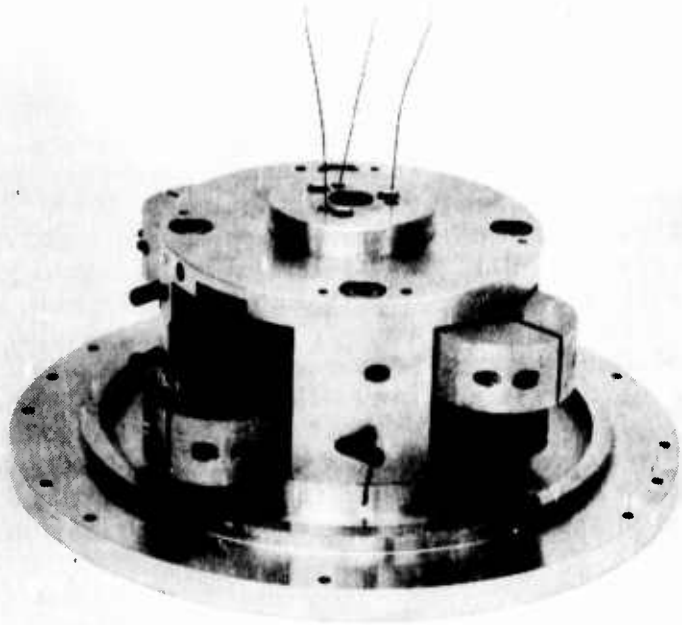
In the initial "hardmounted" gradiometer design, the sensor and its mechanical support systems were mounted on an aluminum alloy base which, in turn, was mounted on a two-axis rotating table permitting orientation at any desired angle with respect to the vertical. The entire assembly was mounted on an aluminum supporting structure which was initially secured directly to the laboratory floor. As a means of reducing excessive floor vibrations from coupling into the sensor, four coil springs were later installed between the floor and support structure and two viscous fluid dampers were mounted to damp the resulting low frequency oscillations. Balance weights were also required to maintain axis orientation of the entire spring supported assembly. (See Figure 5-1.)

The original mechanical support system included: (1) an air bearing supported rotating chamber assembly in which the sensor arms were installed, (2) a servocontrolled magnetic clutch, and (3) an a-c asynchronous motor drive. The rotating chamber contains the sensor arms that are supported by two 0.066 inch diameter torsion wires (see Figures 5-2 and 5-3) and interconnected with a flexural pivot torsion spring to which the piezoelectric strain transducer is affixed. A collect clamp length adjustment of one torsion wire was provided to obtain equal resonance frequency of each arm. A high vacuum was maintained within the chamber to isolate the arms from both acoustic and windage noise. The particular air bearing was selected based on its availability and stiffness; it is not the optimum bearing for future applications, as will be discussed later in this Report.

The sensor rotation drive motor consisted of a six-pole a-c asynchronous shielded motor mounted to the main sensor support frame. The motor was coupled to the sensor by use of a magnetic clutch. The motor was operated at a speed 20 percent above the desired sensor operating speed. The torque transmitted to the sensor was controlled by the magnetic clutch current. The clutch current was servocontrolled by use of a photoelectric position pickoff and appropriate servo electronics.



Figure 5-1. Air bearing supported gravity
gradient mass sensor with eddy current
motor drive under development
for AFCRL



7245

Figure 5-2. Sensor assembly and support structure

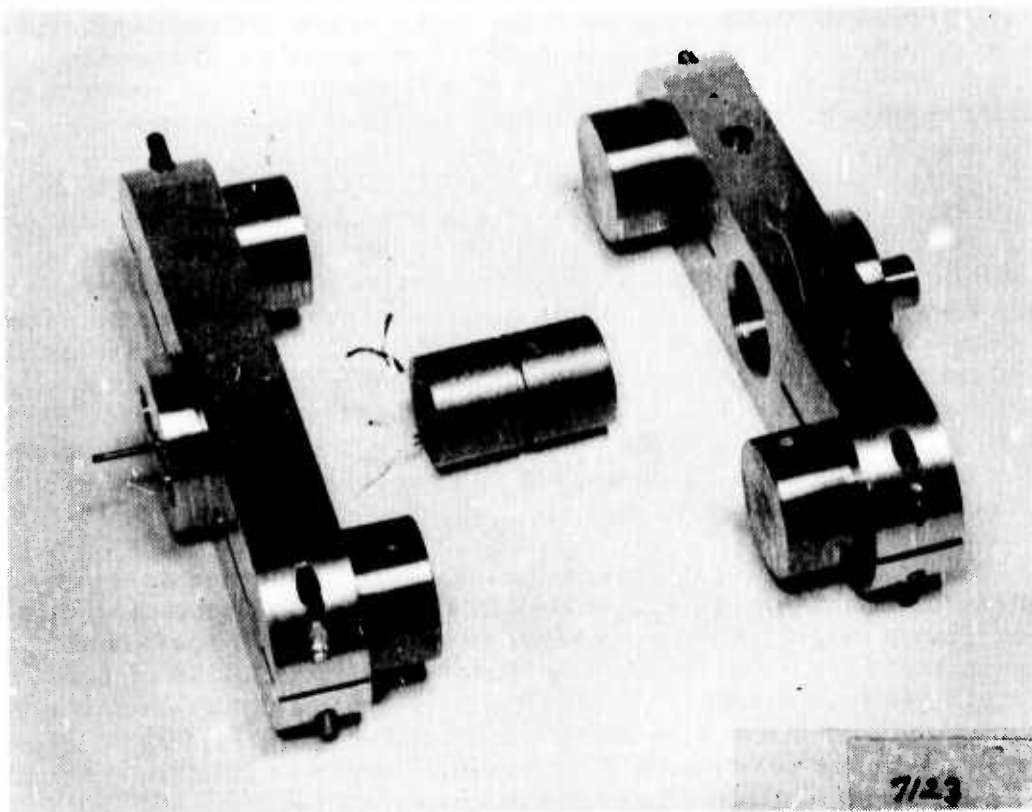


Figure 5-3. Components of sensor arm assembly

The electronic package included assemblies for frequency reference, sensor drive, telemetry, and signal processing, as well as commercial display electronics. The frequency reference and sensor drive system included: (1) a frequency synthesizer, (2) a digital frequency divider, (3) two drive power circuits, and (4) a servocontrol circuit for the hysteresis clutch. The telemetry and signal processing system (see Figure 5-4) amplifies and transmits the signals from the strain transducer, mounted on the flexure pivot, to receiving equipment outside the rotating system. The receiver signal was demodulated and fed into a nulling circuit where the portion of the phase coherent signal was biased out with a portion of the reference signal which was adjusted to phase and amplitude. This nulled signal was fed into a two-phase P.A.R. lock-in amplifier that detects the remaining coherent portion of the signal at twice the sensor rotation speed.

The major problems encountered with the initial design can be grouped into four major categories: (1) sensor arm balance, (2) resonant vibrations and incoherent noise external to the sensor, (3) electronic sensitivity to light, heat and static electricity, and (4) rotational speed control.

The initial attempts to adjust the sensor resonant mode frequency by collet adjustment of the torsion wire length resulted in collet failures. This was first noted from data that showed no significant frequency change with wire length adjustment. From this experience, other design approaches were decided upon for sensor resonant mode frequency adjustment.

Another source of mass unbalance was due to the design and geometry of the flexure pivot. The flexure's non-symmetrical mass distribution, which resulted in arm mass unbalance, was discovered and had to be accounted for, to obtain a satisfactory arm mass balance condition. Also, upon closer examination of the flexure point design, it was found to have the characteristic of non-uniform end moment stiffness versus rotation angle. Although this characteristic should not affect sensor operation when operated in a vertical spin-axis orientation, it could produce a 2ω frequency component when operated in a horizontal spin-axis orientation.

Noise and vibrations external to the sensor chamber assembly were recognized as a problem shortly after starting to obtain test data on the original design. A major source of environmental noise was found to emanate from the laboratory floor. The installation of four coil springs between the floor and the support structure, as previously mentioned, reduced the non-rotating sensor noise from 19,000 E. U. to 2300 E. U. With the bearing air film support, this was further reduced to an equivalent 90 E. U. at 10-second integration time.

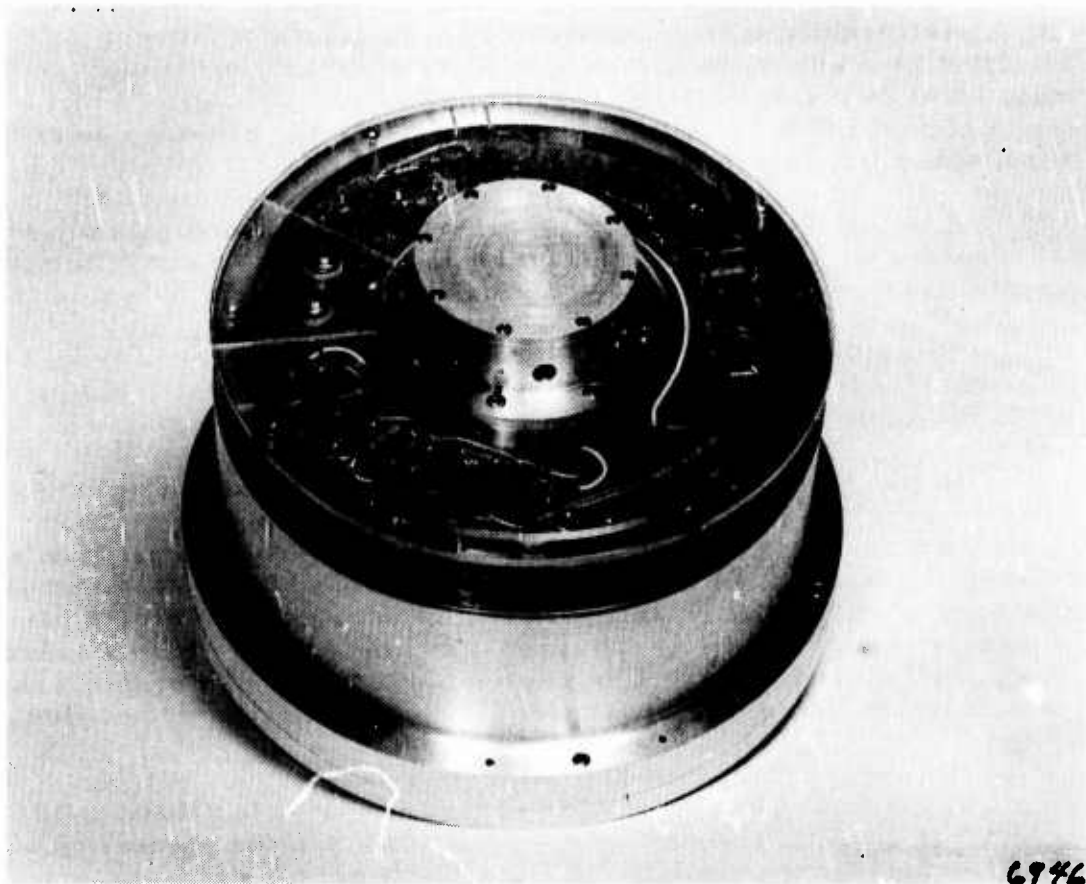


Figure 5-4. Sensor chamber with transmitter electronics

The magnetic clutch support bearings were also a source of excessive noise. Replacement of the original clutch support ball bearings with a high precision set of bearings did not reduce the noise sufficiently. The original six-pole, a-c asynchronous drive motor accounted for a small amount of the total coherent noise. Use of a special flexible elastomeric torsional coupling connecting the motor shaft directly to the air bearing significantly reduced noise transmission into the sensor but presented a speed control problem. It was thereby necessary to develop a drive system that would eliminate rolling element bearings. Replacement of the original asynchronous motor drive and magnetic clutch with a specially designed eddy-current drive motor eliminated these two sources of rolling element bearing noise.

Another speed control problem has only just recently been appreciated. Small second harmonic variations on the speed pickoff disk for example can generate significant coherent noise output. This effect has recently been demonstrated in the laboratory where gain adjustments made in the servo-control system reduced the coherent noise level by a large factor, approximately 40. Operation with a single pickoff pulse per revolution, rather than 10, provided an additional coherent noise reduction effect.

Additional speed variations can occur due to winding assymetry in the motor or random noise on the drive motor power amplifier outputs. These effects have not been studied quantitatively as yet.

Tests revealed erroneous gradient signals that were traced to be electronic component sensitivity to light, heat and static electricity. Small revisions to the electronic package corrected this problem.

Initial tests of the original designed sensor assembly were categorized as: (1) arm balancing tests, (2) static resonance tests, (3) static noise tests, and (4) dynamic tests. The original arm balance procedure resulted in a 20-gram inch static unbalance. This was later improved to within 0.1 gram inch static balance after precision balance on a knife edge. Due to the nonsymmetrical geometry of the flexure pivot, a 4 gram inch correction was required to provide proper arm mass balance. This was incorporated on the most recent modified design.

A static response test of the original sensor indicated a "Q" of 302.2 at 40.8 Hz resonant frequency. The resonant frequency was noted to change approximately 10 Hz with the sensor rotational position. This was later attributed to a fractured collet. Tests of a modified design without a collet showed no resonant shift due to rotational position change. Sensor "Q" has remained near 300 throughout the testing program.

Based on a factor of approximately 30 mV/E. U., the electronic noise level of the transmitted signal was found to be slightly over 1 E. U. peak to peak, while the minimum total static non-running noise has been reduced to 50 E. U.

An improved static balance of the sensor arms reduced the coherent noise during dynamic testing from 400,000 E. U. to 67,000 E. U. Although this coherent signal was biased out, the sensor still maintained a 900 to 1000 E. U. incoherent noise level.

2. Modified Design

The major effort during the past few months was concentrated in a design that would eliminate the foregoing problem areas. The modified system design includes a new sensor support, a broad-band vibration isolation system, and an improved sensor design. The aluminum support structure was replaced by a symmetrical frame within which the motor drive, air bearing and sensor chamber are suspended by four elastomeric springs (see Figure 5-5). This new support provides a 1 Hz resonance vibration isolation system with provision for installation of oscillation dampers if required. The total weight of entire assembly with the sensor installed is less than 100 pounds compared with the approximate 400 pound weight of the original system assembly. Being portable, the entire new assembly was placed on an air supported vibration isolation table.

Sensor mechanical design improvements developed and tested during the past few months include: (1) specially designed eddy-current drive motor that eliminates the original six-pole asynchronous drive motor and magnetic clutch, (2) a new sensor arm support that eliminates the collet and provides for more accurate mass balance and inertia balance of the sensor arms while installed on the rotating assembly and (3) an improved static and dynamic balancing procedure that reduces the coherent output due to non-gravitational sources.

Since the original concept, only minor electronic design improvements were necessary. Among these, as previously mentioned, was a reduction in electronic noise level to 1 E.U. and revisions to eliminate the sensitivity to heat, light and static electricity.

3. Major Achievements

The progress gained under this contract was continual and significant. The importance and drama of measuring gravity gradients was lacking, however, this should not deter the reader from recognizing the importance of the following major achievements:

- a. Significant gain in knowledge of the way in which bias signals and noise are generated;
- b. A corresponding understanding of solutions to bias and noise problems;
- c. Identification of the sensor and system components and tolerances required to achieve the design goals;

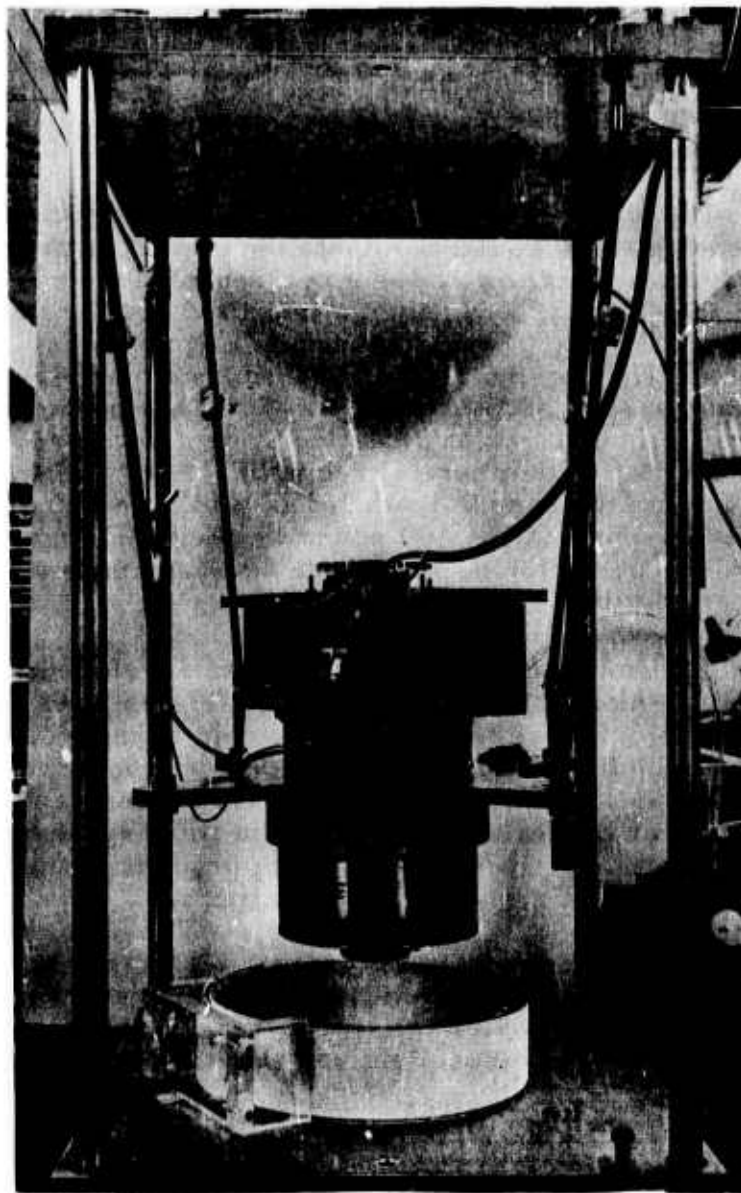


Figure 5-5. Gradient mass sensor vibration isolation system
utilizing latex rubber tubing

- d. A reduction in bias level from 100,000 E. U. to 5,000 E. U.;
- e. A reduction in random noise from 10,000 E. U. to approximately 900 to 1,000 E. U.;
- f. Continued confidence in the feasibility and practicality of the torsionally resonant rotating gradiometer for moving-base applications.

B. Noise Sources

The noise sources that affect the sensor output can be classified in two major types:

- a. Phase and amplitude "coherent" signal sources, i. e., constant signal sources. These occur due to effects of air journal bearing ellipticity; dynamic and static unbalance effects; systematic errors in the sensor speed control system; and effects due to precession, electrical pickup, gravitational-magnetic-and-electrostatic fields. The "coherent" noise level equivalent output of the present laboratory model is currently 5,000 E. U. It must be noted that this type of error can be biased out electronically. Variations in these errors may be caused by environmental changes on the sensor parameters and inputs. Such variations would appear as noise on this coherent signal. Thus, it is desirable to reduce the magnitude of the coherent signal to effect a corresponding decrease in the level of noise.
- b. Phase and amplitude "incoherent" signal sources, i. e., random noise sources. These occur due to effects of drive system mechanical and electrical noise; electronic readout noise; angular rate inputs due to ground vibration and air currents, windage, and journal bearing high frequency air flow noise. These sources act through the basic mechanisms of differential arm mass unbalance, differential inertia-spring unbalance (sum-mode mismatch), and/or angular rate sensitivity. The present incoherent noise level of the laboratory gradiometer is approximately 900 to 1,000 E. U. when measured over an integration time of ten seconds.

1. Sum Mode Mismatch

The gradient error due to differential inertia-spring unbalance (sum mode mismatch) and sensor acceleration about its spin axis is defined by the last major term in Equation (4-23) of Section IV-A. This relation is defined by (5-1).

$$\Gamma_e = \left[\frac{\omega_o^2/Q}{S^2 + \frac{\omega_o}{Q} S + \omega_o^2} \right] \left[\frac{\{(\alpha_1 - \alpha_2) S + (\beta_1^2 - \beta_2^2)\} \dot{\omega}_k}{S^2 + \alpha_{12} S + \beta_{12}^2} \right] \quad (5-1)$$

The magnitude of the coherent gradient error due to sum mode mismatch may be determined by evaluating (5-1) at $S = j\omega_o$. For light damping of the sum mode, this error magnitude may be approximated by (5-2).

$$|\Gamma_e| \cong \left[\frac{\beta_1^2 - \beta_2^2}{\omega_o^2} \right] \dot{\omega}_k(j\omega_o) \quad (5-2)$$

where $\dot{\omega}_k(j\omega_o)$ is that part of $\dot{\omega}_k$ at frequency ω_o .

The degree of balance attainable between the two arms may be ascertained by estimating the error that might exist in the arm inertias after balancing. Assuming balancing accuracy on each mass of 0.0001 inch (probably optimistic), the inertia error produced by this error is

$$\Delta I = 2m(r + \Delta r)^2 - 2mr^2$$

$$\cong 4mr\Delta r = 4(250)(6.35)(0.000394) = 2.5 \text{ gm cm}^2$$

out of a total inertia of 10^4 gm cm^2 or a $\Delta I/I$ of 0.025 percent. This percentage error is proportional to $(\beta_1^2 - \beta_2^2)$ in Equation (5-2) when the support springs are matched, i. e.

$$(\beta_1^2 - \beta_2^2) \cong \left(\frac{\Delta I}{I} \right) \beta_{12}^2 \quad (5-3)$$

Therefore, from (5-2) and (5-3) the sensor torsional acceleration $[(\dot{\omega}_k)(j\omega_o)]$ required to produce a 1 E.U. signal error is

$$|\dot{\omega}_k[j\omega_o]| = \left(\frac{\omega_o}{\beta_{12}} \right)^2 \left(\frac{10^{-9}}{2.5 \times 10^4} \right) \bigg|_{\omega_o \cong 2\beta_{12}} \cong 1.6 \times 10^{-5} \text{ sec}^{-2}$$

The allowable torque input equivalent to this angular acceleration error (assuming a rotor inertia $J = 4 \times 10^5 \text{ gm} \cdot \text{cm}^2$)

$$T_{\text{input}} = J\dot{\omega}_k = 6.4 \text{ dyne} \cdot \text{cm} .$$

This torque level is extremely low compared, for example, to the measured torque required to maintain constant operating speed ($\approx 5 \times 10^5 \text{ dyne} \cdot \text{cm}$ in the existing air bearing).

The implications of the above discussion are significant:

- a. Ellipticity in the air bearing and journal may give rise to second harmonic torques on the rotation speed that can create 2ω coherent signals.
- b. Small variations in torque either from variations in the ellipticity of the bearing, air windage, or noise on the servo speed control current, will give rise to incoherent noise outputs of the sensor.

2. Journal Air Bearing Torque Variations

The viscous torque of an ideal journal bearing consisting of two concentric cylinders is approximately inversely proportional to the gap between the cylinders. The error in this approximation is of the order of the ratio of the gap to the cylinder radius. If the surface boundary projections of the bearing rotor and stator are not perfect circles, the resulting viscous torque will have a time varying component. The intent of this discussion is to make an estimate of the time varying viscous torque based on the assumption that the incremental viscous torque is inversely proportional to the spatially instantaneous gap. Obviously this approach lacks rigor in that inertial forces and turbulence in the lubricant are neglected. Nevertheless, it does provide an indication of the relation between rotor/stator geometry and the time varying torque and serves as the basis for estimation of the magnitudes of various spectral components of this torque.

Rotor/Stator Geometry

Ideally the surface boundary projections of the rotor and stator are perfect circles. The departure from this ideal condition may be described in terms of a spatial Fourier expansion of the radius of the surface boundary projection as shown in (5-4).

$$R \triangleq R_o + \sum_1^{\infty} r_n \cos (n\theta - \phi_n) \quad (5-4)$$

The angular parameter (θ) is defined as the position of the radius vector (\bar{R}) with respect to a coordinate frame fixed in the surface boundary projection as shown in Fig. 5-6.

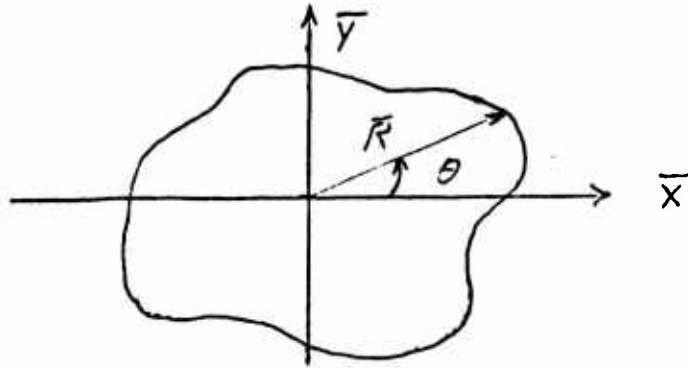


Fig. 5-6

The surface boundary projection represents an "equivalent" surface based on a weighted sum of the actual cross-sections taken along the length of the body.

The "equivalent" surface boundaries of both the rotor and the stator may be described in this manner as shown in (5-5).

$$R_s \triangleq R_{so} + \sum_1^{\infty} r_{sn} \cos(n\theta_s - \phi_{sn})$$

$$R_r \triangleq R_{ro} + \sum_1^{\infty} r_{rm} \cos(m\theta_r - \phi_{rm})$$

(5-5)

An "equivalent gap function" may now be defined as the difference between the stator and rotor radii based on the condition that both the rotor and stator coordinate origins coincide with the bearing spin axis and that the angular orientation of the rotor-fixed frame with respect to the stator-fixed frame is defined by the angle ($\psi \equiv \omega t$). This difference is shown as (5-6) where the parameters of (5-5) have been defined as $m \triangleq n$ and $\theta_r \triangleq \theta_s - \psi$.

$$g \triangleq R_{so} - R_{ro} + \sum_1^{\infty} [r_{sn} \cos(n\theta_s - \phi_{sn}) - r_{rn} \cos(n\theta_s - n\psi - \phi_{rn})]$$

(5-6)

A simplified and normalized form of (5-6) is shown as (5-7) wherein the spatial phase angles (ϕ_{sn}, ϕ_{rn}) are assumed to be zero and the normalized Fourier coefficients are defined as $\gamma_{sn} \triangleq r_{sn}/g_o$, $\gamma_{rn} \triangleq r_{rn}/g_o$, $g_o \triangleq R_{so} - R_{ro}$.

$$g \triangleq g_o \left[1 + \sum_1^{\infty} \left[\gamma_{sn} \cos n\theta_s - \gamma_{rn} \cos (n\theta_s - n\psi) \right] \right] \quad (5-7)$$

Viscous Torque Estimation

The instantaneous incremental viscous torque is assumed to be inversely proportional to the spatially instantaneous gap such that the total torque may be evaluated by integration of the inverse of (5-7) completely around the stator for a given relative rotor angle (ψ) as shown in (5-8).

$$T \triangleq \frac{T_o}{2\pi} \int_0^{2\pi} \frac{d\theta_s}{1 + \sum_1^{\infty} \left\{ \gamma_{sn} \cos n\theta_s - \gamma_{rn} \cos (n\theta_s - n\psi) \right\}} \quad (5-8)$$

Due to the precision of manufacture of the bearing, the maximum value of the series in (5-8) is assumed to be much less than unity.

Thus, the integral of (5-8) may be evaluated by binomial expansion as in (5-9).

$$T \triangleq \frac{T_o}{2\pi} \int_0^{2\pi} d\theta_s \left[1 - f(\theta) + f^2(\theta) - f^3(\theta) \dots \right] \quad (5-9)$$

where

$$f(\theta) \triangleq \sum_1^{\infty} \left[\gamma_{sn} \cos n\theta_s - \gamma_{rn} \cos (n\theta_s - n\psi) \right]$$

and

$$|f(\theta)|_{\max}^2 < 1$$

By symmetry, the definite integral over 2π of the odd powers of the function $[f(\theta)]$ are zero such that (5-9) may be replaced by (5-10).

$$T = \frac{T_o}{2\pi} \int_0^{2\pi} [1 + f^2(\theta) + f^4(\theta) \dots] d\theta_s \quad (5-10)$$

Since the magnitude of the function $[f(\theta)]$ is assumed to be much less than unity, the most significant variable function of (5-10) is contained in the second order term $[f^2(\theta)]$. Thus, equation (5-10) may be approximated as (5-11).

$$T \approx \frac{T_o}{2\pi} \int_0^{2\pi} [1 + f^2(\theta)] d\theta_s \quad (5-11)$$

The square of the series function $[f(\theta)]$ may be obtained from the double sum of (5-12).

$$f^2(\theta) = \sum_{n=1}^{\infty} \sum_{m=1}^{\infty} [\gamma_{ns} \cos n\theta_s - \gamma_{rn} \cos (n\theta_s - n\psi)] [\gamma_{sm} \cos m\theta_s - \gamma_{rm} \cos (m\theta_s - m\psi)] \quad (5-12)$$

The definite integral of the double sum over 2π is zero when the summation indices (rn, n) are not equal; therefore, the integral of (5-11) may be replaced by (5-13).

$$T \cong T_o + \frac{T_o}{2\pi} \sum_1^{\infty} \int_0^{2\pi} \left[\gamma_{sn} \cos n\theta_s - \gamma_{rn} \cos (n\theta_s - n\psi) \right]^2 d\theta_s \quad (5-13)$$

The result of the integral process of (5-13) is shown as (5-14).

$$T \cong T_o \left[1 + \frac{1}{2} \sum_1^{\infty} (\gamma_{sn}^2 + \gamma_{rn}^2) - \sum_1^{\infty} \gamma_{sn} \gamma_{rn} \cos n\psi \right] \quad (5-14)$$

The first summation of (5-14) represents a constant number much less than unity. The second summation of (5-14) is a periodic function of relative rotor position (ψ) and is an approximation to the time varying viscous torque components which we are attempting to estimate.

This estimate of the time varying viscous torque may be stated as a function of rotor velocity (ω) by substitution of ($\psi = \omega t$) into the variable part of (5-14) as shown in (5-15).

$$\Delta T(t) \cong T_o \sum_1^{\infty} \gamma_{sn} \gamma_{rn} \cos (n\omega t) \quad (5-15)$$

Equation (5-15) is interesting in two respects. The time varying torque of (5-15) is proportional to the average viscous torque (T_o); and to the first order, generation of the "nth" harmonic torque of rotor velocity requires spatial components of the "nth" harmonic in both the rotor and the stator, i. e., γ_{sn} and γ_{rn} . This property is unique to the second order term of (5-10); the higher ordered terms of (5-10) will produce much smaller torques containing products of the coefficients of unequal spatial harmonics of the rotor and stator.

Gradiometer Application

The time varying torque components about the gradiometer spin axis acting on the inertia of the rotating assembly (J) will produce angular accelerations of the gradiometer about its spin axis. Such accelerations will be coupled into the sensor through the "sum mode mismatch" of the gradiometer structure. The most significant gradient signal from this source will occur at the second harmonic of angular

velocity (i.e., the tuned resonant frequency of the gradiometer difference mode, $\omega_o = 2\omega$). The magnitude of this signal is stated from (5-15) as (5-16).

$$|\Gamma_e| \cong k_\beta \left[\frac{\beta^2}{\omega_o^2 - \beta^2} \right] \left[\frac{\gamma_{s2} \gamma_{r2} T_o}{J} \right] \quad (5-16)$$

where

k_β = sum mode mismatch factor

β = sum mode frequency

ω_o = difference mode frequency

Equation (5-16) represents the gradient signal that would be produced at the sensor output due to air bearing ellipticity.

It should be noted that only the variation of this signal from its mean value is of concern in terms of a sensor error. The mean value can be biased-out of the sensor output and is therefore in the "coherent" error category. The variation about the mean, then, is the incoherent error of concern. The probable magnitude of this variation might be as much as 10% but it has yet to be measured in the laboratory. Such variations primarily would be due to changes in the mean torque level, T_o , in turn resulting from temperature variation causing air film viscosity changes, and mean gap variations.

A best estimate of the total signal resulting from bearing ellipticity of the present laboratory sensor is made based on the following measurements and assumptions:

1. Sum mode mismatch factor of 1%. Although not directly measured, this appears to be a reasonable estimate of the present sensor's mismatch.
2. $T_o = 4 \times 10^5$ dyne-cm. This is a measured value.
3. $\gamma_{s2} = \gamma_{r2} = 1\%$. This parameter has not been measured, however this is a reasonable estimate based on the present bearing tolerance and techniques used by the vendor in its manufacture.

4. $J = 4 \times 10^5 \text{ gm-cm}^2$, a calculated value based on the present sensor configuration.
5. Sum mode to difference mode frequency ratio $(\beta^2/W_0 - \beta^2) = 1/3$, a measured value. Using these values in equation (5-16),

$$|\Gamma_c| = 10^{-2} \left[\frac{1}{3} \right] [10^{-4}] \text{ sec}^{-1} \cong 300 \text{ E.U.}$$

This, of course, is a coherent signal; the 10% variation on this signal would therefore be equivalent to 30 E.U. of incoherent noise. The above assumptions result in a reasonable estimate, that is, when compared to the laboratory test results.

The reader will recall that the measured coherent signal was 5,000 E.U. and total incoherent signal was approximately 900 E.U. As stated elsewhere in this report, it is felt that other sources of both coherent and incoherent error exist in the present laboratory model and have a significant contribution to the total.

Several means of reducing the estimated 300 E.U. error are possible:

1. Reduction of the average running torque of the bearing (T_0). This can probably be reduced somewhat, possibly by a factor of four.
2. Improvement of the sum-mode mismatch. The magnitude of this improvement, to be accomplished by incorporation of the precision arm balance system, will be at least a factor of 100, and probably more.
3. Reduction of the sum-mode-to-difference-mode frequency ratio $(\beta^2/W_0 - \beta^2)$. This could easily be reduced by a factor of 2 to 4.

Using the foregoing three error reduction possibilities, the present estimated 300 E.U. error value would be reduced to, at most, 0.4 E.U. Most important, since only the variation of this value is of concern, air bearing ellipticity problems are not considered to be a feasibility limitation.

3. Arm Unbalance - Vibration Sensitivity

Another potential source of error is in the arm mass unbalance-vibration sensitivity.

Consider that the mass centers of the sensor arms are displaced from the sensor center of support, as depicted in Figure 5-7, the amount \bar{b}_1 and \bar{b}_2 as indicated. Further consider that the coordinate reference frame of the sensor, x-y, is undergoing an inertial acceleration \bar{A} in the direction θ as depicted. If it is assumed, for the moment, \bar{A} to be constant in both direction and magnitude, then the inertial reaction torque due to the mass unbalance on each arm is

$$\bar{T}_1 = m\bar{b}_1 \times \bar{A}$$

$$\bar{T}_2 = m\bar{b}_2 \times \bar{A}$$

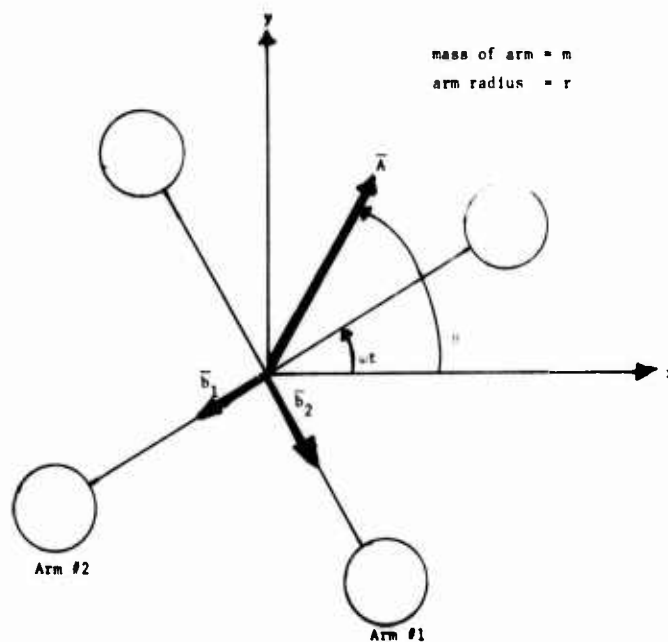


Figure 5-7. Force analysis schematic.

Hence, the differential angular acceleration between the arms is

$$\overline{\Delta a} = \frac{\Delta T}{I} = \frac{m\overline{A} \times (\overline{b}_2 - \overline{b}_1)}{mr^2}$$

or if

$$\overline{h} \triangleq \frac{\overline{b}_2 - \overline{b}_1}{r}$$

is defined, the vector differential mass unbalance distance expressed as a ratio of sensor arm radius,

$$\Delta a = \frac{m\overline{A} \times \overline{h}}{r}.$$

The second order gradient sensor effectively measures, or is sensitive to, this differential angular acceleration and as such, the equivalent gradient error due to this mass unbalance-acceleration effect is

$$\Gamma_e = \frac{m\overline{A} \times \overline{h}}{r}$$

Without developing the details, it can be shown that if the acceleration \overline{A} is oscillatory and occurs at one or three times the sensor rotation frequency, ω , the differential angular acceleration will contain a frequency component at 2ω (the second order gradient sensing frequency). To illustrate the significance of this effect, consider:

Assuming sophisticated balancing techniques are used prior to final assembly of the sensor, a practically achievable value of h is approximately 10^{-5} (0.001 percent) for the sensor radius arm of 2.5 inches. Therefore, allowing a 0.3 E. U. error contribution from this source, the maximum allowable acceleration within the bandwidth of the sensor is

$$A_{\max} = \frac{0.3 \times 10^{-9} \times 2.5}{10^{-5}} = 0.75 \times 10^{-4} \frac{\text{in.}}{\text{sec}^2} \cong 2 \times 10^{-7} g$$

Typical vibration levels on a moving base might be 0.05 g rms. A passive vibration isolation mount could be expected to attenuate this by 100. Thus, it is seen that an improvement in arm balance accuracy, over that attainable in the laboratory, would be

$$\frac{0.05 \times 0.01}{2 \times 10^{-7}} = 2.5 \times 10^3.$$

Balancing in the laboratory model was approximately one order of magnitude worse than that estimated above as being practically achievable, i.e., balance was held to $h \approx 10^{-4}$. This gives a sensitivity to 1 and 3ω accelerations of 10^7 E.U./g. Measured motion of the elastomer mounted sensor platform (measured by using the balancing machine as a displacement pickoff) was 10^{-5} inches. If the elastomer support stand was isoelastic to 0.1 percent (a conservative estimate) then 0.1 percent of the sensor platform motion ($x = 10^{-7}$ in.) would generate a 2ω frequency component in the sensor.

The acceleration amplitude of this motion at 1ω is given by

$$\begin{aligned} a &= \omega^2 x = (2\pi 20)^2 (10^{-7}) = 15,900 \times 10^{-7} \frac{\text{in.}}{\text{sec}^2} \\ &= 4 \times 10^{-6} \text{ g} \end{aligned}$$

This acceleration would, therefore, produce a coherent output of 40 E.U. which, although it is significant, is a small percentage of the current background clutter.

Mass unbalance is probably the only significant error source which generates errors through the arm unbalance mechanism in the laboratory test setup. However, it must be again emphasized that, in an operational system, external vibrations will contain 1 and 3ω components and will more severely constrain the arm balancing requirements.

4. Angular Rate Inputs

The fourth source of error is angular rate susceptibility. One source of errors in this category is caused by the resulting elliptical portion coning motion due to dynamic unbalance. (The ellipticity is brought about through an asymmetry in the sensor stand support.)

This error can be estimated as in the previous section by using the measured dynamic unbalance angular motion of $\approx 10^{-6}$ rad assuming a similar support spring asymmetry (0.1 percent) and calculating the angular rate produced by the 1ω coning angle error. This angular rate (Ω) is given by

$$\Omega = \omega \theta_{el}$$

where

$$\omega = 2\pi(20) = 125.6 \text{ rad/sec}$$

$$\theta_{el} = 10^{-6} \times 10^{-3} = 10^{-9} \text{ rad}$$

Therefore, $\Omega = 1.26 \times 10^{-7} \text{ rad/sec}$.

The equivalent gradient is given by

$$\begin{aligned} \Gamma_{eq} &= \Omega^2 = 1.57 \times 10^{-14} \text{ sec}^{-2} \\ &= 1.57 \times 10^{-5} \text{ E.U.} \end{aligned}$$

which is not significant.

The above calculation assumes that the test stand itself is isoinertial about any axis in the x-y plane.

In actual tests, significant differences in coherent output were obtained by adjusting the lateral inertias of the sensor support platform, however, only when there was significantly more dynamic unbalance in the rotor than the final tolerance. After dynamic balancing, stand inertia changes made no appreciable difference in sensor output.

Another source of angular rates is the stand motion induced by air currents and ground vibrations. These vibrations, because of their random nature, are a source of incoherent noise outputs from the sensor.

A reasonable estimate for the stand random angular motion due to air currents is somewhat less than 0.02 degrees = 3.5×10^{-4} rad. For the following calculation this figure will be used as an upper limit on the stand motion.

If it is assumed that this motion "rings down" at the resonant frequency of the stand (≈ 1 Hz) the maximum angular rate inputs are $\Omega = 2\pi f\theta = (6.28)(3.5 \times 10^{-4}) = 2.2 \times 10^{-3} \text{ rad/sec}$. The sensor output due to these random inputs is $\Gamma_e = \Omega^2 = 4.85 \times 10^{-6} \text{ sec}^{-2} = 4,850 \text{ E.U.}$

The sensor time constant attenuates this signal by at least a factor of 10. Therefore the maximum noise level would be expected to be no more than 500 E.U. of incoherent noise.

Although the above result is based on a crude estimate of test stand angular motion, it may well explain a significant portion of the observed 900 - 1000 E.U. noise level. In a follow-on program, detailed attention will be given to controlling the laboratory environment.

BLANK PAGE

VI. APPLICATION CONSIDERATIONS

A. Airborne Motion Isolation System

1. Baseline Configuration

Comparison of the expected aircraft motion environment to the susceptibility of the sensor to this environment with servo controlled arm balancing has established a set of requirements for a motion isolation system. In addition, a need for some major sensor design changes from the current laboratory model has become evident. During the course of these preliminary investigations, several alternative isolation systems and sensor configurations have been conceived and briefly analyzed. As a result of these considerations an overall system concept has been developed which appears to provide the required sensor/isolation system performance goal of 1 E.U. sensitivity. The baseline mechanization is best illustrated by the building block concept shown in Figure 6-1.

The gravity gradient sensor(s) is supported by a very low friction air knuckle bearing joint that provides high frequency-small amplitude angular motion isolation. The knuckle joint is supported by a three-gimbal platform whose inner, inertially stabilized element provides the basic vertical and azimuth alignment reference. The knuckle platform is servocontrolled to follow only the long time average orientation of the three-gimbal platform stable element. The three-gimbal platform thus provides the gross, low frequency large amplitude angular isolation and stabilization, while the secondary knuckle bearing and servo provide the high frequency small amplitude-angular isolation.

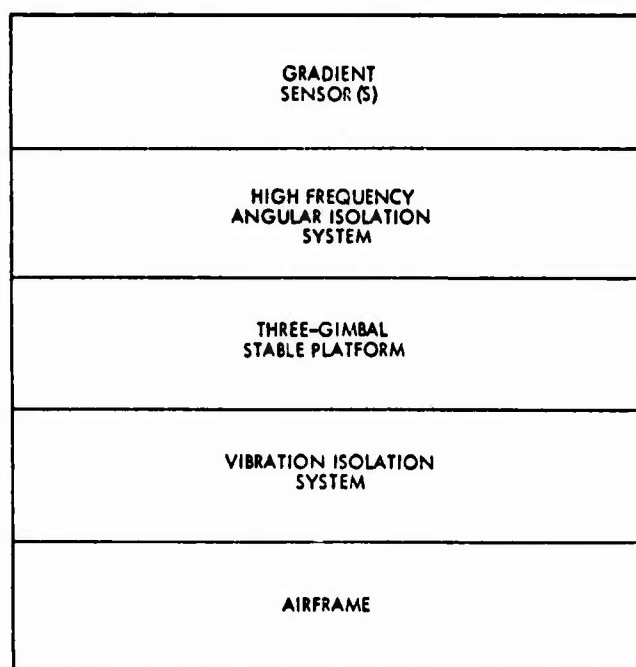


Figure 6-1. Baseline system mechanization building block concept.

The base of the three-gimbal platform is supported by a vibration isolation system. This component primarily provides the isolation of translational aircraft vibrations from the sensor, and secondarily provides a certain degree of angular vibration isolation, depending on the specific mechanization of this subsystem.

It should be pointed out that the baseline configuration is only one alternative of a number of possible designs. Design alternatives were the subject of a study performed for the petroleum industry. The conclusions of the petroleum report, as outlined on the last page, are still valid with one notable exception: it is now realized that sensor arm bending can be compensated for, in part, by sensor arm stretch. This new requirement is reflected in Section IV-D of this Report as a requirement for arm isoelasticity.

2. Inertial Platform Vendor Survey

A preliminary survey of a representative sample of inertial platform manufacture was conducted to ascertain the feasibility, availability, and approximate cost of the inertial platform portion of the baseline motion isolation system. The procurement specification used for this survey is included in Appendix B. The specification requested a bid on the three-gimbal platform portion of the baseline system and in addition requested quotes on any other system mechanization meeting the overall sensor system motion isolation requirements. Due to the preliminary and tentative nature of the request, replies were brief and limited. Table 6-1 summarizes the pertinent findings of the survey.

None of the inertial platform vendors queried proposed a system already in existence. It is highly probable that a development effort will be required to provide a platform meeting the stability and payload requirements for the three-sensor cluster.

For a single-sensor flight test evaluation program, it is possible that an existing inertial platform could be modified; however, the vibration isolation system and the knuckle bearing/servo system would have to be developed if the above described baseline configuration were selected.

TABLE 6-1. SUMMARY - PRELIMINARY INERTIAL
PLATFORM VENDOR SURVEY

Manufacturer	Response	System Configuration Proposed	Delivery	Cost Development of 1st Unit	Small Quan. Production	Comments
Aeroflex Laboratories, Inc.	Letter Only	Three Gimbal Platform Only.	No Estimate Received	\$300K	\$150K	Requires special development. Does not provide adequate long term level accuracy due to use of low-cost inertial components and analog computer.
Carco Electronics	Technical Proposal	Three gimbal platform, platform management computer, knuckle air bearing and servo, vibration isolation mount.	12 months ARO	\$475K	\$300K	Requires special development. Company has experience in spherical air bearings and gimbal systems, but little experience in inertial stabilization and navigation systems. Development cost estimate is probably low.
Koelsman Instrument Corp.	No Bid					
Xearfott Systems Div. Singer-Gen'l Precision Inc.	Letter Only	Instrument Navigation Platform and Management Computer only. No sensor mount capability.			\$75-80K	Quote not responsive since it does not provide for a sensor support and stabilization system.
Honeywell, Inc.	No Bid					
Northrop Corp., Electronics Div. Norwood, Mass.	Technical Proposal	Wide angular freedom spherical air bearing platform, platform management computer, and vibration isolation mount.	No Estimate Received	\$2700K (verbal reply)		Requires special development. Some analysis and design already completed. Would probably result in unusually large development effort and cost due to new mechanization approach. Unsolved problems of transmitting sensor spin motor power and sensor air bearing supply without inducing large disturbance torques when large platform angles exist. Proposed vibration isolation mount appears to be inadequate.

B. Mass Noise Effects

A preliminary study of the feasibility question of the proximity effects of the aircraft mass distribution on the desired measurements has been made. In the Air Force gravity survey application, a KC-135 aircraft is assumed as the carrying vehicle. In a previous study conducted by Hughes for an oil company consortium, a DC-3 aircraft was assumed as the carrying vehicle.

Results of this oil company study indicated that the influence of the aircraft proximate masses was of secondary importance compared to that of the sensor support system. Thus, the DC-3 study is reproduced here to illustrate that mass proximity effects must be considered but do not present a feasibility question.

DC-3 MODEL

A mass distribution model for the DC-3 has been assumed based on data provided by McDonnell Douglas. The sensor is assumed to be placed 6 inches above the cabin floor level centered 34.3 feet from the nose of the aircraft. An xyz coordinate system used throughout the analysis, is centered at this assumed sensor location as indicated in Figure 6-2. Except for discussions of aircraft heading (yaw) displacement, it is assumed that the sensor x-axis is aligned with the projection of the aircraft x-axis on a horizontal plane.

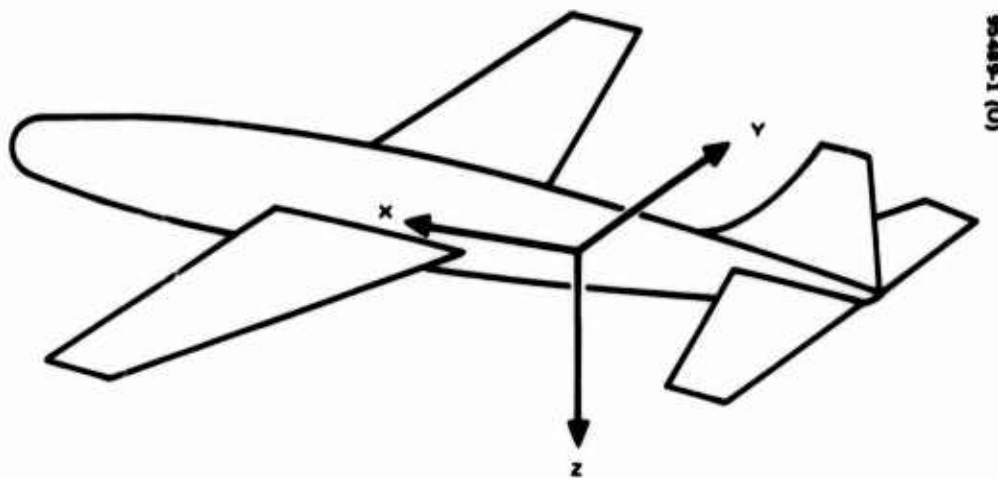


Figure 6-2. Coordinate System

The assumed mass distribution in terms of this coordinate system is presented in Table 6-2.

TABLE 6-2. DC-3 MASS DISTRIBUTION

Part	Total Weight, pounds	Assumed Distribution	Coordinates, feet
Tail + tail gear	700	Point mass	$x = -12$ $y = 0$ $z = -5$
Engines + landing gear (up)	6700	Two point masses (3350 pounds each)	$x = +18$ $y = \pm 8$ $z = +2$
Wings	3500	Line masses linearly decreasing from center	$x = +10$ $-50 < y < +50$ $z = +2$
Fuselage	1500	Uniform cylindrical shell	$-20 < x < +35$ $y = 0$ $z = +2$ } center
Floor + miscellaneous	500	10 uniform rods	$1.5 < x < 35$ $-20 < x < -1.5$ $y = -2, -1, 0, +1, -2$ $z = 0.5$
Fixed* equipment + crew	3600	Point mass	$x = +25$ $y = 0$ $z = -2$

* Assumes passenger seats, etc. have been removed and crew stationary.

FUEL MODEL

The fuel is stored in four tanks of 200 gallons each. There are two tanks in each wing, located between the fuselage and the thrust plane (see Figure 6-3).

The fuel in each tank is assumed to be represented by a point mass. However, because of fuel consumption, the masses decrease and change location. Assuming no sloshing, the values and locations of the point masses at various stage of fuel consumption are listed in Table 6-3.

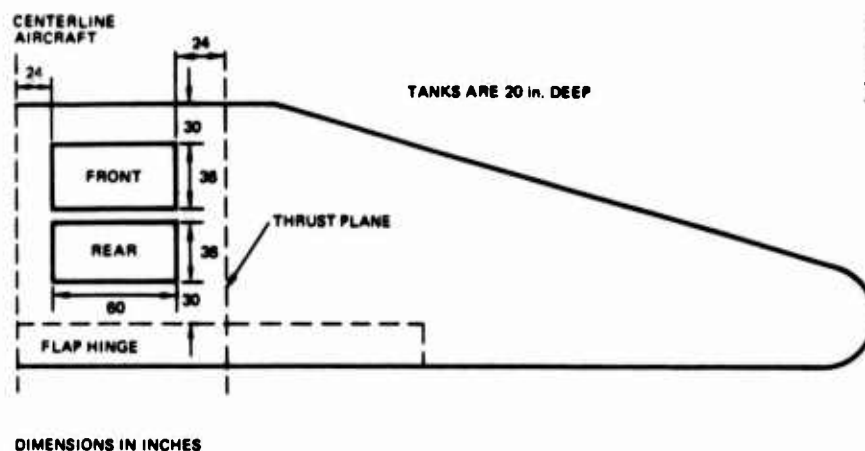


Figure 6-3. Location of Fuel Tanks

TABLE 6-3. FUEL MASS DISTRIBUTION

Fuel Status	Front Tanks		Rear Tanks	
	Mass pounds	Location, feet	Mass pounds	Location, feet
Full	2400	x = 15.5 y = ± 4.5 z = 2	2400	x = 13.5 y = ± 4.5 z = 2
3/4 full	2400	x = 15.5 y = ± 4.5 z = 2	1200	x = 13.5 y = ± 4.5 z = 2.5
1/2 full	2400	x = 15.5 y = ± 4.5 z = 2	0	—
1/4 full	1200	x = 15.5 y = ± 4.5 z = 2.5	0	—
Empty	0	—	0	—

INERTIAL PLATFORM MODEL

The gimbals of the inertial platform are an important consideration because of their proximity to the sensor (see Figure 6-4). The three gimbals are assumed to be square line masses. The dimensions and total masses of each gimbal have been postulated as follows:

<u>Gimbals</u>	<u>Size, inches</u>	<u>Mass, pounds</u>
Inner	20	25
Middle	24	35
Outer	28	50

The gimbals were assumed to be in the xy plane at $z = +1$ foot. Ideally, the gimbals could be assumed to be centered at the sensor. However, the effects of being off center were also investigated.

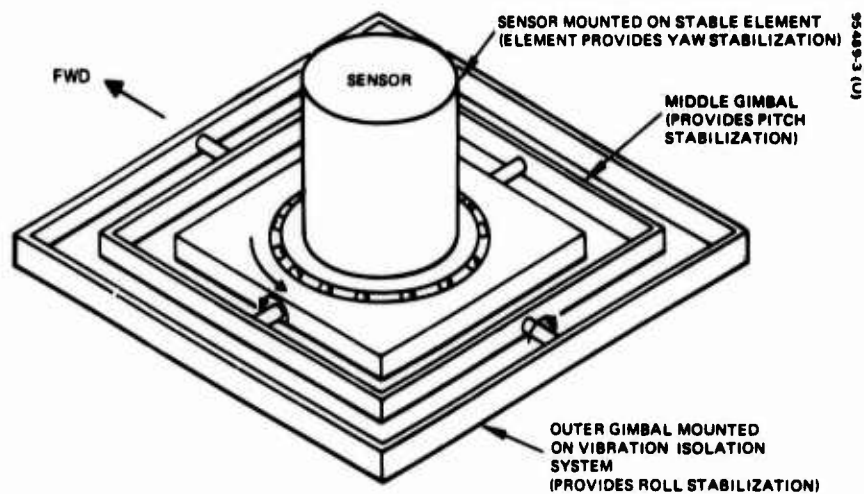


Figure 6-4. Inertial Platform

GRAVITY GRADIENT

An increment of gravity potential resulting from an increment of mass at a point x, y, z is given by

$$d\phi = - \frac{G dM(x, y, z)}{(x^2 + y^2 + z^2)^{1/2}}$$

where

$$G = 34.4 \times 10^{-9} \text{ ft}^4/\text{lb-sec}^4$$

$$dM(x, y, z) = \text{increment of mass at } x, y, z$$

$$(x^2 + y^2 + z^2)^{1/2} = \text{distance from sensor to } dM$$

The second-order gradient of the gravitational potential of an increment of mass is given by the tensor

$$\begin{bmatrix} \frac{\partial^2 d\varphi}{\partial x^2} & \frac{\partial^2 d\varphi}{\partial x \partial y} & \frac{\partial^2 d\varphi}{\partial x \partial z} \\ \frac{\partial^2 d\varphi}{\partial y \partial x} & \frac{\partial^2 d\varphi}{\partial y^2} & \frac{\partial^2 d\varphi}{\partial y \partial z} \\ \frac{\partial^2 d\varphi}{\partial z \partial x} & \frac{\partial^2 d\varphi}{\partial z \partial y} & \frac{\partial^2 d\varphi}{\partial z^2} \end{bmatrix}$$

where

$$\frac{\partial^2 d\varphi}{\partial u \partial v} = d\Gamma_{uv}$$

These increments of gravity gradient can be integrated over the various mass distributions to determine the total gradient produced by the entire mass of interest. In the case of a point mass, no integration is necessary. Thus, for a point mass, the gravity potential function is:

$$\varphi = - \frac{GM}{(x^2 + y^2 + z^2)^{1/2}}$$

and the corresponding second-order gradients are:

$$\Gamma_{xx} = \frac{\partial^2 \phi}{\partial x^2} = GM \left[\frac{1}{(x^2 + y^2 + z^2)^{3/2}} - \frac{3x^2}{(x^2 + y^2 + z^2)^{5/2}} \right]$$

The other gradients can be expressed in a similar manner.

In the case of the distributed masses, a computer program was written to perform the necessary integrations.

The gravity gradients resulting from the DC-3 mass distribution (Table 6-2) for a straight and level flight, are listed in Table 6-4. The gravity gradients measured by a single sensor oriented with its spin axis aligned in either the x, y, or z directions are indicated in the table, and in all subsequent tables in this section.

TABLE 6-4. AIRCRAFT STRUCTURE FIXED MASS EFFECTS, EU

Part	y Spin Axis Orientation		z Spin Axis Orientation		x Spin Axis Orientation	
	$\Gamma_{xx} - \Gamma_{zz}^*$	Γ_{xz}	$\Gamma_{xx} - \Gamma_{yy}^*$	Γ_{xy}	$\Gamma_{yy} - \Gamma_{zz}^*$	Γ_{yz}
Tail + gear	- 0.76	-0.36	- 0.9	0	0.15	0
Engines and gear (up)	- 2.25	-0.23	- 1.83	0	-0.42	0
Wings	- 1.94	-0.4	- 1.73	0	-0.21	0
Fuselage	- 0.81	Negligible	- 0.03	0	-0.84	0
Floor + miscellaneous	- 7.03	Negligible	- 5.95	0	-1.08	0
Fixed equipment + crew	- 0.75	0.03	- 0.75	0	Negligible	0
Totals	-13.54	-0.96	-11.19	0	-2.40	0

*The gradients are tabulated as differences because these are the actual quantities measured by the sensors.

Since signals as small as 1 EU are to be sensed, the values found in Table 2-3 indicate the need for sensor compensation to account for the effects of aircraft mass.

In Table 6-5, the gradients caused by the fuel at various levels of consumption for straight and level flight are listed.

TABLE 6-5. GRADIENTS CAUSED BY FUEL, EU

Fuel Status	$\Gamma_{xx} - \Gamma_{zz}$	Γ_{xz}	$\Gamma_{xx} - \Gamma_{yy}$	Γ_{xy}	$\Gamma_{yy} - \Gamma_{zz}$	Γ_{yz}
Full	-4.25	-0.64	-3.88	0	-0.37	0
3/4 full	-2.92	-0.46	-2.70	0	-0.22	0
1/2 full	-1.62	-0.21	-1.52	0	-0.10	0
1/4 full	-0.81	-0.128	-0.76	0	-0.05	0
Empty	0	0	0	0	0	0

These results indicate that compensation for fuel mass is also necessary and, in addition, the compensation must be made a function of fuel level. Table 6-5 illustrates that some of the terms could change by as much as 4 EU if the entire fuel load was consumed during a flight.

Table 6-6 shows the gravity gradient effects of the inertial platform gimbals. Both centered and off-centered conditions are considered.

This table indicates the necessity for compensating the gimbal gravity gradient effects. These quantities grow rapidly as the mounting location of the sensor approaches the plane of the gimbals. For $z = 0$ and the sensor off center, the gravity gradients are tabulated in Table 6-6C which illustrates this trend. A more accurate and detailed study of the gimbal mass effects should be conducted when a more detailed specification of the three-gimbaled platform becomes available.

TABLE 6-6. GRAVITY GRADIENT EFFECTS
OF PLATFORM GIMBALS, EU

Gimbal	$\Gamma_{xx} - \Gamma_{zz}$	Γ_{xz}	$\Gamma_{xx} - \Gamma_{yy}$	Γ_{xy}	$\Gamma_{yy} - \Gamma_{zz}$	Γ_{yz}
A. Sensor Centered in x and y with z = 12 inches						
Inner	9.2	0	0	0	9.2	0
Middle	5.4	0	0	0	5.4	0
Outer	2.1	0	0	0	2.1	0
B. Sensor Off-Center by 4 inches along x and y Axis and 12 inches along z Axis						
Inner	12.54	-0.06	0	0.32	12.54	-0.06
Middle	9.2	-1.23	0	0.45	9.2	-1.23
Outer	5.6	-2.1	0	0.55	5.6	-2.1
C. Sensor Off-Center by 4 inches along x and y with z = 0						
Inner	-88	0	0	6.9	-88	0
Middle	-60	0	0	3.65	-60	0
Outer	-48	0	0	2.34	-48	0

SENSITIVITY TO ROLL, PITCH, AND YAW

Since calibration of the nominal gravity gradient effects of the DC-3 masses has been shown to be necessary, the next question that arises is that of the sensitivity of the effects to roll, pitch, and yaw. Table 6-7 presents the effects attributed to the DC-3 fixed mass distribution caused by roll, pitch, and yaw of ± 10 degrees each. These results for ± 10 degrees of roll, pitch, and yaw indicate that some compensation for DC-3 structural masses in terms of aircraft pitch and yaw may be desirable. Roll effects are negligible.

Roll, pitch, and yaw will also affect the gimbal compensations since the gimbals will move about the stabilized sensor. The effects are summarized in Table 6-8 for the off-centered sensor cases of being above the plane of the gimbals and being located in the plane of the gimbals.

TABLE 6-7. EFFECT OF AIRCRAFT MASS - GRADIENT CHANGES
CAUSED BY 10 DEGREE ATTITUDE AND HEADING CHANGES, EU

Part	Rotation Angle	$\Delta[\Gamma_{xx} - \Gamma_{zz}]$	$\Delta\Gamma_{xz}$	$\Delta[\Gamma_{xx} - \Gamma_{yy}]$	$\Delta\Gamma_{xy}$	$\Delta[\Gamma_{yy} - \Gamma_{zz}]$	$\Delta\Gamma_{yz}$
Tail + gear	Roll	-	-	-	-0.04	-0.01	0.03
	Pitch	0.36	0.18	0.18	-	0.18	-
	Yaw	0.03	-	0.04	0.144	-0.03	0.06
Engines + gear (up)	Roll	0.01	-	-0.01	-0.04	0.02	0.07
	Pitch	0.27	0.38	0.13	-	0.13	-
	Yaw	0.05	-	0.1	0.31	-0.05	0.04
Wings	Roll	0.005	0.005	-0.005	-0.07	0.01	0.03
	Pitch	0.38	0.32	0.18	-	0.18	-
	Yaw	0.05	0.005	0.09	0.29	-0.05	0.07
Fuselage	Roll	0.025	-	-0.025	-	0.05	0.15
	Pitch	0.05	0.15	0.025	-	0.025	-
	Yaw	-	-	-	-	-	-
Floor + miscellaneous	Roll	0.03	-	-0.03	-	0.06	0.16
	Pitch	0.4	1.2	0.2	-	0.2	-
	Yaw	0.16	-	0.32	1.0	-0.16	-
Fixed equipment + crew	Roll	-	-	-	-	-	-
	Pitch	0.06	0.12	0.03	-	0.03	-
	Yaw	0.02	-	0.04	0.12	0.02	-
Totals	Roll	0.045	0.005	-0.045	-0.15	0.08	0.29
	Pitch	1.47	2.20	0.72	-	0.72	-
	Yaw	0.31	0.005	0.59	1.86	-0.27	0.17

TABLE 6-8. EFFECT OF GIMBAL MASS - GRADIENT CHANGES
CAUSED BY ATTITUDE AND HEADING CHANGES

Rotation Angle	$\Delta[\Gamma_{xx} - \Gamma_{zz}]$	$\Delta\Gamma_{xz}$	$\Delta[\Gamma_{xx} - \Gamma_{yy}]$	$\Delta\Gamma_{xy}$	$\Delta[\Gamma_{yy} - \Gamma_{zz}]$	$\Delta\Gamma_{yz}$
Sensor Offset 4 inches in x and y and 12 inches in z						
Roll*	-0.83	0.115	0.83	-0.35	-1.67	1.1
Pitch**	-3.06	2.68	1.0	-0.5	-1.6	0.32
Yaw***	-0.44	0.27	0.88	-0.05	-0.44	0.27
Sensor Offset 4 inches in x and y only						
Roll*	1.33	0.37	-1.33	0.04	2.67	8
Pitch**	6.00	18.00	3.0	0.10	3.00	1
Yaw***	4.3	0	8.6	0.8	4.3	0

*Only the outer gimbal rotates relative to the sensor.

**Both outer and middle gimbals rotate relative to the sensor.

*** All three gimbals rotate relative to the sensor.

The magnitude of these gradient changes is about the same as those for DC-3 structural masses. Therefore, some compensating function of roll, pitch and yaw is desirable. Note that if the sensor center is closer than 12 inches from the plane of the gimbals, these effects increase rapidly and an accurate compensation scheme would be necessary.

Fuel sloshing effects, caused by roll, pitch, and yaw motion when the tanks are partially full, had been considered a potential mass noise problem. However, as shown in Table 6-9, sloshing effects can be ignored. Even the gradient changes caused by roll, pitch, and yaw when the tanks are full are small and require only crude compensation. This low sensitivity to fuel mass effects is a result of the relatively large distance (approximately 14 feet) between the sensor and the fuel tanks.

TABLE 6-9. GRAVITY GRADIENT CHANGES
CAUSED BY FUEL SLOSH, EU

Tanks	Sloshing	Rotation Angle	$\Delta[\Gamma_{xx}-\Gamma_{zz}]$	$\Delta\Gamma_{xz}$	$\Delta[\Gamma_{xx}-\Gamma_{yy}]$	$\Delta\Gamma_{xy}$	$\Delta[\Gamma_{yy}-\Gamma_{zz}]$	$\Delta\Gamma_{yz}$
Front full	No sloshing	Roll	-	0.003	-	0.035	-	0.016
		Pitch	0.23	0.28	0.12	0	0.12	0
		Yaw	0.045	-	0.09	0.25	0.045	0.035
Front half full	Slosh to rear	-	-0.08	0.002	-0.06	-	0.02	-
	Slosh to side	-	-0.04	0.008	-0.03	0.035	0.01	0.0075
Rear full	No sloshing	Roll	-0.0075	0.006	-0.0075	0.07	-0.015	0.045
		Pitch	0.425	0.464	0.212	0	0.212	0
		Yaw	0.066	0.006	0.132	0.396	0.066	0.07
Rear half full	Slosh to rear	-	-0.09	0.006	-0.045	-	0.045	-
	Slosh to side	-	-0.02	0.03	0.004	0.05	-0.02	0.008

SENSITIVITY TO HEADING

In the preceding analysis, it was assumed that the platform x, y, z coordinate system was aligned with the aircraft body x, y, z directions. However, as a survey pattern is flown which requires 90, 180, and 270 degree headings, the compensation schemes must reflect this function of heading. Table 6-10 shows the sensitivities of the sensed gravity gradients for changes in headings of 90 and 180 degrees.

TABLE 6-10. EFFECT OF HEADING CHANGE
Gravity Gradient Change from 0 Degrees Heading, EU

	Heading, degrees	$\Delta[\Gamma_{xx} - \Gamma_{zz}]$	$\Delta\Gamma_{xz}$	$\Delta[\Gamma_{xx} - \Gamma_{yy}]$	$\Delta\Gamma_{xy}$	$\Delta[\Gamma_{yy} - \Gamma_{zz}]$	$\Delta\Gamma_{yz}$
DC-3 structural masses	90	11.19	0.96	22.38	0	-11.19	0.96
	180	0	1.92	0	0	0	0
Full fuel	90	3.86	0.64	7.72	0	-3.86	0.64
	180	0	1.28	0	0	0	0
Gimbals* off center, z = 1	90	0	3.39	0	-2.64	0	3.39
	180	0	6.78	0	0	0	0
Totals	90	15.05	4.99	30.1	-2.64	-15.05	4.99
	180	0	9.98	0	0	0	0

*The symmetry assumed for the gimbals makes these results optimistic.

EFFECT OF PERSONNEL PROXIMITY

The worst-case gravity gradient caused by the proximate mass of a 200-pound man has been calculated to demonstrate how far away operating personnel must be situated when gradient readings, accurate to 1 EU, are being recorded by the gradiometer. Alternatively, the operator can be stationed at a fixed position with limited movement, and a calibration applied to the result.

The maximum gradient is given by

$$\Gamma = \frac{2 G M}{R^3}$$

Using ft/lb-sec units

$$G = 34.4 \times 10^{-9} \text{ ft}^4/\text{lb-sec}^4$$

$$M = \text{Mass} = \frac{200 \text{ lb}}{32.2} = 6.2 \text{ slugs (simulating the man by a point mass for simplicity)}$$

$$R = \text{distance in feet to gradiometer of mass } M.$$

The following tabulation illustrates the gravity gradient produced by a 200-pound man at various distances from the sensor:

R, feet	2	4	8	12	16
Γ (EU)	53.3	6.66	0.832	0.247	0.104

It is desirable to keep the unknown errors down to 0.1 EU because an rms summation of all the errors should be less than 1 EU. Consequently, it can be seen that it will be desirable to keep the operator 16 feet or more away from the gradiometer unless he were severely restricted in his body motions.

Since the slope $\frac{\partial \Gamma}{\partial R}$ is so high, even at 8 feet (0.62 EU/ft), it seems impractical to have the operator close enough to the instrument to make adjustments except between the taking of calibration points on the ground. There will be times during flight, such as the turnaround following a data-taking run, when the operator can approach, check, or adjust the instrument if this should prove desirable.

MASS NOISE EFFECTS CONCLUSIONS

- 1) The structural masses of the DC-3 contribute nominal gravity gradient "noise" as large as 13 EU; therefore, compensation must be provided to detect signals as small as 1 EU.
- 2) Pitch and yaw rotations of 10 degrees cause changes in the DC-3 structural mass fixed-nominal gravity gradient as large as 2 EU. Compensation is required.
- 3) The mass of a full load of fuel contributes gravity gradients as large as 4 EU. Hence, nominal compensation must be provided. Clearly, these effects decrease to zero as fuel is consumed. Thus, it is also necessary to make this compensation as a function of fuel quantity.
- 4) Changes in gravity gradient contributed by the fuel caused by roll, pitch, and yaw, and fuel sloshing are negligible.
- 5) The nominal gravity gradient effects caused by gimbals could be quite large (200 EU), depending on their position relative to the sensor.
- 6) Roll, pitch, and yaw could cause changes in gravity gradients contributed by the gimbals as large as 20 EU.
- 7) Proximity and motion of personnel within the aircraft must be severely restricted while the sensor is in use or is being calibrated.
- 8) Since roll, pitch, and yaw will cause significant changes in the gravity gradients compensation is required as a function of these rotation angles. Measurement of these angles to 0.1 degree accuracy is required and can be accomplished without difficulty.

- 9) A calibration procedure will be necessary to determine the exact compensation required for roll, pitch, and heading (as well as simultaneous combinations thereof) and fuel consumption. This procedure must be conducted using the actual aircraft with the sensor, stable platform, and all other system-related equipment mounted in place and operating.

VII. SUMMARY AND CONCLUSIONS

This Section of the Final Report is written in four parts:

- A. Sensor Error Sources
- B. Laboratory Development Summary
- C. Operational System Considerations
- D. Conclusions

The purpose of this Section VII is to provide the reader with an overview of the work performed for AFCRL under the subject contract; it both summarizes and discusses conclusions.

The reader will note that great detail is devoted in this Report to sensor problems (error sources). Such detail is meant to illustrate the breadth of knowledge gained during the conduct of the contract. Detailed problem explication must not be confused with the important overall conclusion that the hard bearing concept is both feasible and practical. Thus, a moving base gradiometer appears achievable and practical using the rotating, torsionally-resonant sensor configuration to measure and phase detect the strength and direction of a gradient field.

A. Sensor Error Sources

Any second order gradient sensor responds to both gravitational and inertial force gradients. When the sensor is used for the purpose of measuring gravitational force gradients, care must be exercised to limit, or compensate for, any inertial force gradients present, since they would appear as errors in the measurement of the desired quantity. In a practically realizable sensor, additional error sources are introduced due to mechanical construction tolerances as well as inherent sensitivity to other inputs such as thermal noise and gradients, electromagnetic radiation, etc.

Because the Hughes torsionally-resonant gradiometer is rotated (at a rotation frequency ω), it is an a.c. device. Hence, only inputs to the sensor which modulate its output at 2ω , (the torsional resonant frequency or the gradient sensing frequency), appear in the output of the demodulated signal.

1. Inherent Angular Rate Sensitivity

Inertial force gradients occur as a result of precessional rates of the sensor's spin-axis. The sensor's output is proportional to the square of the angular rate normal to its spin-axis. Thus, the sensor must be operated in such a way as to limit these angular rates to tolerable magnitudes. Alternatively, these angular rates may be sensed and used to compensate the sensor's output.

2. Mechanization Related Errors

Although an "ideal" gradiometer is not sensitive to accelerations, all practically realizable designs do have some acceleration sensitivity due to various mechanical unbalances in the instrument due to tolerance accumulation.

The critical acceleration sensitivities of the Hughes sensor are generated as follows:

a. Angular Acceleration Sensitivity

The sensor can respond to inertial angular accelerations about its spin-axis if they occur at the 2ω torsional resonant frequency. The sensitivity of a given sensor to this input is dependent upon its sum-mode mismatch. Sum-mode mismatch refers to the amount by which the ratio of each arm's mass moment of inertia to end pivot torsional spring rate differ. (See pages IV-29 V-10)

b. Translational Acceleration Sensitivity

The sensor can respond to certain translational acceleration inputs. Again, due to the a.c. nature of the device, translational vibrations occurring at frequencies of ω or 3ω can result in a signal output at 2ω . Its sensitivity to these vibration inputs is dependent upon its arm mass unbalance difference, i. e., the vector difference between each arm's mass center. (See page V-10).

A second mechanism which results in sensitivity to translational accelerations is arm anisoelasticity. Arm anisoelasticity results if the arm's bending stiffness differs from its axial stiffness. This effect results in a sensor 2ω output which is proportional to the square of the applied acceleration. Hence, due to arm anisoelasticity, constant as well as oscillatory accelerations can cause a sensor output. The sensor arms can be designed to be isoelastic, however, construction tolerances will result in slightly anisoelastic properties. (See page IV-29).

A third mechanism resulting in sensor response to translational acceleration is torsional coupling non-uniformity. This effect would be maximum in a horizontal spin-axis orientation. The torsional pivot is nominally insensitive to loads or end moments normal to its torsional axis. However, it can have a second order sensitivity to such loadings. If the pivot sensitivity to such loadings varies two times per revolution, an erroneous 2ω signal would be generated in the sensor output.

c. Other Environment-Related Errors

If the gradiometer is to be used to measure gravitational force gradients, care must be taken to assume that the gravitational force gradients of interest are separated from those caused by the carrying vehicle. For example, motion of the stabilization system support gimbals creates a change in the gravity force field thus causing a change in sensor response. These effects, referred to as "mass noise", must be calibrated and appropriately used to compensate the sensor's output.

Other effects which may result in erroneous sensor outputs include:

- thermal noise in the sensor arms as well as in the signal processing and transmission system
- sensitivity to electromagnetic radiation
- sensitivity to acoustic noise

B. Laboratory Development Summary

The experimental portion of this development program was directed toward the assembly and test of a breadboard model gradiometer. The goal was to achieve a hard bearing sensor capable of accurately detecting gravity gradients in the laboratory environment.

Significant factors were learned during the course of the contract. These discoveries helped to explain the difficulty in achieving a low level of noise. Accordingly, much is now known as to the contribution of the component parts to the total noise output of the sensor. Although noise sources can not be completely separated at this time, the most significant contributors have been determined. Methods of correcting and/or compensating these sources are described in this Report.

One measure of the empirical progress gained during this program may be illustrated by examining the reductions achieved in coherent and incoherent noise levels. Thus, during the past ten months, coherent noise was reduced from 100,000 E.U. to 5,000 E.U. and random (incoherent) noise, measured over a ten second integrating time, was reduced from 10,000 E.U. to approximately 900 to 1000 E.U.

1. Sensor Design

The sensor used as the laboratory breadboard model went through several modifications, with the basic goal of providing improvements in arm and inertia balance capability (sensitivity to these unbalances is discussed in Section IV-A and V-B) and in providing an integral structure that could be balanced after assembly in the operational configuration.

Important points of the initial design were:

- a. Spuds on the arms fit into eccentric holes in the end masses. This mounting arrangement enabled rotation of the end masses to provide coarse balance adjustments.
- b. One arm-to-case torsion pivot was designed with an adjustable collet type clamping device to allow adjustment in the torsional spring constant and provide some compensation for initial sum mode mismatch (see discussion under Section V-B-2).
- c. Adjustment screw balance weights were provided for fine mass and inertia balancing.

- d. A balancing fixture was designed which was used to balance each arm individually by providing linear vibrational inputs to the sensor arm supports. This method proved to be ineffective in providing balance capability because the fixture could not prevent the cross-coupling between linear and angular accelerations. This cross coupling varied in quantity every time a change was effected on the sensor arm center of mass.
- e. Rotor balance was accomplished by static balancing of each component as it was added to the air bearing. No attempt was made at that time to correct for dynamic unbalance.

Arm balancing on the initial design proved very difficult and balancing results were uncertain. Vibration generated by dynamic unbalance and resonant modes of the support structure generated large quantities of coherent and incoherent noise signals through the mechanisms of arm mass and inertia unbalance. Rebalancing of the sensor arms was difficult as it required complete disassembly and reassembly each time it was attempted.

The first modification made on the sensor design was to revise the arm balancing method. This revision included the following: 1) The eccentric mass type of coarse balancing was eliminated as it added more adjustment than was needed and augmented unbalance rather than aiding its correction. The use of the vibrating balance fixture was deleted and the sensor was thereafter balanced on knife edges. 2) The collet clamping device had been questionable in its clamping reliability and was modified to take a better "bite" on the adjustable torsion spring.

Tests on this first modification showed reduction in the coherent noise by a factor of 2 to 3.

The collet clamping device was still providing reliability problems and did not exhibit the fineness of adjustment in providing the "sum-mode match" required. "Sum mode match" (or mismatch) would vary as torque on the collet nut was increased and a precise match could not be attained.

It was decided to provide a more comprehensive redesign of the sensor which would retain the knife edge mass balance methods and provide non-adjustable torsion springs thereby eliminating the need for the collet.

"Sum mode mismatch" errors then were corrected by arm inertia adjustment using signals generated by driving the sensor in a oscillatory mode.

At this time it was also discovered that, because of its geometry, the central flexure pivot was contributing to the arm unbalance problem by adding half of its dynamic unbalance to each arm as a direct differential arm unbalance. Compensating balance weights were added to the sensor to correct this problem.

This new sensor design provided much more consistent balance data than had been obtained before and led to an estimate of differential arm mass unbalance to be approximately .01% (.0002 inch) and sum mode mismatch to be approximately 2%.

The final improvement in the sensor assembly technique was improving dynamic unbalance and obtaining a measurable dynamic unbalance motion, at operating speed, of 10^{-5} inches by use of a dynamic balancing machine.

This attainment of dynamic balance reduced this coherent noise due to elliptical coning of the sensor spin axis by a factor of approximately 6.

2. Electronics

The data readout electronics originally designed for the sensor have required only minor modifications throughout the program. Because of the high noise levels, several stages of gain were bypassed in the preamplifier circuit. This increased the noise of the sensor readout electronics to between 10 and 50 E. U. (still well below the level of the sensor incoherent noise output). Early in the program the electronics scale factor proved to be sensitive to light, heat and static charge, but minor circuit adjustments alleviated these sensitivity problems.

3. Speed Control

a. Servo System

The speed control system did not come under close scrutiny until near the end of the contract. Basically, a lack of proper speed control can result in error signals being produced. Because of sum mode mismatch, the sensor responds to oscillatory angular accelerations occurring at or near the 2ω (torsional resonant) frequency. (See Section IV-A and Section V-B).

Initially, speed control was provided by a magnetic servo controlled clutch which attenuated torsional noise inputs to the sensor.

Use of a special flexible elastomeric torsional coupling connecting the motor shaft directly to the air bearing significantly reduced

incoherent noise transmission into the sensor but presented a speed control problem. It was then deemed necessary to develop a drive system that would eliminate rolling element bearings. Replacement of the original synchronous motor drive and magnetic clutch with a specially designed asynchronous eddy-current drive motor and servo eliminated these two sources of rolling element bearing noise.

Another speed control problem has only just recently been appreciated. Small second harmonic variations on the speed pickoff disk for example can generate significant coherent noise output. This effect has recently been demonstrated in the laboratory where gain adjustments made in the servo-control system reduced the coherent noise level by a large factor, approximately 40. Operation with a single pickoff pulse per revolution, rather than 10, provided an additional coherent noise reduction effect.

Additional speed variations can occur due to winding assymetry in the motor or random noise on the drive motor power amplifier outputs. These effects have not been studied quantitatively as yet.

b. Air Bearing

The effect of air bearing characteristics on speed-torque control is the latest subject to be investigated in detail.

The air bearing used on the sensor system was not designed for this specific application. It was chosen on the basis of availability and reasonable cost. Certain design aspects of the bearing are very suitable to our requirements. For example, the bearing air duct design eliminates any residual bearing torques while the sensor is not rotating.

However, requirements on drag torque, operating pressure; race ellipticity, air flow etc. were not specified for this particular application.

Two bearings of the same type were used interchangeably; they demonstrated a significant difference in coherent noise level. The second bearing provided intrinsically lower coherent noise generation (by approximately a factor of four). However incoherent (random) noise did not appear to be different between the two bearings. Operating pressure affected both coherent and incoherent noise levels but the effect was not too consistent between repeated tests.

Recent analysis (Section V-B-2) demonstrates that specifications on drag torque, operating pressure, rotation speed, air flow rate, ellipticity, and stiffness will have an appreciable effect on reducing the torque noise output generated by the bearing. Signal variation of less than 0.4 E. U. can be anticipated by simple modifications (See page V-18). Reduction in the effect of these noise sources can also

be accomplished by additional reduction in sensor "sum mode mismatch." It is expected that the servo arm balance system discussed in Section IV-D will be used to provide arm inertia corrections as well as arm mass balance control thereby reducing sum mode mismatch.

c. Windage

Windage effects have not been detected at present operating noise levels. However it is anticipated that these effects would have become significant somewhere below the 500 E. U. noise level with the current level of sum mode mismatch. In the future, provision will be made to provide arm-inertia balancing to reduce all the sum mode mismatch errors of the type discussed on page V-10, including windage. In addition, a co-rotating windage shield will be considered in the design of the next instrument.

4. Supporting Structure

Two diametrically opposite approaches have been taken on the design of a supporting structure for the laboratory sensor.

By mounting the sensor bearing structure solidly to the ground, the problems of angular rate input into the sensor are eliminated. However, ground vibrations can produce spurious noise signals acting through mass and inertia unbalances. Isolating the bearing structure from the ground provides reduction of ground noise, but allows air currents to generate cross axis angular rates. Both methods have been used with the isolated support method providing the lower noise level. (This system is shown in Fig. 5-5) When this system was mounted on a vibration isolation table, which provided an additional stage of ground noise isolation, the sensor noise level was not further reduced. This indicates that the latex tubing isolation system is reducing ground vibration noise to levels below other noise sources. However, this system did not provide complete angular rate isolation. Simple shielding by a wind screen structure about the isolated sensor system resulted in no further reduction of the existing noise levels. Therefore, it is concluded the noise generated by air currents in the room must be below the noise level due to other sources.

C. Operational System Considerations

The environment which exists during laboratory testing and demonstration of the sensor is much less severe than that expected in any of the earth-bound moving base applications. A requirement will exist, in most applications, for operation of three orthogonally mounted sensors. It has, therefore, become necessary to consider the requirements imposed on the overall moving base gradiometer system as they affect: 1) sensor design, 2) sensor supporting system design, and 3) data compensation, interpretation, and processing techniques. At this point in the development of a moving base gradiometer system, differences in design requirements imposed by the several different moving base applications have not been discriminated.

1. Sensor Attitude Stabilization

The gravity gradient data measured by a three sensor cluster must be referenced to some geodetic level reference. The angular position accuracy requirements developed in Section IV-B dictate that this reference must be established, in the moving base application, through use of an inertially stabilized platform. A suitably sized three gimbal stabilized platform would support the three-sensor cluster.

The sensed gravity gradient data must also be referred to a geodetic position reference. Various possible implementations exist which complement the implementation of the attitude stabilization system.

- a. The sensor support platform could utilize the required high precision inertial sensors and thus serve as the primary geodetic position reference.
- b. Lesser quality inertial sensors could be used to stabilize the sensor support platform with the primary geodetic position reference being supplied by a separate high quality inertial navigator. In this case, the position outputs of the separate inertial navigator would be used to compensate for long term drift errors of the sensor attitude stabilization system.

2. Angular Rate Isolation

The foregoing attitude stabilization techniques will provide a large amount of angular rate isolation. However, conventional inertial platforms (using ball type gimbal bearings) will not provide sufficient isolation to reduce gradiometer angular rate noise outputs to levels below 1 E.U. There is, therefore, a requirement in an operational system to include additional angular rate isolation. Several techniques have been considered:

- a. The three-sensor cluster would be supported by a low-friction three-axis knuckle bearing which in turn would be mounted to the stabilized element of the three gimbal platform. The upper knuckle platform then would be servo controlled to follow the long time average orientation of the three gimbal platform. The low-friction coupling would provide the required small amplitude, high frequency isolation.
- b. Use of a specially developed three-axis attitude stabilization platform utilizing low friction bearings.
- c. Provide inherent angular rate isolation within the basic sensor element itself. A spherical bearing sensor configuration has been given some preliminary consideration.

Because the attitude stabilization system will probably be mechanized to provide locally level orientation, inertial angular rates proportional to earth's rate, plus a vehicle transport rate, will be introduced into the sensor. Provision will therefore have to be made to compensate the sensor output for this effect.

The angular stabilization and isolation problem is discussed in detail in Sections IV-B, IV-C, VI-A, and VII-D.

3. Vibration Isolation and Sensor Arm Balance

As stated in VII-A, the sensor will respond to translational vibrations normal to its spin-axis occurring at ω and 3ω only. In addition, it will respond to angular acceleration about its spin-axis occurring at 2ω . The extent to which the sensor responds to these inputs is governed by the magnitude of the motion inputs and by the amount of arm mass unbalance and sum-mode mismatch that exists. Because of the extreme sensitivity of the sensor to such inputs, it is necessary to both reduce the magnitude of these inputs to the sensor and to de-sensitize the sensor's response thereto.

One precision balancing system has been devised which is capable of providing both arm mass balance control and sum-mode mismatch control. A description of this system is contained in Section IV-D. Alternate implementations of such a precision balancing system have been suggested.

Isolation of translational vibration inputs has been studied in some detail. A broadband isolation system supporting the entire three sensor-cluster and three gimbal platform is discussed in Appendix A. Such a system is relatively simple to mechanize and can provide an attenuation of 100 at the 1ω sensor frequency, with larger attenuation at higher frequencies. It can also provide significant attenuation of angular vibration inputs to the three gimbal platforms. More sophisticated vibration isolation techniques utilizing an active feedback servo control could be designed to provide additional attenuation if necessary. (See Appendix A)

As stated above, minimization of spin-axis angular acceleration inputs is also required. As stated in Section VII-B, three sources of angular acceleration noise which occur in the lab environment are: (1) drive motor and speed control servo noise, 2) sensor spin-axis support bearing noise, and 3) windage noise. In the moving base application, an additional noise source is introduced or magnified via the speed control servo. Angular acceleration of the sensor support, to which the speed reference photocell is attached, will appear as a driving function to the speed control servo. The magnitude of these accelerations, as well as the extent to which the sensor can be desensitized to such accelerations, will determine the severity of this problem. Techniques are available, such as providing acceleration compensation to the servo and arm inertia balance techniques to minimize this error source.

4. Isoelasticity

The system requirement of measuring all of the tensor components of the gradient field implies mechanization of a system of three orthogonal gradiometers. It is therefore impossible to maintain a vertical spin axis for all three sensors. Analysis has shown that the gradiometer has a " g^2 " sensitivity due to compliance of the arms. The magnitude of this problem is no longer negligible with horizontal spin axis operation. This problem has been analyzed and design solutions are discussed in Section IV-D. The results of this design study are that the " g^2 " sensitivity of a horizontal spin axis sensor can be overcome by design of an isoelastic arm combined with a relatively precise knowledge of the acceleration environment.

A similar type of sensitivity is generated by non-uniformity of the sensor torsional couplings. This is discussed on page VII-3 and is mentioned here because the problem only becomes significant when the sensor operates in a non-vertical spin axis orientation.

5. Scale Factor and Bias Errors

Equally important are two other performance parameters of the sensor, i. e., its bias stability and its scale factor stability. These parameters become significantly important in applications of the sensor requiring timewise integration of its outputs over long periods. In some applications, long term drift errors of the sensor can be compensated. Several compensation techniques exist, e. g.: comparison of the integrated sensor output with (1) a gravimeter carried on the vehicle, (2) known gravity check points, and (3) correlation with cross traverse gradiometer surveys, etc.

Preliminary system application studies should be carried out to better define the bias and scale factor stability requirements to be imposed on the sensor.

6. Mass Noise

Any systems application must consider the presence of proximate masses as a source of background clutter. A study of one such systems application "mass noise sensitivity" problem indicated that mass noise will not be a significant problem provided the gradiometer system is calibrated by physically determining the effort of the angular positional relationship between the sensor, platform and carrying vehicle to reasonable accuracy ($\approx \pm 1^\circ$). See page VI-4.

D. Conclusions

While it is true that gravity gradients were not detected and measured by the hard bearing sensor, it is true that valuable information has been gained which properly identified problem areas. In addition, a perspective has been achieved which not only identifies, but ranks those problems related to achieving a hard bearing sensor operating in both the laboratory and the dynamic environments, and specifies future plans of action. To date, the work accomplished continues to indicate that the Hughes rotating instrument is not only feasible, but the preferable method of detecting and measuring gradients in a moving-base environment.

The problems inherent in the successful achievement of a gravity gradiometer for a moving base application seem numerous. This should not be surprising since the desired gradient signal is of extremely small magnitude and the environmental demands are severe. It is important to note that many of the problems described herein would be common to a gradiometer mechanized as either a dynamic (rotating) or a static (non-rotating) instrument.

Gravity gradients were not measured during the conduct of this contract because the incoherent noise level of the various sensor configurations was never less than 900 to 1000 E.U. The magnitude of a convenient laboratory source of horizontal gravity gradients has been limited to approximately 600 E.U.; thus, gravity gradient signals from this source were masked by approximately 300 E.U. of incoherent noise.

The sources of noise, which are discussed in detail in this Report, have become well understood. Noise sources include:

- torque variations introduced by the supporting bearing, by windage on the rotating assembly, and by errors in the drive system;
- linear vibrations introduced through the support structure and by dynamic unbalance; and
- angular rates due to dynamic unbalance of the rotating assembly and/or external influences (air currents, ground vibrations, etc.)

The following specific conclusions are drawn. Note: They are applicable to the sensor operating in both the laboratory and the moving base environments but not necessarily to a zero-g environment.

1. Precision Arm Balance and Vibration Isolation Will Definitely be Required.

Precision arm balance and vibration isolation are both mandatory and complementary. A successful system requires both. The stringency of the demands upon each factor are a function of the operating environment. At this point in time, the objective must be to achieve the best balance and highest attenuation.

"Arm Balance" refers to both mass balance of the arms (coincident centers of mass) and inertia balance (identical arm inertia - spring constant ratio of each arm). Preliminary analysis has indicated feasibility of the piezoelectric scheme described in Section IV-D. Because of the importance of this requirement, it is necessary that the feasibility of a precision balance scheme be verified in the next contractual phase.

Achievement of the greatest precision in the balance scheme will relax the requirements imposed upon: 1) the vibration isolation system, 2) the drive system, 3) the spin axis support bearing, and 4) allowable windage torque. Thus, the importance of this one parameter can not be overemphasized. Incidentally, it should be remembered that the support level of the subject contract precluded the inclusion of a precision balance mechanization in the models constructed.

Vibration isolation has been stated to be necessary and complementary to precision balancing. The converse to a previous statement may be made: the more attenuation provided by the isolation system, the less stringent are the demands placed upon the precision balance scheme.

Vibration isolation systems with attenuation capability of 100 are well within the state-of-the-art. Thus, vibration isolation becomes a matter of feasibility only if precision balance can not be achieved and large attenuation factors (e. g. , 10,000) are demanded.

As stated above, the first order of attention in the next contract remains with the verification of feasibility of a precision arm balance method.

2. Angular Rate Isolation and Angular Position Stability Are Definite Requirements.

Any gravity gradiometer requires that angular inputs be minimized. The sensitive axes differ according to the type of gradiometer, however all gradiometers have the same amplitude of basic sensitivity to angular rate inputs. In the case of the torsionally resonant rotating gradiometer, the spin axis must be isolated from angular rate inputs and held to a given position in inertial space. See Sections IV-B, C, V-B, VI, and VII-A of this Report.

Feasibility is not thought to be a prime question since one or more potential solutions appear practical. For example, a stage of angular isolation may be added in series with a conventional three gimbal inertial platform. This addition is presently thought of as a knuckle bearing and servo system. (See Section IV-C).

An alternative solution would utilize any new developments in inertial platform technology which would eliminate present day problems associated with ball bearing "hang-off" errors. Thus, an air gimbal bearing inertial platform might be well suited to provide the high frequency, low amplitude angular isolation required by the sensor.

A second alternative design solution suggests that the sensor and its vacuum enclosure become the inner race of a spherical bearing. The outer race would be attached to the drive mechanism. Viscous drag would keep both inner and outer races of the bearing rotating at approximately the same speed. The orientation of the sensor axis would be maintained by the angular momentum vector being self-aligning along the sensor major moment of inertial axis.

The relative merits of the potential solutions will require analysis in the early stages of the next contractual effort.

3. Angular Accelerations about the Sensor Spin Axis Must Be Minimized.

Non-gravity-gradient-induced torque variations (noise) must be minimized. Torque noises can be induced by: 1) the spin axis bearing, 2) the drive system, and 3) windage on the rotating assembly.

Feasibility does not appear to be a prime question except as this topic is interrelated with the achievement of a precision arm balance system. The contributions of noise from the above sources will be minimized by careful design of the contributing components.

In the case of the spin-axis support bearing, recent analysis (Section V-B-3) indicates that an erroneous gradient signal can occur due to air bearing ellipticity. To a large extent, this signal can be biased-out. The remaining variation, probably no more than 10% of the bias value, is then, a source of incoherent noise. In the present laboratory model sensor, the total magnitude of this error is estimated to be 300 E.U., with an incoherent component equal to less than 30 E.U. Several means of reducing the estimated 300 E.U. error are both feasible and available. Incorporation of these changes would result in a minimum reduction of the total error to 0.4 E.U., thus, the incoherent variation would become negligible.

Careful selection of the bearing parts will reduce ellipticity. Trade-off analyses will be made regarding other controllable bearing parameters. For example, air bearing noise can be reduced by increasing the gap dimensions, by reducing the pressure, by use of a less viscous gas in an air bearing, and by reducing the sensor rotation speed. At the same time consideration will be given to other types of bearings, e.g., magnetic. Many of these considerations will relate to either a cylindrical or spherical configuration.

Similarly, the next design effort will call for careful selection of the drive system, i.e., the motor, speed pick-off, electronic servo control system, and the coupling device. Primary consideration will be given to reducing the servo bandwidth to a level which will provide adequate isolation from external disturbing torques yet hold the speed precisely within the resonant band of the sensor.

Angular acceleration effects generated by random air windage on the rotating assembly (as differentiated from the arms which rotate in a vacuum) have not yet proven to be of significant magnitude. Windage effects will be considered in future sensor design configurations. Windage is another factor closely related to sum-mode-mismatch. Thus, once the degree of precision balance achievement is known, the relative importance of windage will be known. Several potential solutions are available for consideration if windage proves to be a significant source of sensor noise.

In summary, solutions to angular acceleration problems are to be found by straight-forward engineering design efforts.

4. Horizontal Spin Axis Operation Imposes Additional Requirements.

During this contract, the laboratory testing was limited to sensor operation with a vertical orientation of the spin axis. Thus any anisoelastic properties of the rotating arms and their flexural couplings were of no concern. In the future, however, when the system requires sensors to operate with an off-vertical spin axis orientation, isoelasticity will be required of the rotating members.

Solutions to this problem require accurate design of the arm and the flexural pivot configurations; they appear to be achievable by present-day manufacturing techniques. Thus, feasibility is not thought to be a consideration.

5. Additional Effects Must Be Considered.

Although variations in temperature, acoustic noise, electrostatic and magnetic fields have not yet affected the sensor noise level, these factors must be considered in any design for moving base applications. It is not anticipated that these items will provide any stringent technical difficulties in any system design.

Similarly, requirements imposed on the motion isolation system and the navigation system will vary, depending upon the particular application. Studies in this area will be required to define the expected vehicle motion environment, the resultant requirements on the motion isolation system, and the navigation system requirements.

It therefore is necessary to perform a system application study to define the above parameters in light of the actual mission dependent data requirements. Such a study could be performed by Hughes or the ultimate system users. However, since the results of such a study significantly influences the sensor design parameters, at least in the areas of scale factor stability, bias stability, and navigation requirements, it is imperative that such studies be performed as soon as possible.

6. Design Review Milestone Is Desirable.

A logical sequence of events for a continuing effort to demonstrate the capabilities of a hard bearing sensor calls for a two phase effort:

- a. The known problem areas will be the first subject of a comprehensive analysis and design phase. The interrelationship of all components to the program performance goals will be considered. A simultaneous effort in the laboratory will be required to verify and augment the analytical efforts. A design review will be conducted at the termination of this phase.
- b. The second phase will complete the design efforts. Manufacture, assembly and test of the hard-bearing prototype sensor will be accomplished to determine conformance to program goals.

The foregoing sequence of events will provide the desired level of confidence to indicate that the design alternatives have been fully considered, and that the resulting hardware will demonstrate the required capabilities.

APPENDIX A

GRAVITY GRADIOMETER BROADBAND ISOLATION SYSTEM

ABSTRACT

A unique gravitational gradient sensor capable of measuring gradients with accuracies from 10^{-8} sec⁻² to 10^{-9} sec⁻² range (10 E. U. to 1 E. U.) in a quiet laboratory environment has been developed and tested at Hughes Research Laboratories. One of the many applications for this type of instrument is in an airborne environment to measure the earth's gravity gradients at various points for geophysical information and exploration purposes. An application of this kind would involve some form of mounting of the gradient sensor to the aircraft structure. Since the sensor is sensitive to linear and angular vibrations within the aircraft structure as well as the angular oscillatory motion of the aircraft, some form of inertial platform isolating system will be required.

This report presents one design of three such isolation systems capable of providing attenuation factors of at least 100 to those linear and angular vibrations which might have a deleterious effect on sensor performance.

BLANK PAGE

INTRODUCTION

Comparison of the expected aircraft motion environment to the susceptibility of the gradiometer to this environment has established a set of requirements for a motion isolation system. During the course of these preliminary investigations, several alternative isolation systems and sensor configurations have been conceived and briefly analyzed. As a result of these considerations an overall system concept has been developed which appears to provide the required sensor/isolation system performance goal of 1 E.U. sensitivity. The baseline mechanization is best illustrated by the building block concept shown in Figure A-1.

The gravity gradient sensor(s) is supported by a very low friction air knuckle bearing joint that provides high frequency-small amplitude angular motion isolation. The knuckle joint is supported by a three-gimbal platform whose inner, inertially stabilized element provides the basic vertical and azimuth alignment reference. The knuckle platform is servocontrolled to follow only the long time average orientation of the three-gimbal platform stable element. The three-gimbal platform thus provides the gross, low frequency large amplitude-angular isolation and stabilization while the secondary knuckle bearing and servo provide the high frequency small amplitude-angular isolation.

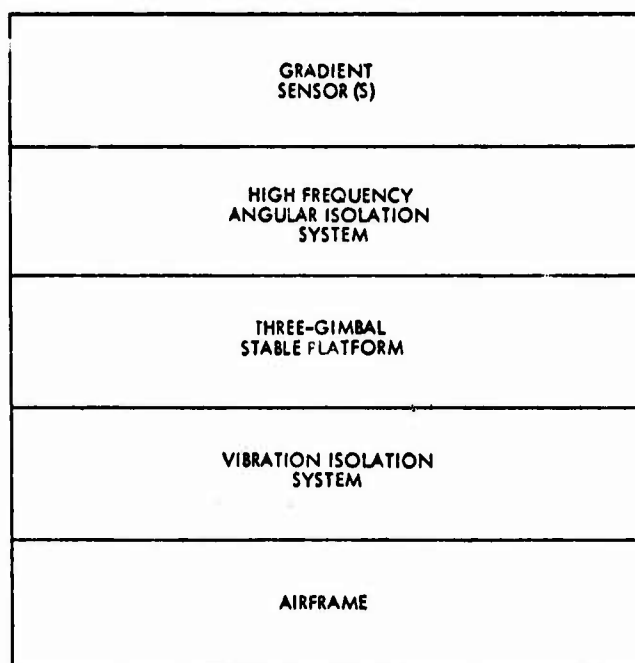


Figure A-1. Baseline system mechanization building block concept.

The base of the three-gimbal platform is supported by a vibration isolation system that primarily provides the isolation of translational aircraft vibrations from the sensor and secondarily provides a certain degree of angular vibration isolation, depending on the specific mechanization of this subsystem.

This report presents an analysis of three types of Passive Broadband Isolation Systems that could be used to support the Three-Gimbal Stable Platform. In the evaluation of each system, consideration was given to the size of the system and the ability to maintain the design requirements over extended periods of time with a minimum of servicing and component replacement.

AIRCRAFT ENVIRONMENT - MOTION AND VIBRATION

Since the aircraft motion and vibration have an influence on the sensor output, an investigation as to the frequency and magnitude of disturbing forces is pertinent. Although specific data from an actual instrumented aircraft test were not available, some pertinent data from aircraft users that provided order-of-magnitude information of this type were obtained and proved useful.

To provide an operational gravity gradient sensor capable of a 1 E. U. threshold sensitivity in an aircraft with these conditions, a vibration isolation system with a maximum resonant frequency of 1 Hz and a damping ratio of no less than 0.1 is necessary. The analysis is based on a design to provide isolation of both translational and angular vibrations while supporting a combined dead weight load of approximately 1000 pounds.*

*This weight estimate was made early in this program. Sensor weight was estimated based on conservative projections of the then current laboratory model sensor. The weight of the required support system for a three-sensor cluster, i.e., the knuckle bearing servo system, the three gimbal platform, and the vibration isolation system, was similarly based on this early estimate of sensor weight. These estimates were made based on a need for an early, specific application to a special test aircraft to be used in gravity surveying. In such an application, the sensor size and weight would be traded off for early operational capability. No specific attempt was made to minimize sensor and support system size and weight. Thus, the reader is cautioned not to draw direct inferences as to the size and weight of a productized sensor and support system.

VIBRATION ISOLATION SYSTEMS

The types of Vibration Isolation Systems that are considered appropriate for this application and that were selected for investigation are

1. Elastomer Suspended Mass System
2. Coil Spring Suspended Mass System
3. Air Column Supported Mass System

1. Elastomer Suspended Mass System

A method of providing the required low resonant frequency broadband isolation system is to suspend the mass consisting of the entire inertial platform-sensor assembly from elastic cords. The types of cords investigated for this report are aeronautical shock absorber (Bungee) cord and Amber Latex Rubber Tubing.

Shock Absorber Cord

The aeronautical shock absorber cord tested is classified as Type I of Specification MIL-C-5651B that differs from the Type II or Bungee cord only to the extent that the Bungee is supplied in an endless ring whereas the Type I tested consists only of a straight section. An example of some of the more pertinent physical properties of 3/8 inch diameter cord as outlined in specification MIL-C-5651B are

Ultimate elongation - percent - minimum	140
Drift - percent, maximum	20
Set - percent, maximum	10
Flexing cycles, minimum	5×10^4
Load change at low temperature, percent	+50

Physical Properties after Aging:

Percent change in load for 100 percent elongation	-35 to +20
Percent decrease in breaking strength, maximum	40
Percent decrease in ultimate elongation, maximum	20
Flexing cycles, minimum	5×10^3

Most applications using Bungee cord utilize the cord shock absorbing features with little concern for isolating specific vibrations as part of a low frequency broadband isolation system. Therefore, the information presented in MIL-C-5651B is not sufficient for the required design and a series of laboratory tests were necessary to determine the pertinent properties of the cord.

An illustration of the results are listed in Table A-1. The first four cords tested (samples 1 through 4) are of the type III listed in the specification and have a single braided cover enclosing multiple continuous strands of polyisoprene rubber. In reviewing the data it was found that although three of the cords are within 0.005 inch difference on the outside diameter the corresponding spring rates are not the same. This condition is illustrated better by determining the "incremental spring rate" which is the average spring rate for a one inch length of cord.

$$S = \frac{W}{\Sigma}$$

$$S_I = S/L ,$$

where

W = applied weight, pounds

Σ = elongation, inches

S = spring rate, lb/in.

L = Length of Sample, inches

S_I = Incremental Spring Rate, lb/in/in.

Although the samples one through four do not represent the size and type of cord that would best fit the design requirements, the large variation in spring rate for different applied loads is of interest.

More extensive spring rate tests were conducted on Samples Nos. 5 and 7 having an outside diameter of 0.275 inch and 0.375 inch, respectively, which sizes seemed appropriate in suspending a 1000-pound mass system. These were of the type I and II construction that consists of multiple polyisoprene rubber strands encased in a double cotton braided cover, the outer braid consisting of more fibers than the inner braid. The tabulated results of data obtained during these tests are listed in Table A-2, and an illustration of the spring rate curve for each sample is shown in Figures A-2a and b. It can be noted from the data and curves that the spring rate approaches linearity only within certain lengths of elongation. The elongation of 1 inch increments marked along the cord length revealed that the cord did not stretch uniformly. Up to 22 percent increment stretch variation was recorded. Post test measurement of the 1 inch increments revealed up to 15 percent yielding in some areas although none of the

Table A-1. Spring Rate Test "Bungee" Shock Cord

SAMPLE NO.	① DIA.	② APPLIED WEIGHT LBS.	③ ORIGINAL LENGTH IN.	④ EXTENDED LENGTH IN.	⑤ TOTAL STRETCH IN.	⑥ 1" INCREMENT LENGTH				⑦ MEAN INCR. STRETCH	⑧ SPRING RATE LB/IN		INCR. RATE LBS/IN
						1	2	3	4		SPRING RATE	INCR. RATE	
1	.208	3.55 3.25 6.97	9 10 10	13.30 14.82 * 20.03	4.3 4.82 * 10.03	1.46 1.50 1.50	1.46 1.50 1.50	1.46 1.50 1.50		13.14 15.00	.827 .675 .694	.858 .650 .694	7.45 6.75 6.94
2	.195	3.55 3.25 6.97	9 10 10	9.30 10.44 16.80	0.3 0.44 6.80	1.04 1.05 1.72	1.04 1.05 1.62	1.04 1.05 1.64		9.36 10.50 16.60	11.83 7.39 1.03	9.86 6.50 1.06	106.3 73.9 10.3
3	.190	6.50 8.63 10.87	9 10 10	10.20 11.25 13.25	1.20 1.25 3.25	1.13 1.12 1.32	1.13 1.12 1.32	1.13 1.12 1.32		10.17 11.20 13.20	5.42 6.91 3.35	5.56 7.19 3.39	48.7 69.1 33.5
4	.195	8.63 10.87 21.38	10 10 10	11.35 13.25 * 18.32	1.35 3.25 * 8.32	1.12 1.32 1.82	1.12 1.37 1.83	1.13 1.31 1.83		11.23 13.33 18.27	6.89 3.35 2.57	7.01 3.27 2.58	63.9 33.5 25.7
5	.275	8.63 10.87 21.38	10 10 10	12.75 15.80 * 22.78	2.75 5.80 * 12.78	1.18 1.50 2.18	1.25 1.56 2.25	1.32 1.69 2.37		12.50 15.83 22.67	3.14 1.88 1.67	3.45 1.87 1.69	31.4 18.8 16.7
6	.280	8.63 10.87 21.38	9 9 9	12.07 15.07 19.20	3.07 6.07 10.20	1.32 1.63 2.12	1.35 1.65 2.15	1.35 1.67 2.12		12.06 14.85 19.17	2.81 1.79 2.09	2.82 1.86 2.10	25.9 16.1 18.8
7	.375	21.38 42.70	9 9	9.38 13.81	0.38 4.81	1.05 1.53	1.03 1.50	1.05 1.53	1.65	9.39 13.97	56.2 8.88	54.7 8.41	506 79.9
8	.525	42.70 76.50	10 10	11.96 17.50	1.96 7.50	1.04 1.56	1.13 1.68	1.09 1.68	1.25	11.28 16.20	21.8 10.4	33.3 12.3	218 104

* NEAR MAX STRETCH

specimens was subjected to loads exceeding the maximum as stated in the specification. It was not definitely determined whether the yielding occurred in both the multiple stranded rubber core and the cotton braided covering or in just the braided covering. From the braided construction of the covering it is likely that some of the cotton fibers could have repositioned themselves during the cord elongation and did not relocate to their original position when the load was removed. There is also the possibility of dirt getting caught between the braid when extended, resulting in distortion of the cover. Unless some of the rubber strands of the core had failed, it is unlikely that the core yielded to the extent that a permanent set of the core would be noticeable. One definite characteristic of the braided covering is that it offers some resistance to cord elongations for small load applications. This is shown on Figure A-2 and is probably due to static friction between adjacent fibers in the braided covering. The amount of resistance or friction would be a function of the amount of contact area between adjacent surface fibers and the amount of binding force on the fibers due to tightness of the braid. The resistance of the cord covering could thereby be changed by increasing or decreasing the number and size of fibers and also by changing the braid pattern.

The test results indicate that a certain amount of damping exists within the cord material that is not present in a normal coil spring designed for a comparable application. Several tests were conducted on the 0.275 inch diameter (sample No. 5) cord and the results comparable curves depicting viscous and coulomb damping, respectively. Figure A-3 shows curves representing conditions of pure viscous damping and coulomb or constant friction damping. With pure viscous damping the mass system will have a damped natural frequency less than that of an undamped system and is represented by

$$\omega_{nd} = \frac{k}{m} - \left(\frac{c}{2m} \right)^2$$

where

ω_{nd} = damped natural frequency rad/sec

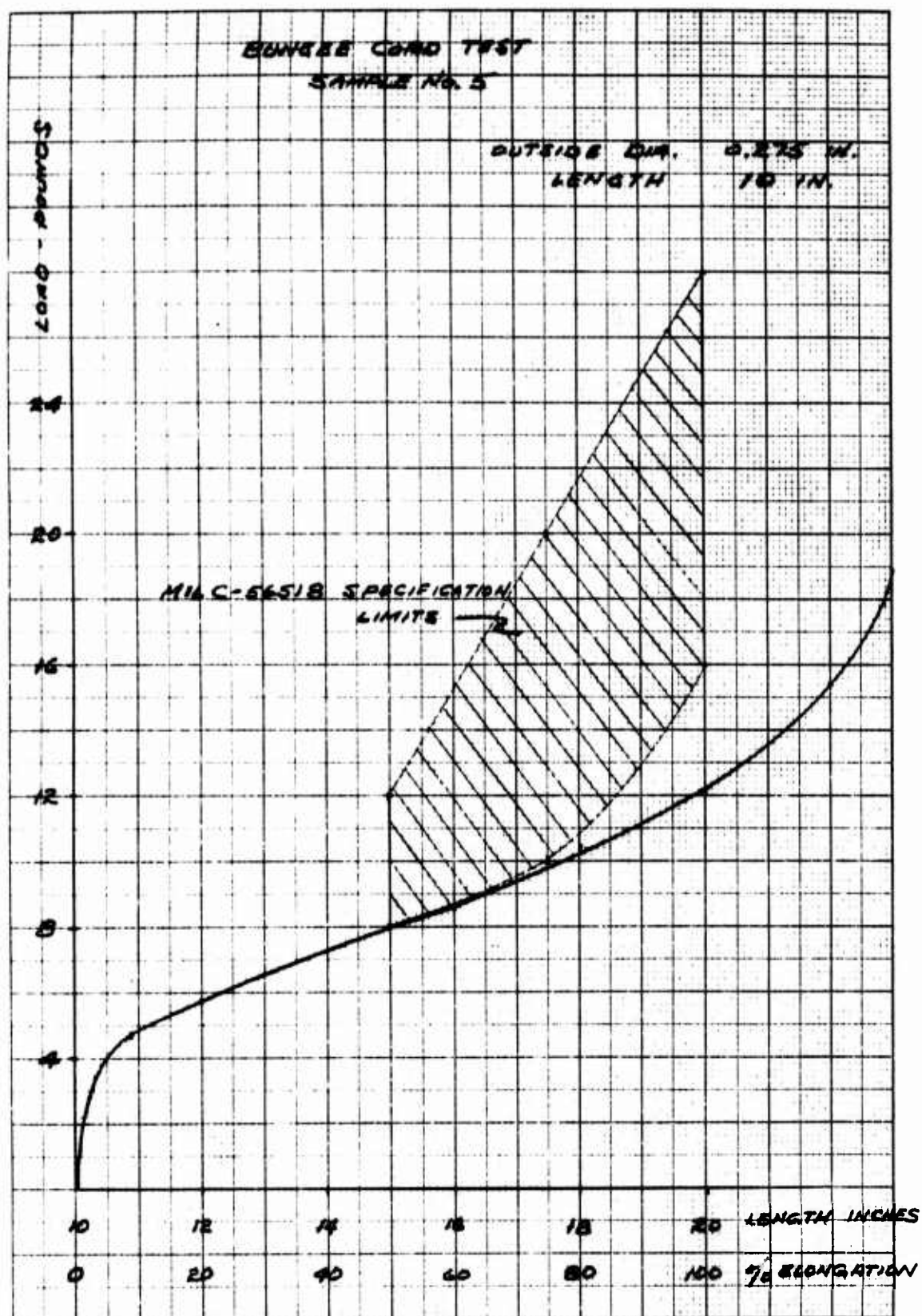
k = spring rate, lb/in.

m = suspended mass, lb/sec²/in.

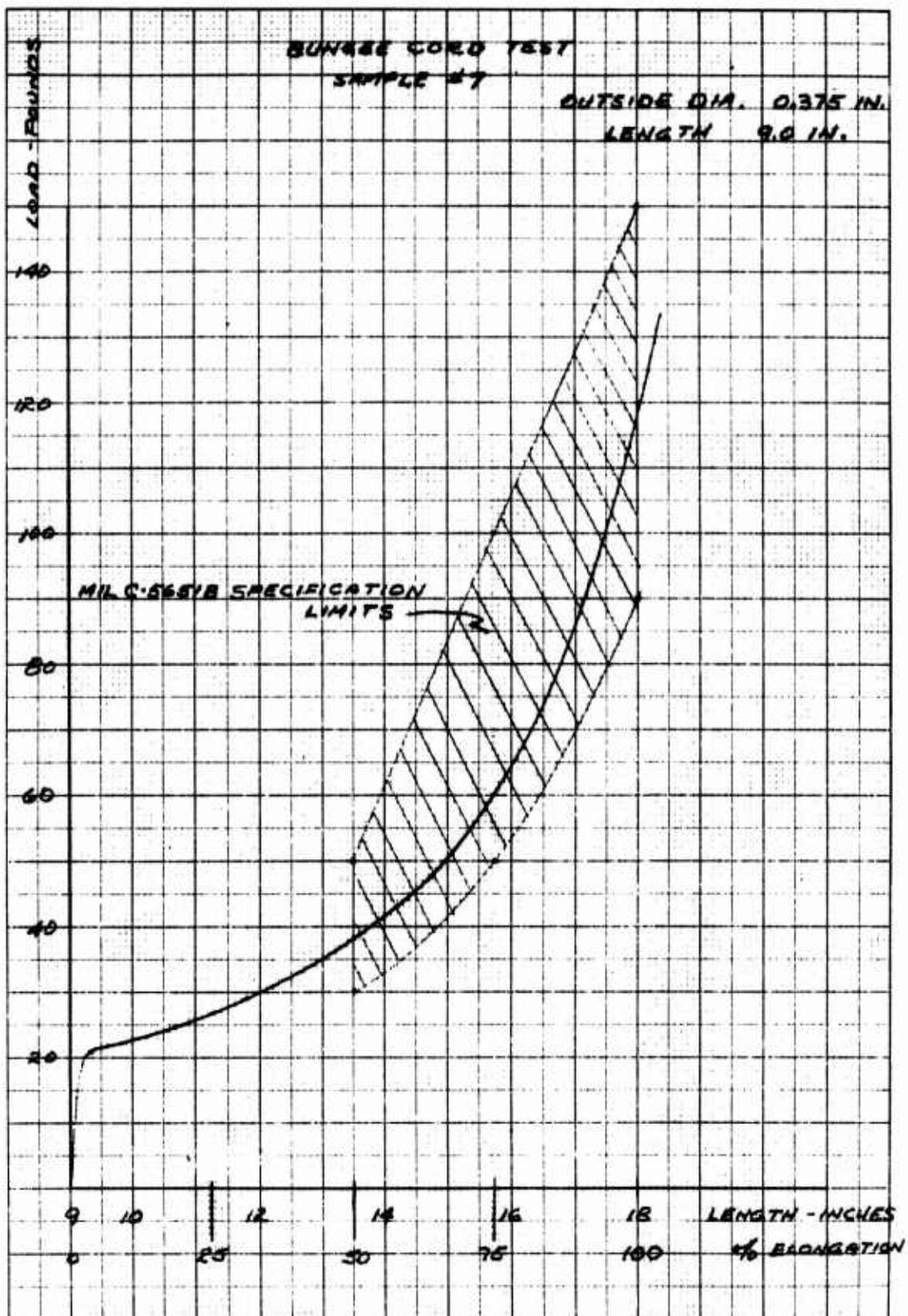
c = damping factor, lb/sec/in.

The curve as illustrated in Figure A-3a for viscous damping follows the equation

$$x = x_0 e^{-\left(\frac{c}{2m}\right)t} \cos \omega_{nd} t$$



a. "Bungee" Sample No. 5
Figure A-2. Spring rate curve.



b. "Bungee" Sample No. 7
Figure A-2. Spring rate curve

where

x_0 = initial mass displacement, inches

x = displacement at any given time, inches

c = damping factor, lb/sec/in.

m = suspended mass, lb/sec²/in.

t = time of period, second

ω_{nd} = damped natural frequency rad/sec.

The curve depicting coulomb damping shown in Figure A-3b differs in respect to that illustrating viscous damping in that the boundary lines of the decay curve are straight. An analysis of the motion is obtained from work and energy considerations and the results utilizing the energy equation are

$$x_{1/2} = x_0 - \frac{2F}{k}$$

and

$$x_1 = x_{1/2} - \frac{2F}{k}$$

where

x_0 = initial mass displacement, inches

$x_{1/2}$ = amplitude after 1/2 cycle, inches

x_1 = amplitude after 1 cycle, inches

F = friction force, pounds

k = spring rate, lb/in.

Therefore, the amplitude decreases at a constant rate of $4F/k$ per full cycle.

Test results to determine the type and amount of damping are illustrated by the curve in Figure A-4. It can be noted that the shape of the curve for the first several cycles indicates that viscous damping is predominant. Assuming the presence of only viscous damping for the first several cycles the damping factor can be determined by measuring

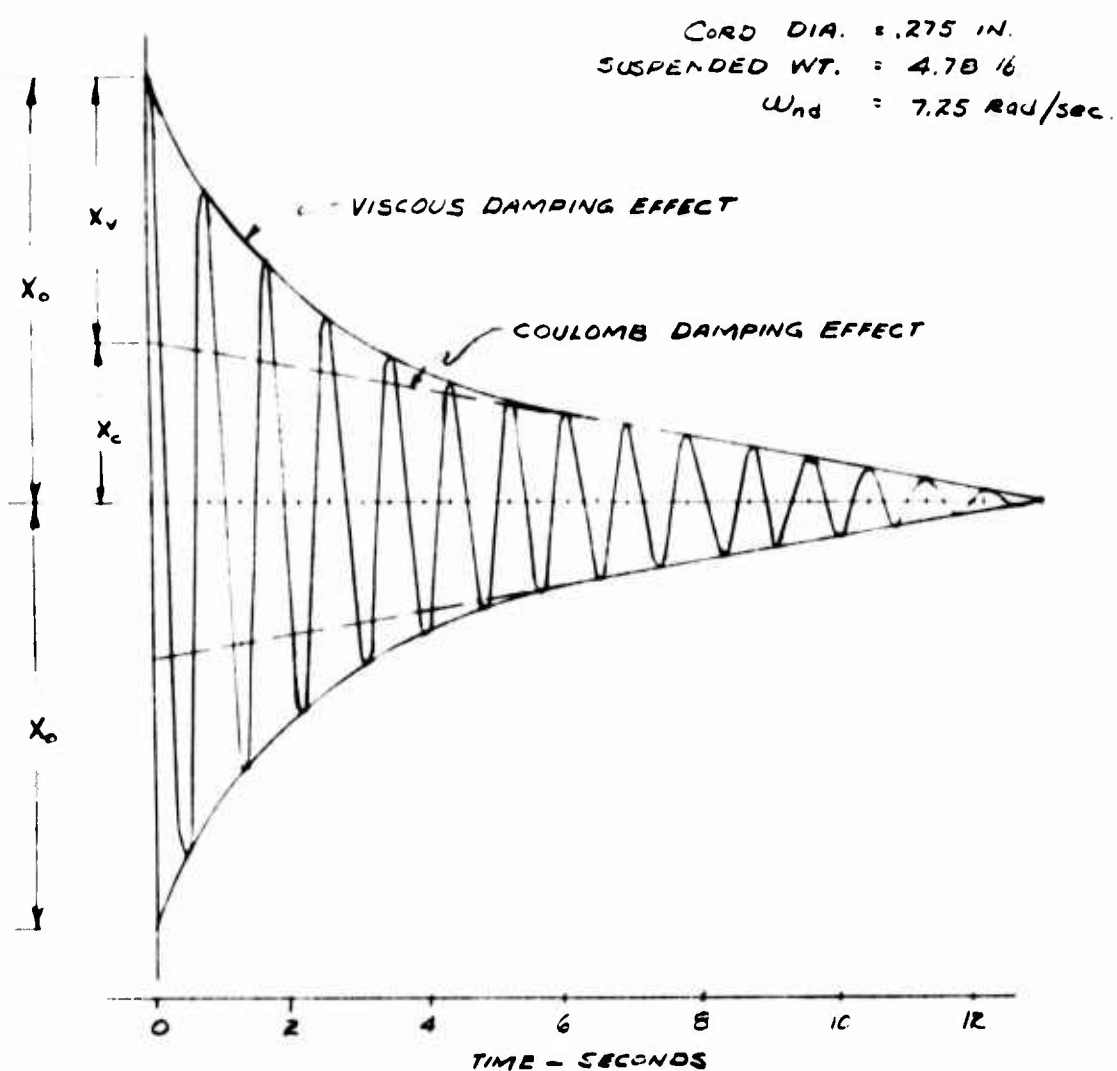


Figure A-4. Vibration damping of "Bungee" cord.

the initial mass displacement and the maximum amplitude after a definite number of cycles, thereby obtaining the damped cyclic frequency by timing the oscillations the damping factor is found by

$$\frac{x_n}{x_{n+1}} = e^{\frac{\pi c}{m \omega_{nd}}}$$

or

$$\log_e \frac{x_n}{x_{n+1}} = \frac{\pi c}{m \omega_{nd}}$$

and

$$c = \frac{m \omega_{nd}}{\pi} \left(\log_e \frac{x_n}{x_{n+1}} \right).$$

where x_n and x_{n+1} are the maximum amplitudes of successive cycles. To determine whether only viscous damping exists after 10 cycles during decay of the motion, the maximum amplitude can be calculated after 10 cycles and compared to that measured. The difference between the calculated and measured amplitude is then the approximate loss due to dry friction or coulomb damping.

"Bungee" Suspended System Design. To provide the required vibration isolation, the system design is based on having a resonant frequency of 1 Hz or less with a damping ratio of no less than 0.1. To provide vibration isolation in the "x," "y" and "z" axes along with angular rate isolation, a number of "Bungee" cord rings can be utilized to suspend the mass as illustrated in Figure A-5. This design would require 16 Bungee endless rings used as soft springs each with a spring rate of 6.38 lb/in. This is determined by

$$\omega_n^2 = \frac{16k}{m}$$

$$k = \frac{\omega_n^2 W}{16g}$$

$$k = 6.38 \text{ lb/in.}$$

where

$$\omega_n = 1 \text{ Hz} = 6.28 \text{ rad/sec}$$

$$W = 1000 \text{ pound}$$

$$g = 386 \text{ in/sec}^2$$

$$k = \text{spring rate}$$

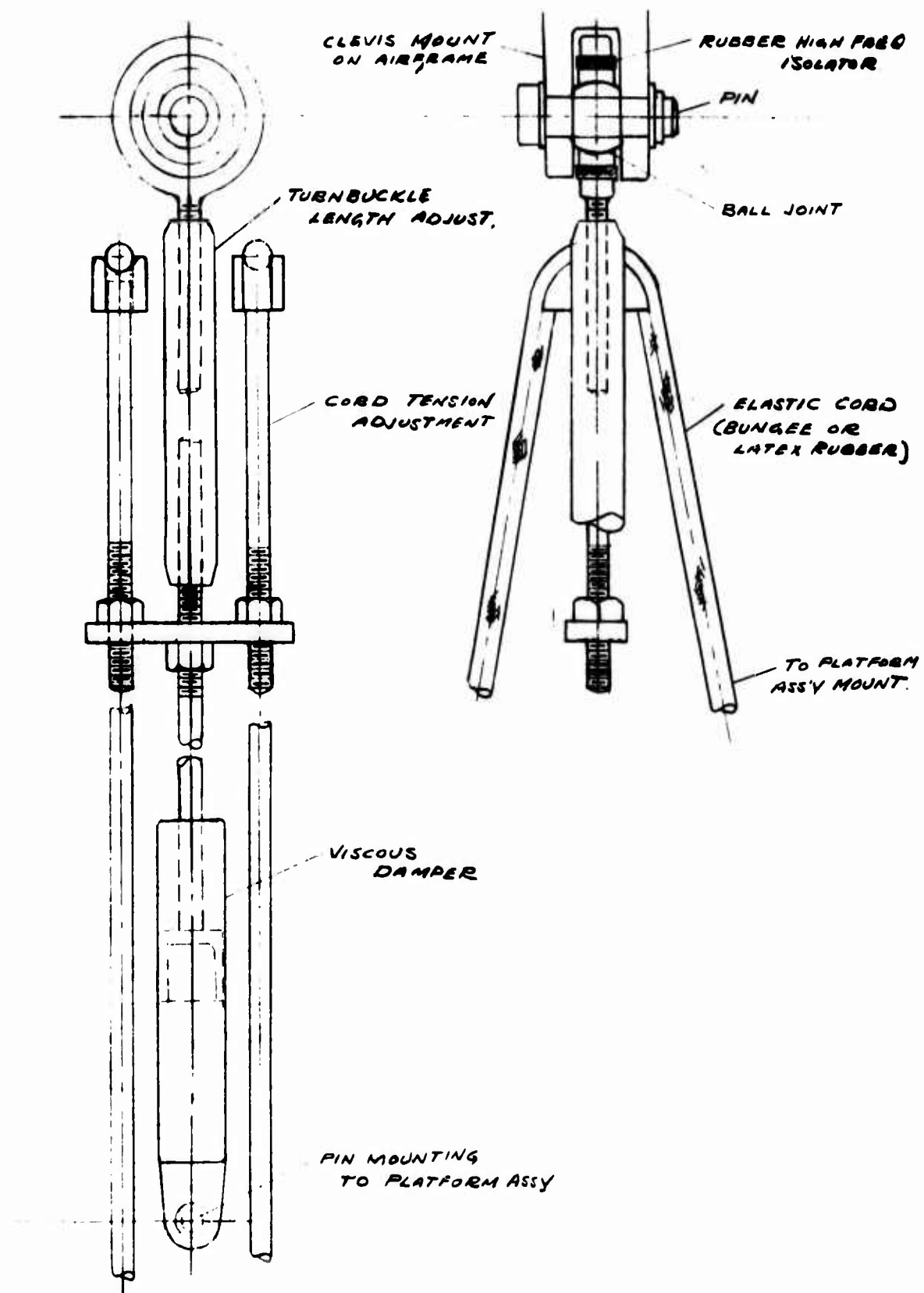


Figure A-5. "Bungee" suspension with viscous damper.

With the mass suspended as shown in Figure A-6, each of the top "Bungee" rings will be loaded to 240 pounds. This will include a 63 pound preload. The Mil Spec Requirements for 3/8 inch diameter cord indicate a load range between 180 and 300 pounds will result in a 100 percent cord elongation. Considering 100 percent cord elongation, for a 240-pound load, the elongation of each cord based on a 6.38 pound/inch spring rate would be

$$\frac{F}{K} = \frac{240 \text{ lb}}{6.38 \text{ lb/in.}} = 37.7 \text{ inches.}$$

The total length of the elongated cord would then be

$$37.7 \times 2 = 75.4 \text{ inches.}$$

The eight bottom Bungee rings will each be preloaded with 63 pounds and have an installed length of 36.6 inches of which 9.9 inches will be elongation. The design criteria is based on the test results and specification limitations of the "Bungee" cord (Figure A-7).

The type of suspension utilizing "Bungee" cord rings as illustrated in Figure A-6 will permit the coulomb damping properties inherent in the cord to dampen low frequency rotational oscillations of the suspended mass about the vertical axis. The installation of an adjustable viscous damper as shown will suppress the translational very low frequency vibrations. A means of adjustment will be required such as that shown in Figure A-5, to assure that the mass load can be equally distributed and that the tension in each cord is equal.

Amber Latex Rubber Tubing

Another elastomeric suspension approach is the use of amber latex rubber tubing. The amber latex rubber tubing investigated is the type commonly used in the laboratory for the conveyance of fluids and gases. The tubing sizes tested were found to be not adequate in strength to support the required load, and the largest size commercially produced, 1/2 inch I. D. x 1/8 inch wall tubing, was not currently available. Based on the results of tests conducted on the smaller size tubing, a spring rate curve was computed for the larger unavailable size. Results of the spring rate tests of the two samples and the computed spring rate curve (dashed line) are shown in Figure A-8. The resulting curves indicate that neither spring rates of the Bungee nor the rubber tubing are linear. Whereas the spring rate of the "Bungee" cord increased for increased loads, the spring rate of the rubber tubing decreased when more load was applied. Although springs with a linear spring rate are more desirable, elastomer materials can be utilized effectively in designing vibration isolation

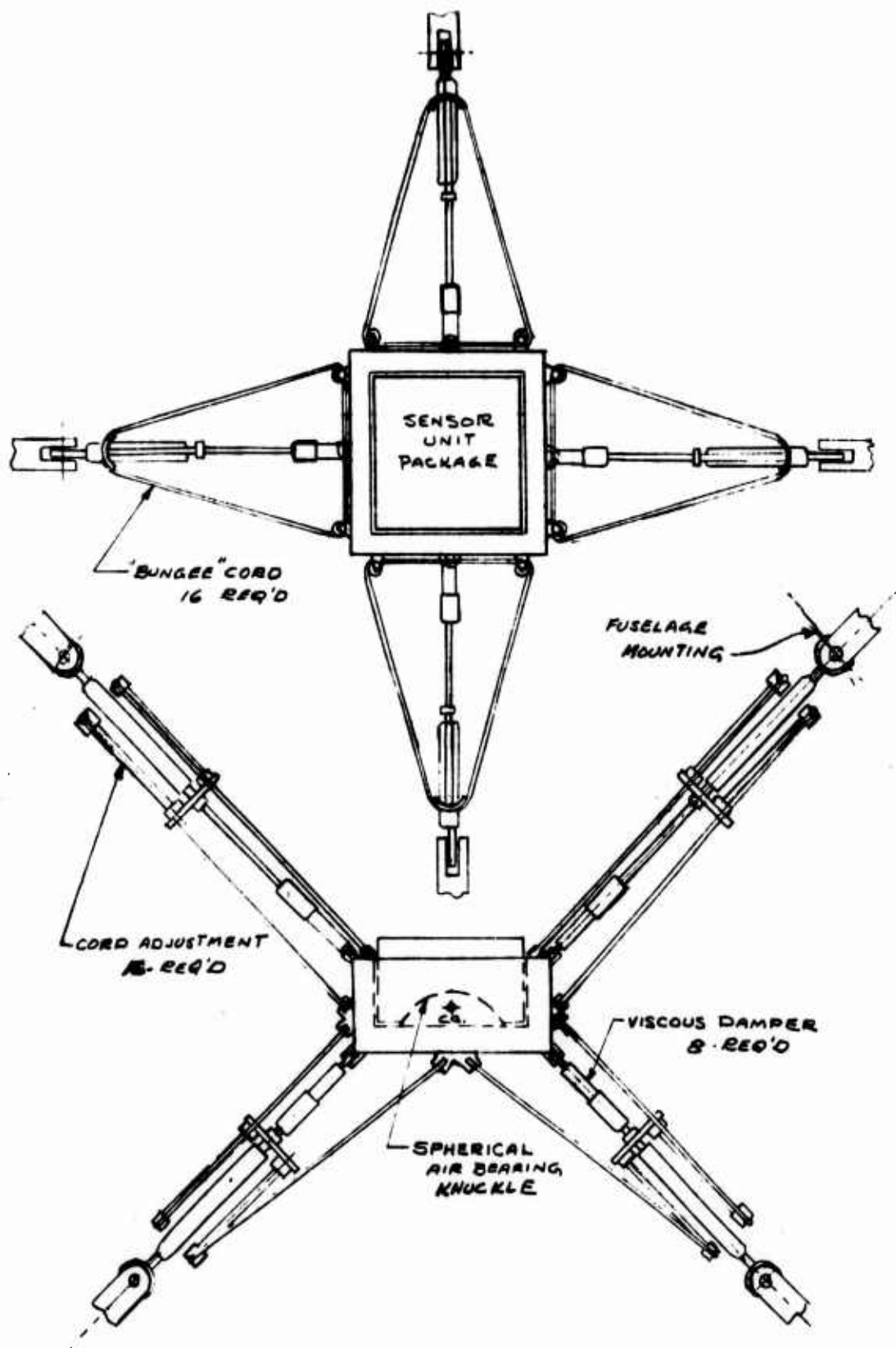


Figure A-6. "Bungee" spring-mass vibration isolation system.

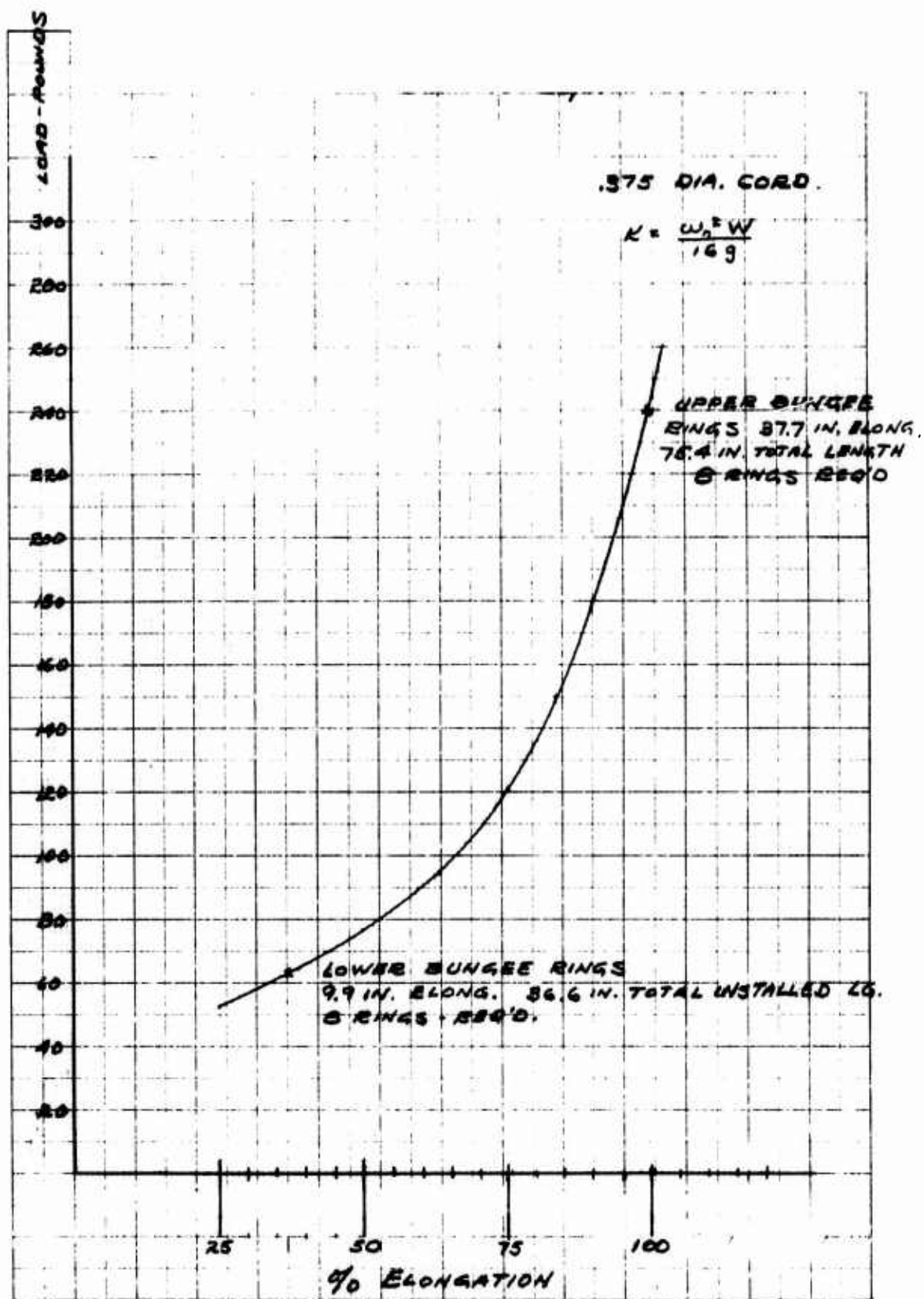


Figure A-7. "Bungee" spring-mass suspension characteristics.

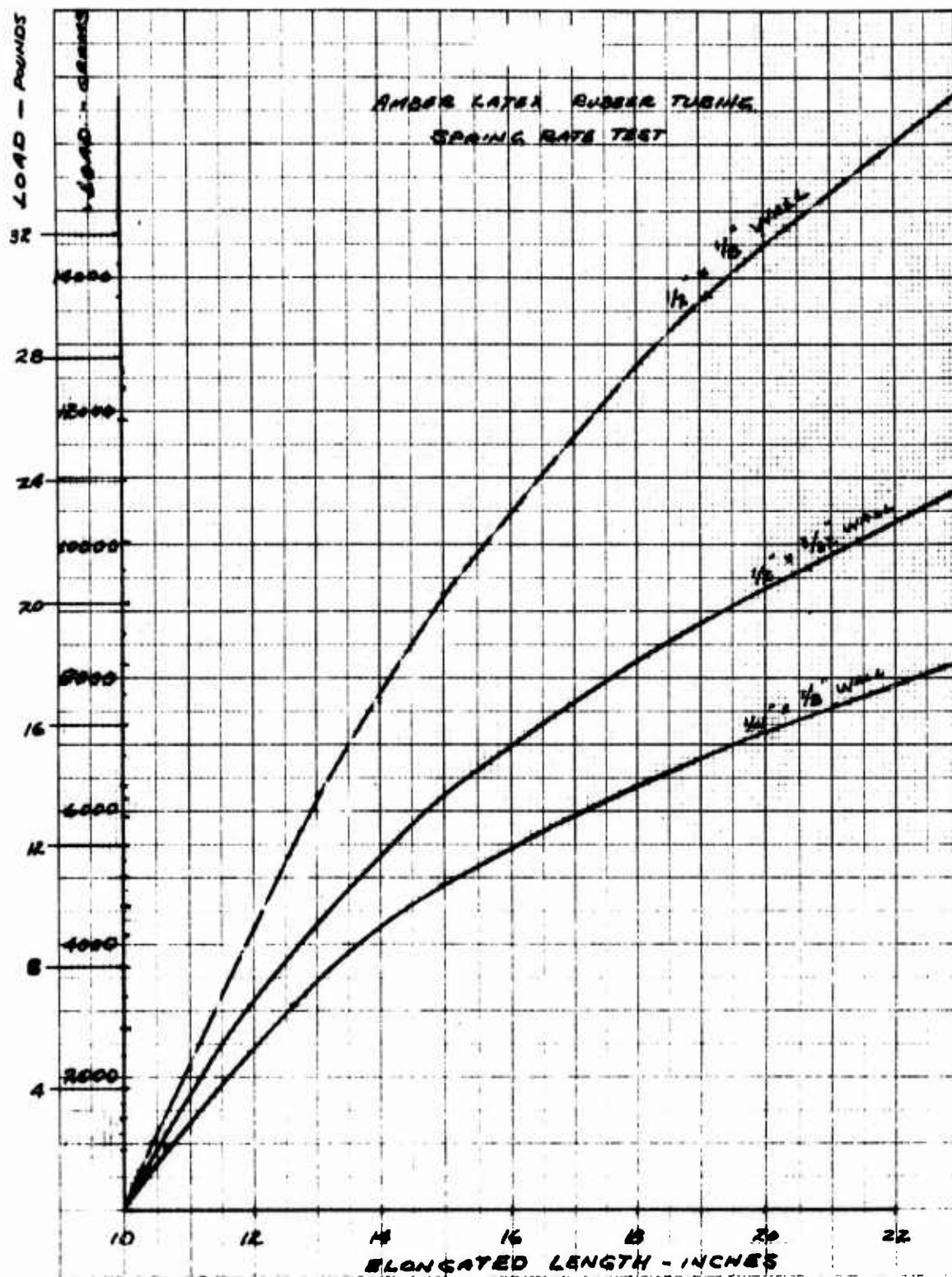


Figure A-8. Rubber tubing spring rate test.

systems when their material properties are known. Figure A-9 illustrates points on the spring rate curve at which 1/2 inch I. D. rubber tubing can be used to obtain a 1 Hz resonant suspension system supporting a 1000 pound mass. Using this tubing in ring form, a total of 64 rings are required. The number of rings could be reduced if larger size latex rubber tubing could be provided. Only sizes that presently are commercially available were considered for test purposes.

Figure A-10 shows the results of the amount of damping that is present in a ten inch length of 1/2 inch x 3/32 inch wall rubber tubing. A significantly less amount of material damping was found to be present in the rubber tubing as compared to that found in the "Bungee" cord tested. The curve indicates very little if any coulomb damping and could be considered similar to the damping characteristics found in a helical coil steel spring. A suspension system design using latex rubber tubing would be very similar to utilizing "Bungee" shock cord rings except that the number of rubber tubing rings would be greater.

The basic disadvantages of using any kind of elastomer in the design of a vibration isolation system of this type is the material drift and set characteristics which would have a decided effect in changing the spring rate after a short period of time. These material properties were previously noted in MIL-C-5651B for the Bungee shock absorber cord and were later verified by test. Although no pertinent specification was found for the particular latex rubber tubing tested, the results of a load elongation test revealed that the rubber tubing also exhibited yielding and permanent set.

Figure A-11 illustrated the rate of elongation that occurred in a 19.4 inch length of 1/4 inch ID x 0.060 wall rubber tubing over a 7-day period under a constant load of 4.93 pounds. The amount of permanent set measured was 0.264 inches or 1.35 percent of the original length. A decided change in color of the elongated portion of the rubber tubing was also evident during the elongation test.

This color change in the rubber was examined and found to be crystallization which takes place when latex rubber is subjected to freezing or maintained in a stretched condition over a period of time. Crystallization in rubber takes place by local rearrangements of portions of molecules rather than by bulk movement of molecules as occur in a liquid. The length of the crystallites are only 100 to 1000 Å whereas the length of a molecule average about 20,000 Å. The crystallization process involves a definite structural change, or change of state, which is accompanied by the usual manifestations - latent heat of crystallization and change of specific volume. Since this characteristic results in a change in material elasticity, it would effect cord spring rate during the period of crystallization.

The very limited fatigue life and effects of aging on material properties also present a major problem when using elastomers.

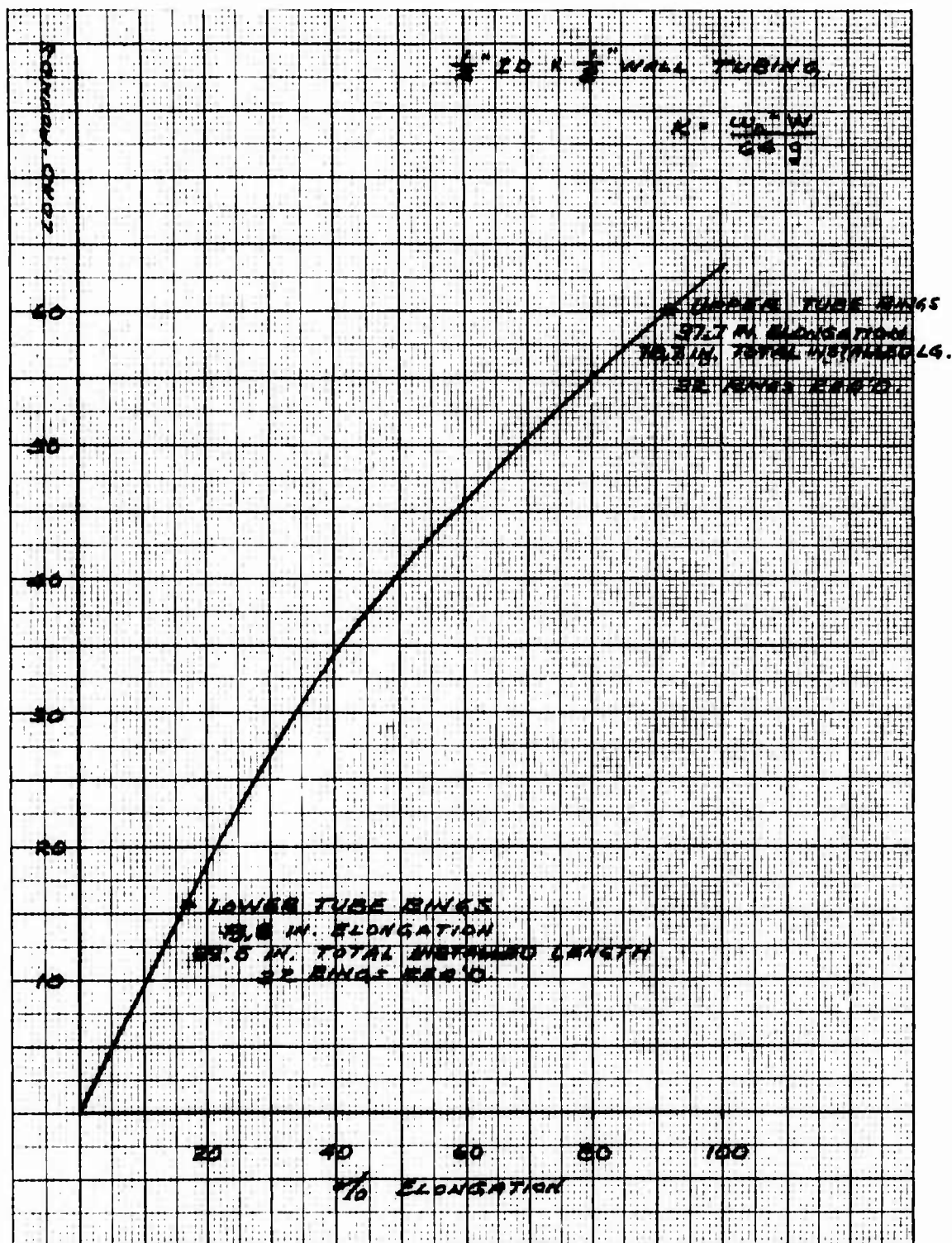


Figure A-9. Rubber tubing spring mass suspension characteristics.

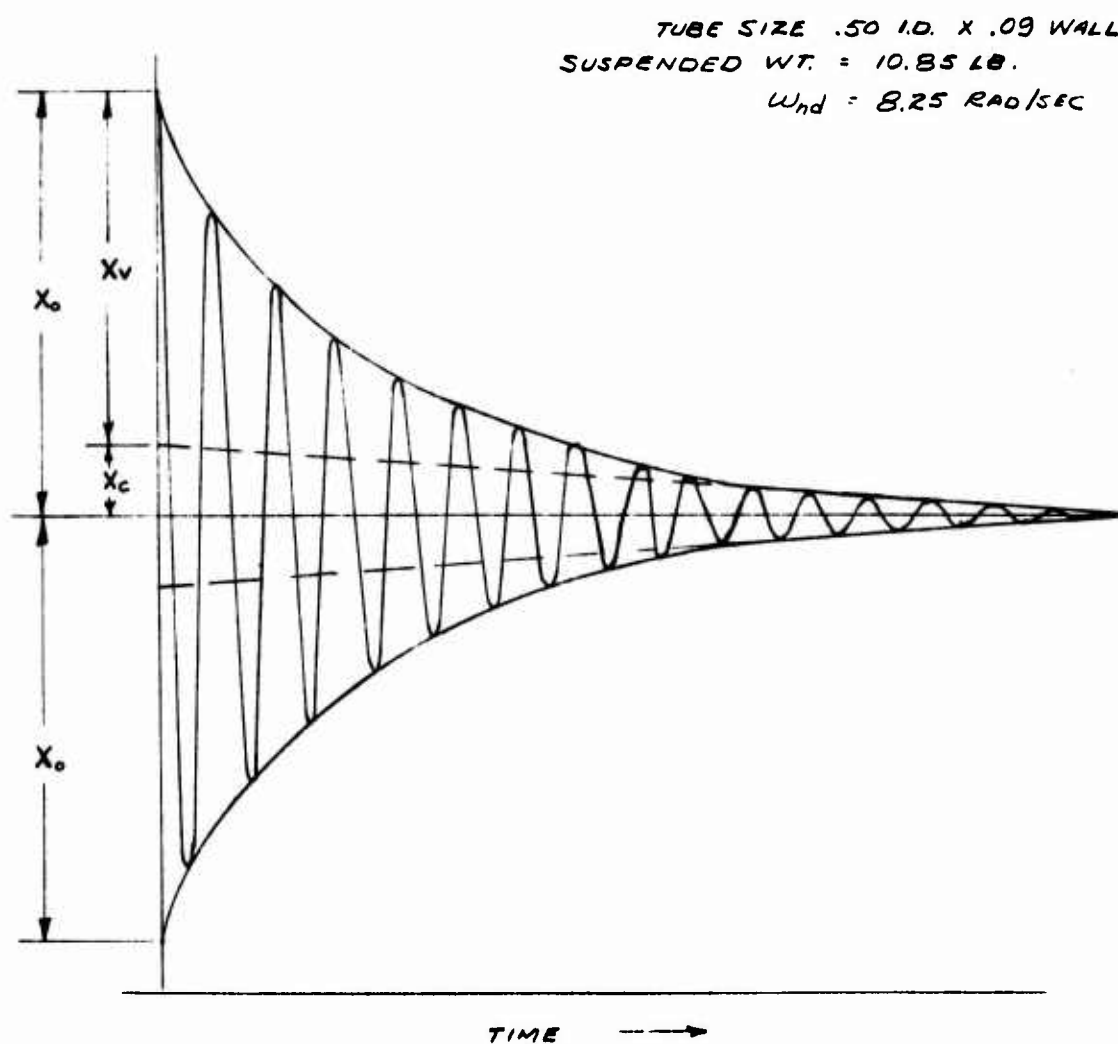
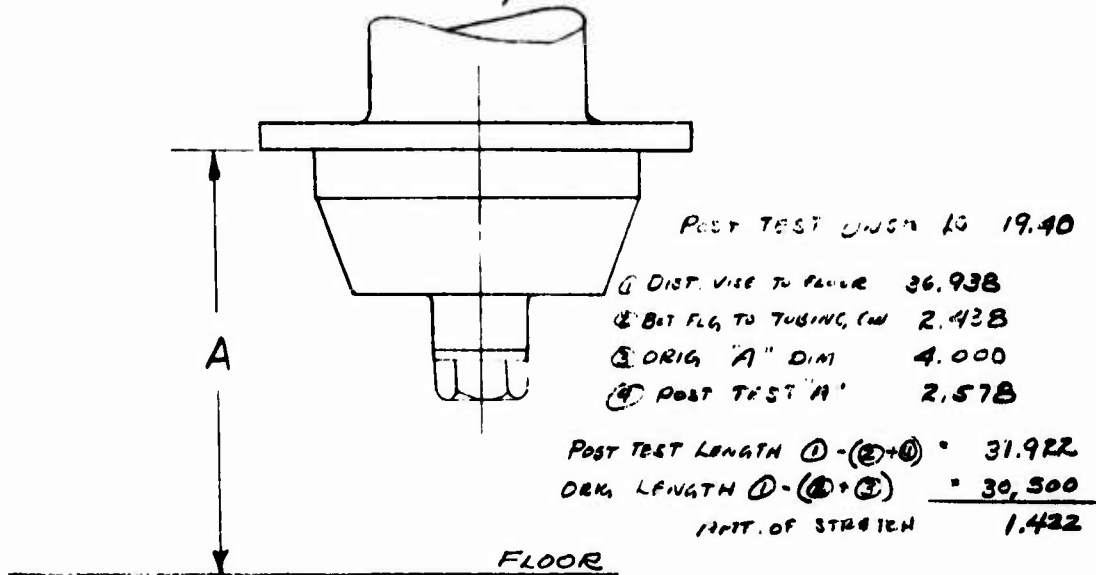


Figure A-10. Vibration damping of rubber tubing.

SUSPENDED WEIGHT 2231 Grams : 4.93 LB.



DATE	TIME	A	ΔA	ΔA/MIN	ΔA/HR	TIME LAPSE MIN.	TOTAL STRETCH INCH
7-24	9:15	4.00					
	10:25	3.80	0.20	0.00286		70	0.20
	12:00	3.70	0.10	0.00105		165	0.30
	14:05	3.60	0.10	0.00080		290	0.40
	17:05	3.485	0.115	0.00064		470	0.515
7-27	9:10	3.330	0.155		0.00242	3845	0.670
7-28	10:10	3.255	0.075		0.00300	5345	0.745
7-29	11:10	3.210	0.045		0.00180	7145	0.790
7-30	10:25	3.160	0.050		0.00220	8555	0.840
	9:45	3.110	0.050		0.00214	9955	
8-3	9:40	3.736					
	10:10	3.485	0.251	0.008		30	0.251
	14:45	3.000	0.485				0.736
	8:40	2.813	0.187				0.923
8-5	9:15	2.813					
8-7	11:40	2.578					

Figure A-11. Rubber tubing drift and set test.

The fatigue life and effects of aging is a major problem with elastomers. This was previously outlined for the "Bungee" shock absorber cord for which minimum specification requirements are available and, considering the test results, would be similar for the latex rubber tubing.

A gravity gradient sensor assembly including drive system, air bearing and rotating chamber was suspended from a support frame with latex rubber tubing. The assembly, a 1.2 resonant vibration isolation system, is shown in Figure A-12. Test results indicated that with this suspension the environmental noise level mainly from the floor, was reduced by a factor of 300. Although the suspended mass for this application was 40 pounds, the results indicate that with a more sophisticated design the rubber tubing could provide an adequate isolation in systems with larger masses.

2. Coil Spring Suspended Mass System

A more common approach to vibration isolation is to utilize a system of helical coil springs in conjunction with viscous dampers. A system of this type designed to have a resonance of 1 Hz maximum would have a maximum vibration transmissibility of 0.02 for a disturbing

M 7433

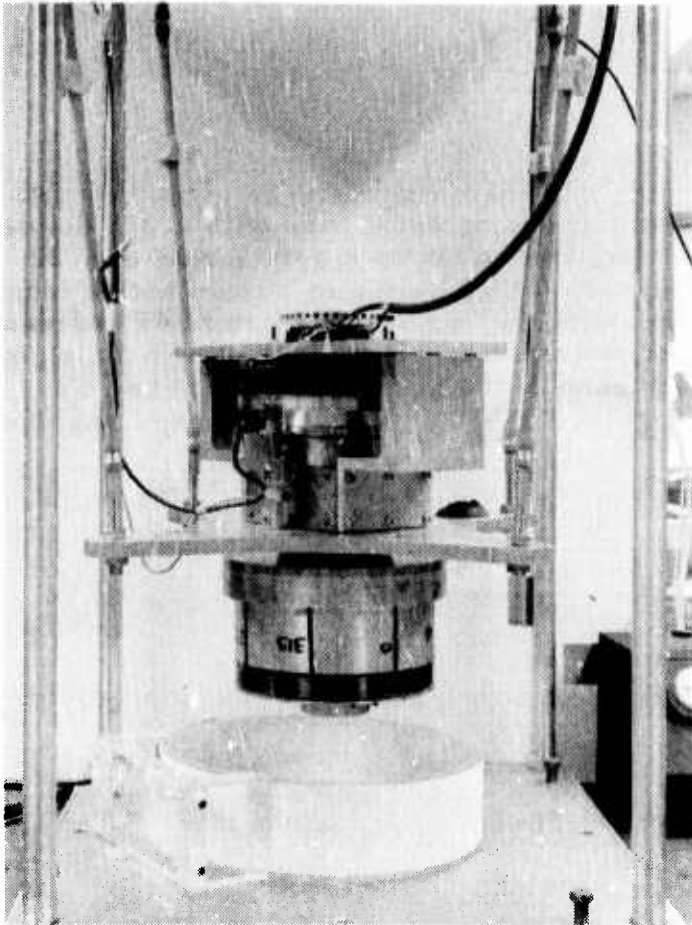


Figure A-12
Gradient mass sensor vibration isolation system utilizing latex rubber tubing.

frequency of approximately 10 Hz. The system illustrated in Figure A-13 consists of 16 coil springs, each with a spring rate of 6.38 pound per inch suspending the 1000 pound inertial-platform-sensor assembly. This being a conventional type coil spring application, the design can be based on using the formula:

$$K = \frac{Gd^4}{8nD^3}$$

or

$$n = \frac{Gd^4}{8KD^3}$$

where

G = shear modulus of elasticity

d = wire diameter, inches

D = mean coil diameter, inches

n = number of coils

K = spring rate, lb/in.

Considering a 2 inch diameter coil spring using wire with 0.218 diameter, a total of 69 active coils are required to obtain a spring rate of 6.28 pounds per inch. Each spring would then have a minimum active length of 69×0.218 or 15.1 inches. With the springs mounted at 45 degrees as shown in Figure A-13, and considering a total preload for the eight top springs, the total load for each of the top springs would be.

$$P_s = \frac{\frac{W}{\cos \theta} + W_p}{N} = 240 \text{ pound}$$

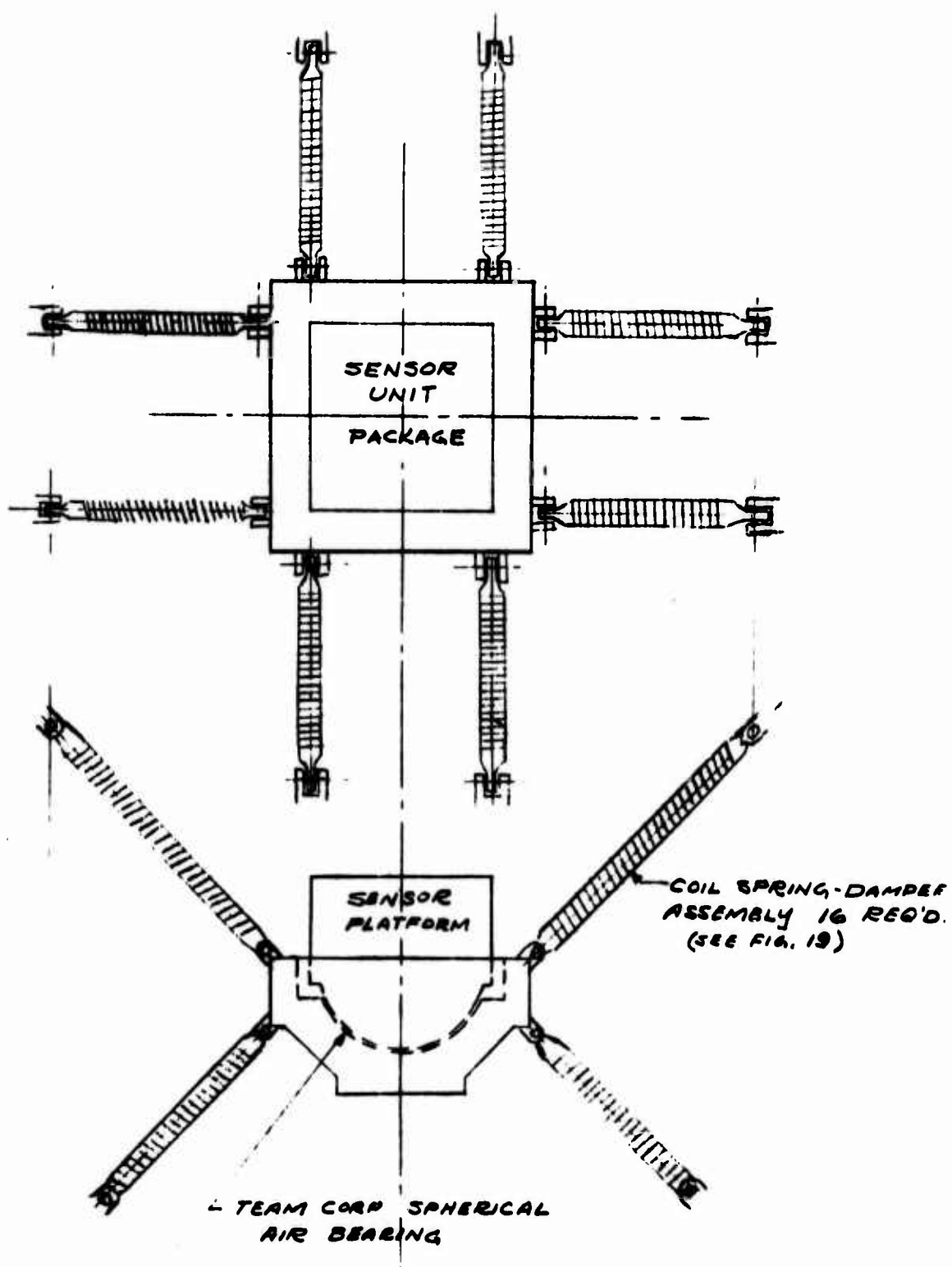


Figure A-13. Coil spring-mass vibration isolation system.

where

P_s = load per spring

W = 1000 pounds

W_p = preload = 500 pounds

N = Number of springs

The total extended length for each top spring would be

$$L_1 = L_A + \frac{P_s}{K} = 52.7 \text{ inches}$$

where

L_1 = spring extension lg.

L_A = 15.1 inches

P_s = 240 pounds

K = 6.28 lb/in spring rate

Since the eight bottom springs would be only subjected to the total preload of 500 pounds, the load per spring would be 62.5 pounds and the total extended length would be 24.9 inches.

The minimum translational resonance of the system can be determined by assuming eight of the springs in parallel each with a tension load along the spring axis and eight springs in bending. The spring rate for the four top springs in bending would be:

$$K_1 = \frac{2EI}{L_1^2} = 2.4 \text{ lb/in}$$

and

$$\omega_n = \sqrt{\frac{4K}{M}} = 1.92 \text{ rad/sec}$$

for the four bottom springs

$$K_2 = \frac{2EI}{L_2^2} = 10.8 \text{ lb/in}$$

and

$$\omega_{n_2} = \sqrt{\frac{4K}{M}} = 4.09 \text{ rad/sec.}$$

where

E = modulus of elasticity

$$= 30 \times 10^6 \text{ psi}$$

I = wire moment of inertia

$$= \frac{\pi d^4}{64} = 1.11 \times 10^{-4} \text{ in}^4$$

L_1 = top spring length

L_2 = bottom spring length

K_1 = spring rate (top)

K_2 = spring rate (bottom)

The resonant frequency of the system with the eight remaining springs in tension is

$$\omega_{n3} = \sqrt{\frac{8K}{M}} = 4.44 \text{ rad/sec}$$

the translational resonance of the system would then be

$$\omega_{n_t} = \sqrt{(\omega_{n1})^2 + (\omega_{n2})^2 + (\omega_{n3})^2} = 6.34 \text{ rad/sec.}$$

The angular rate or rotational resonance of the system is determined knowing the mass inertia and spring rate of the spring in torsional bending. Considering the mass concentrated at a 10-inch radius from the mass center the mass moment of inertia is

$$I = Mr^2 = 386 \text{ lb. in. sec}^2$$

where

r_g = radius of gyration

= 10 inches

the spring rate of each spring in torsional bending is found by

$$K_r = \left(\frac{Ed^4}{32nD} \right) \left(\frac{1}{1 + E/2G} \right)$$

$$K_r = 6.98 \text{ in. lb/rad.}$$

where

$E = 30 \times 10^6 \text{ psi}$

$G = 12.5 \times 10^6 \text{ psi}$

$d = 0.218 \text{ inch diameter wire}$

$D = 2.0 \text{ inch coil diameter}$

$n = 69 \text{ coils.}$

The angular rate or rotational resonant frequency is then determined by

$$\omega_{n_r} = \sqrt{\frac{8K_r}{I}} = 0.38 \text{ rad/sec.}$$

A preliminary stress analysis of the coil spring as designed indicates that it is adequate even if ordinary spring steel is used. Based on a shear modulus of elasticity of $G = 12,500,000$ psi and an allowable unit stress of 125,000 psi and an allowable unit stress of 125,000 psi the safe working load for each spring is

$$P = 0.1963 d^3 S_v = 255 \text{ pounds}$$

where

S_v = allowable unit stress

d = wire diameter

Since the maximum load on any one spring will be 240 pounds when the mass is equally distributed, there should be no difficulty in suspending the 1000 pound mass as illustrated.

A coil spring vibration isolation system must be provided with some type of rubber isolator to keep high frequencies from being transmitted along the spring wire. These isolators are installed at the spring ends as illustrated in Figure A-14 and will serve to isolate those high frequency vibrations that normally would be conducted by the spring wire.

To be effective in damping low frequency oscillations, each coil spring is coupled with an individual viscous damper. The springs are therefore designed so that a hydraulic damper will fit within the spring coils as shown in Figure A-14. These viscous type dampers are adjustable to obtain the optimum amount of damping with minimum reduction in vibration isolation rate and little change in variation of the system resonant frequency. A standard curve depicting the damped ω_n and for various damping ratios is shown in Figure A-15. The transmissibility at various impressed vibration frequencies is shown in Figure A-16 for damping ratios between 0.1 and 0.5. A coil spring suspended mass isolation system as illustrated can be designed and fabricated to utilize standard commercial type components and will be able to provide the required isolation of the broad band frequency vibrations experienced during normal aircraft operation.

3. Air Column Supported Mass System

A very effective method of broadband vibration isolation is the use of servocontrolled pneumatic components to support the mass of the inertial platform-sensor assembly. This type of isolation system is

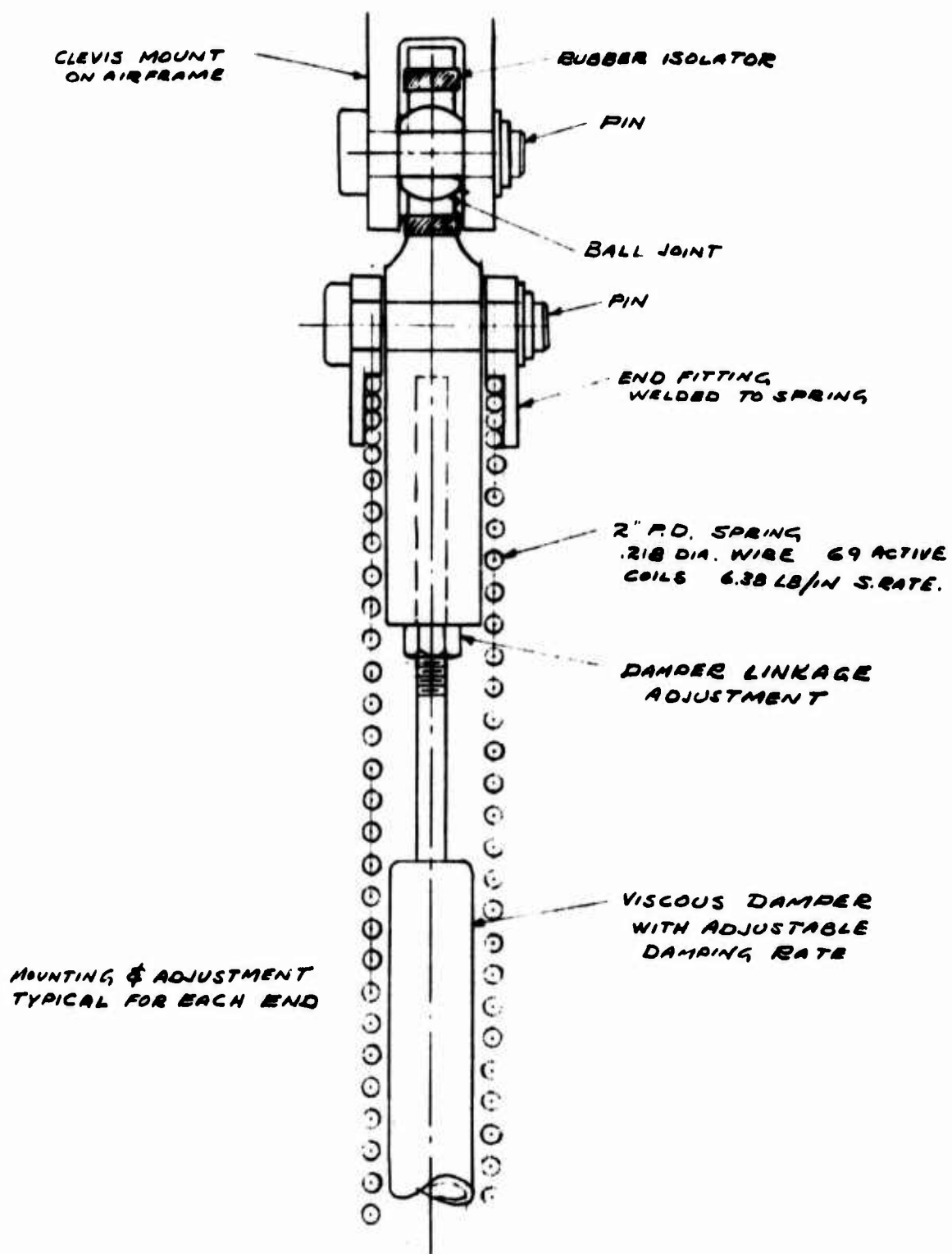


Figure A-14. Coil spring-viscous damper installation.

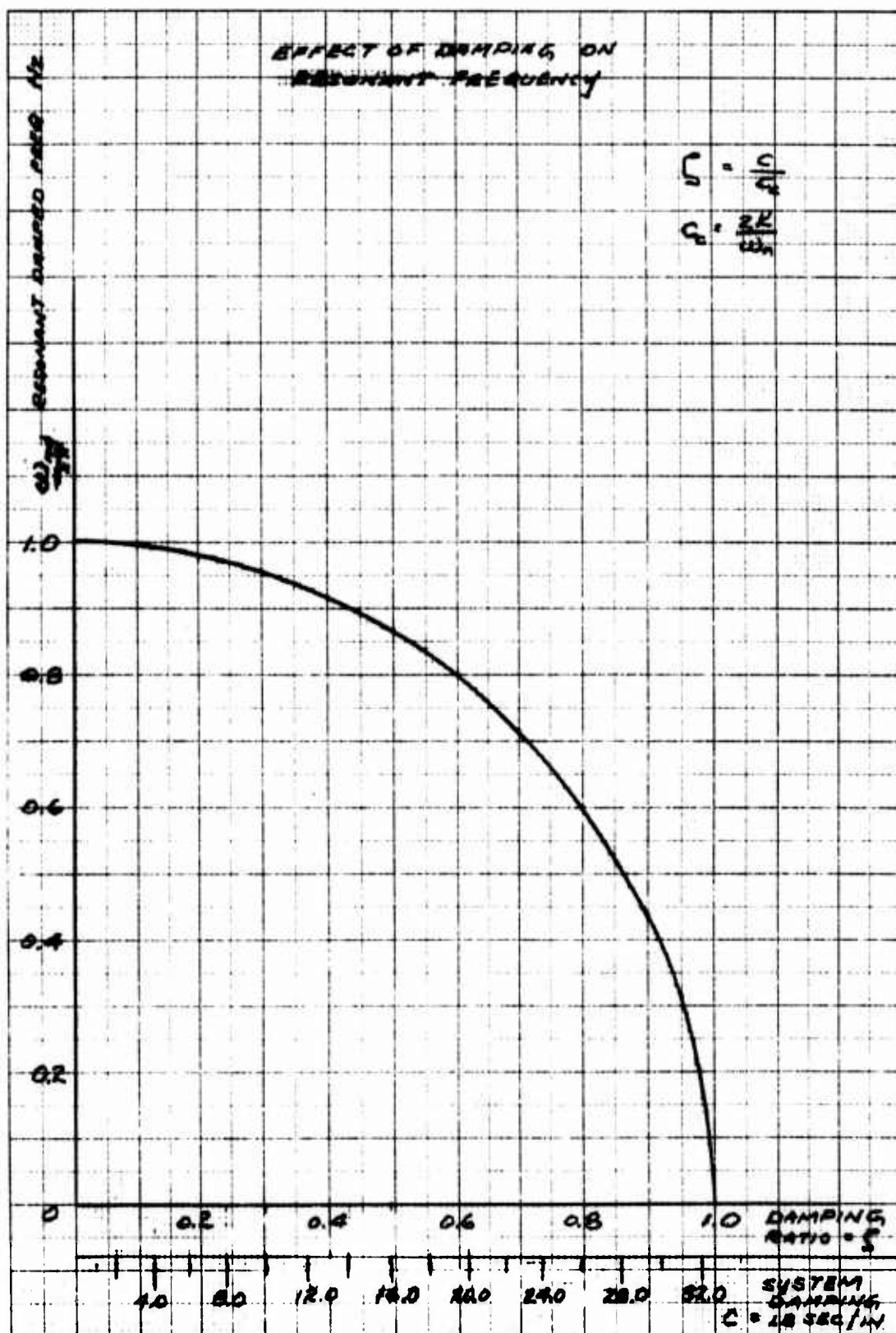


Figure A-15. Effect of damping on resonant frequency.

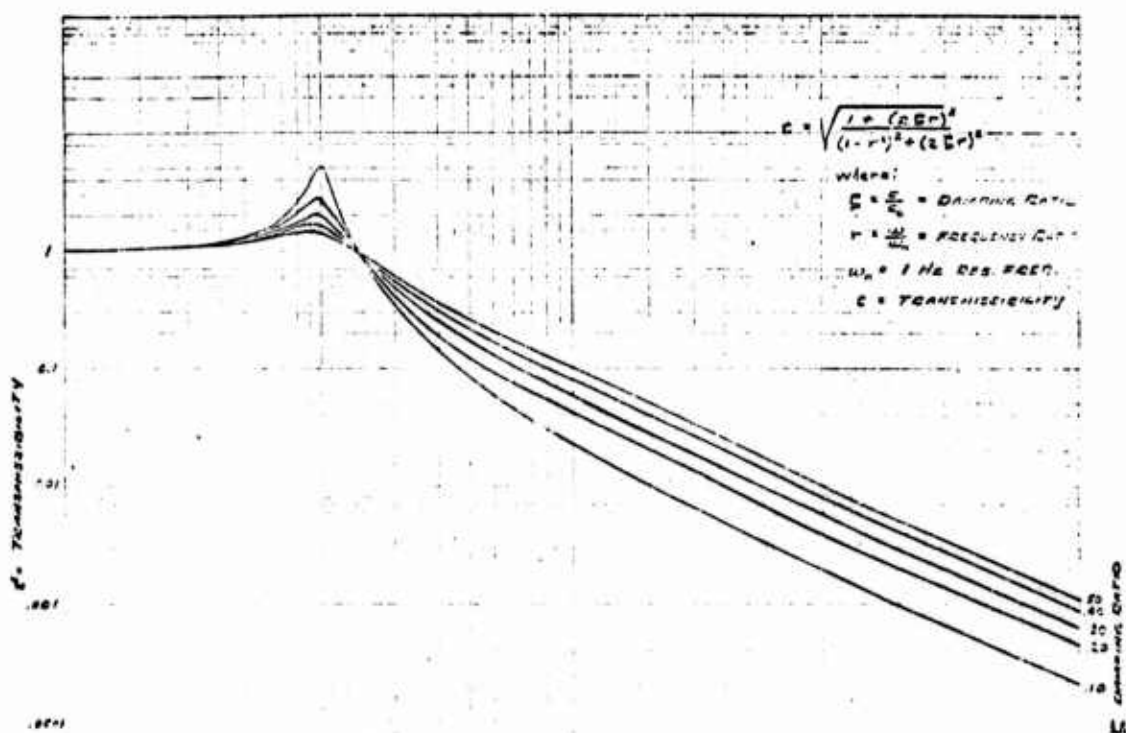


Figure A-16. Coil spring isolation system characteristics with viscous damping

commonly used for installations where close level conditions and high efficiency vibration isolation is required such as test platforms for guidance systems and calibration of optical equipment. Special applications have also been utilized in aircraft for vibration isolation of highly sensitive instrumentation.

One type of air column servocontrolled isolation currently used in applications of this type is the Barry Servo-Level illustrated in Figure A-17. Four of these units can be arranged in a system so that they are located uniformly with respect to the centroid of the supported mass. The isolator units are active air springs controlled by a height sensing servo valve which automatically returns the supported mass to its original preset orientation whenever mass is added to or removed from the system. In operation, air or gaseous nitrogen is fed to the air spring system. This air column supports the total mass sensor assembly so that the weight of the assembly will determine the air

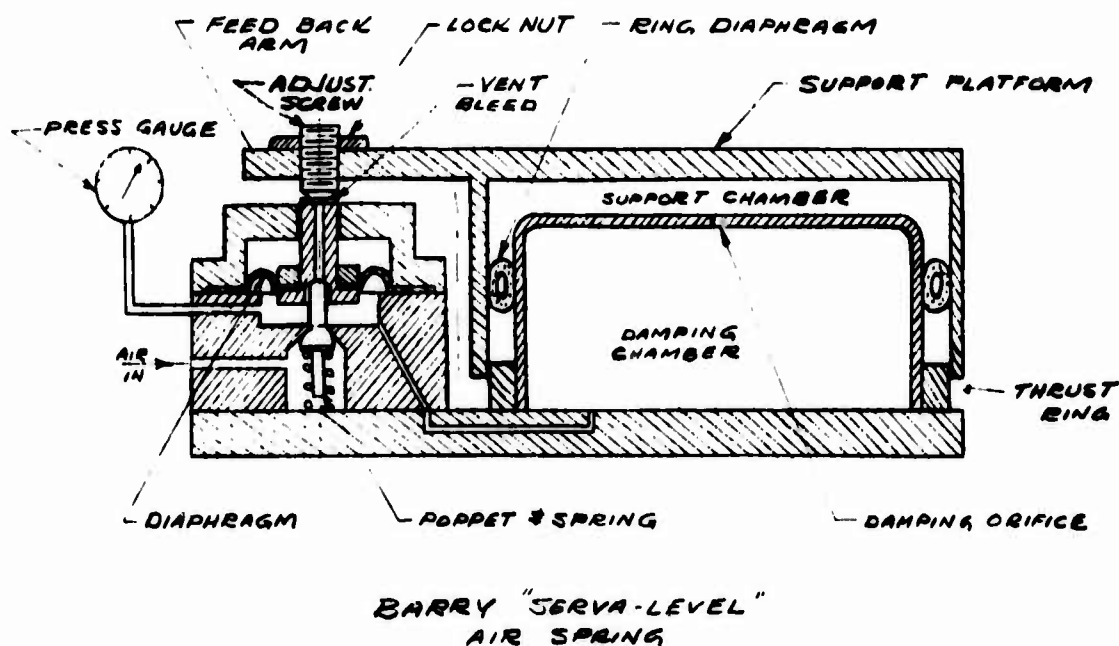


Figure A-17. Air column servo-level isolator.

pressure. When the load on each isolator unit is balanced by the air pressure, both ends of the servo valve remain closed. When the load increases, the valve opens to the air supply, providing compensating pressure. Conversely, when the load decreases, the "bleed" end of the valve opens, releasing pressure to maintain dimensional stability. The air flow to and from the support chamber is controlled by an orifice in the damping chamber providing a time delay sufficiently long to avoid a response under vibration, yet short enough to adjust promptly should the static load conditions change. In this manner the air column isolator system will function as a low frequency (1 Hz) isolator with near critical damping. Figure A-18 shows a series of curves that illustrate how an air column spring-damped system limits resonant amplifications to values normally provided by a critically damped isolator, while the isolation efficiency of a completely undamped isolator is provided at higher frequencies.

Another kind of air column vibration isolator is that contained in the legs supporting vibration isolation tables. This isolator basically consists of an air piston fastened to a rolling diaphragm that enables the piston to act as a frictionless piston with a constant area. Air is introduced into a chamber below the piston which is sized to obtain a system resonant frequency of 1 Hz. A surge chamber which serves as a pneumatic dashpot is located below the piston chamber. Connecting the two chambers is a specially designed damping orifice which together with the surge tank serves to reduce vibration transmissibility

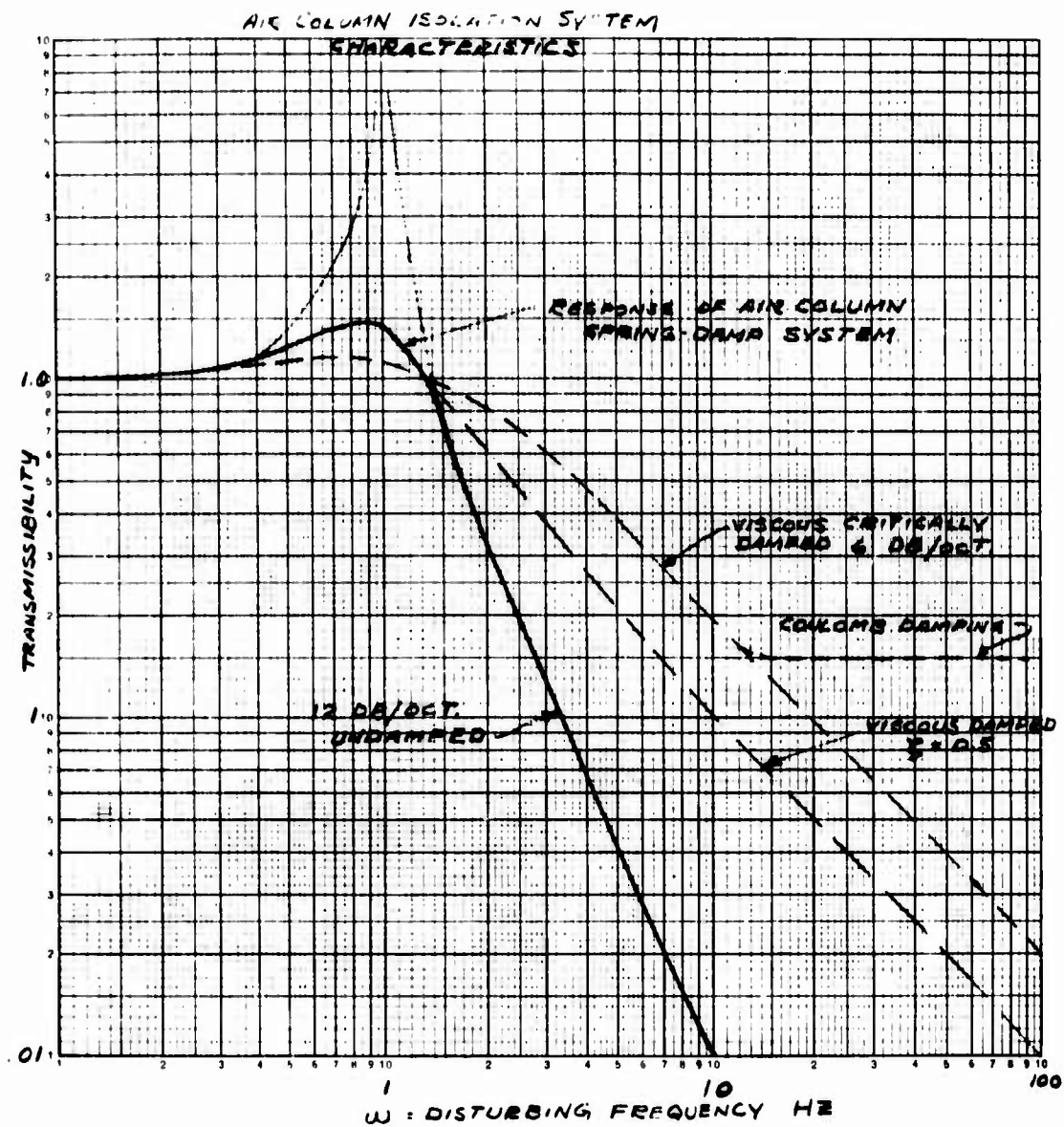


Figure A-18. Air column isolation system characteristics.

at resonance. Figure A-19 is an illustration of this type of air column isolator.

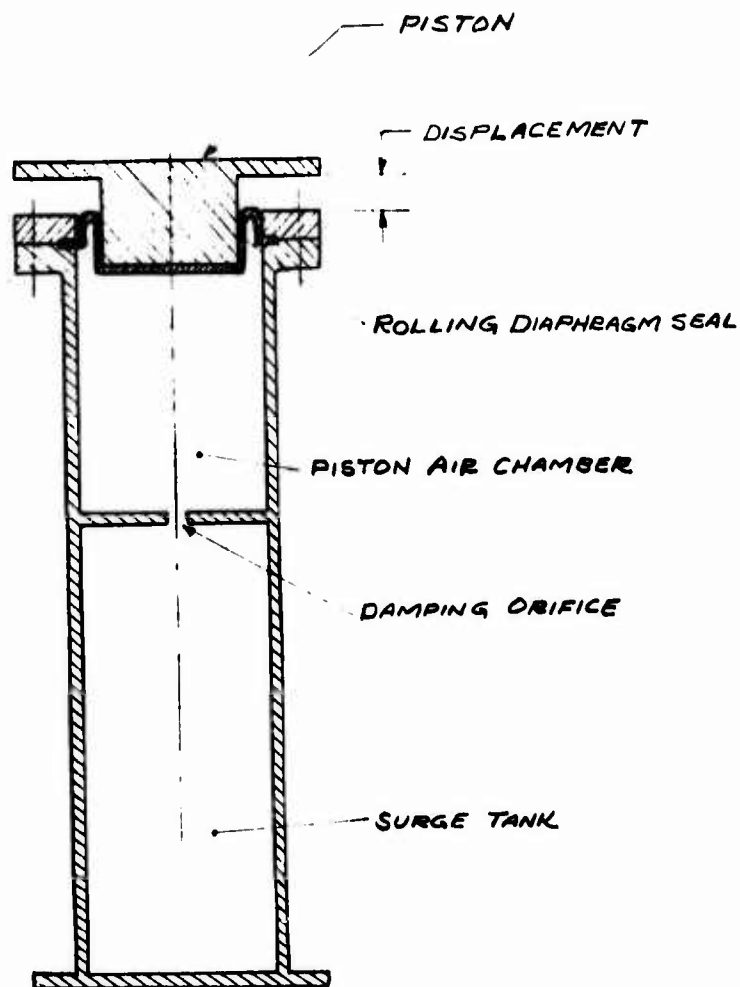


Figure A-19. Air column isolator with piston and rolling diaphragm.

The resonant frequency of an air column isolation system can be lowered by either increasing the supported mass or increasing the air pressure in the piston chamber which has the effect of increasing the spring rate. The resonant frequency of an air piston is mass dependent and only dependent on the ratio of the piston area to the air chamber volume. The equation for the resonant frequency of an air piston can be determined beginning with the gas laws governing polytropic change for a perfect gas.

$$P_1 V_1^n = P_2 V_2^n$$

since

$$P_1 = \frac{F}{S}$$

and

$$V_1 = V_2 - SX$$

where

K = spring rate, lb/in.

M = mass, lb sec²/in.

F = force, pound

X = displacement, inch

S = piston surface area, inch

P₁ = original air pressure, pounds per square inch

W = supported weight

P₂ = air pressure after displacement

V₁ = original tank volume, in³

n = $\frac{C_p}{C_v}$ = specific heat ratio air = 1.4

then substituting in original equation

$$\left(\frac{F}{S}\right) (V_2 - SX)^n = P_2 V_2^n$$

$$F = \frac{(SP_2 V_2^n)}{(V_2 - SX)^n}$$

since $K = df/dx$ letting $X \rightarrow 0$.

then

$$K = \frac{nP_2 S^2}{V_2} = \frac{nP_1 S^2}{V_1}$$

substituting $PS = W = Mg$

$$\therefore K = \frac{nMgS}{V_1}$$

since

$$f = \sqrt{\frac{K}{\frac{M}{2\pi}}}$$

then substituting for K and M

$$f = \sqrt{\frac{\frac{ngS}{V_1}}{\frac{1}{2\pi}}}$$

$$f = c \sqrt{\frac{S}{V_1}}$$

where

$$c = \sqrt{\frac{ng}{2\pi}}$$

Air pistons provide vertical isolation and have resonant frequencies as low as 1.0 Hz, but the resonant frequency for horizontal vibration isolation is usually higher due to the characteristics of the rolling diaphragm. The rolling diaphragm used to seal the air pistons in this type of isolation system must be preloaded to act as nonstretchable membranes. Below this preload condition the diaphragm interferes with the performance of the air piston. For the piston to act as a mass independent system, the operating pressure must be above 30 psi which will be above the preloaded condition of the diaphragm in most designs. For safe operation the operating pressure should not exceed 90 psi. An optimum designed system should have a horizontal resonant frequency between one and two Hz.

One of the basic advantages of this concept of vibration isolation is that the maximum transmissibility is limited to less than 1.3 without the amplitude sensitivity or sacrifice in higher frequency isolation efficiency common to other conventional damping systems. Aging will be less of a problem since the only application of elastomeric components are for the impregnation of the rolling diaphragm fabric. There will be no elements that would cause a drift or set that is evident with systems having steel coil or elastomeric springs. The fatigue life is limited to the cycle life of the rolling diaphragm which is comparable with that of conventional coil springs and far exceeds the fatigue life of the components in an elastomer suspended system. An air column supported system would have a vibration isolation rate of 12 dB per octave above approximately three times the natural frequency, which is at least twice the isolation efficiency of other conventional damped isolators.

Figures A-20 and A-21 illustrates how air column isolators can be used in conjunction with a spherical air bearing knuckle joint to provide a system with torsional vibration isolation as well as isolating translational resonances. A 10-inch spherical air bearing knuckle having a projected load bearing area of 40 square inches will support a 1000-pound inertial platform sensor assembly with a minimum pressure of 30 psi. Results of a load test on a bearing this size produced by Team Corporation of Los Angeles, California, are listed in Table A-3. The air column isolator is sized to support the 1000-pound mass with a pressure of 50 psi. To obtain a 1 Hz resonant system the piston size and volume of the air chamber can be determined by:

$$f = \sqrt{\frac{ng \frac{S}{V}}{2}}$$

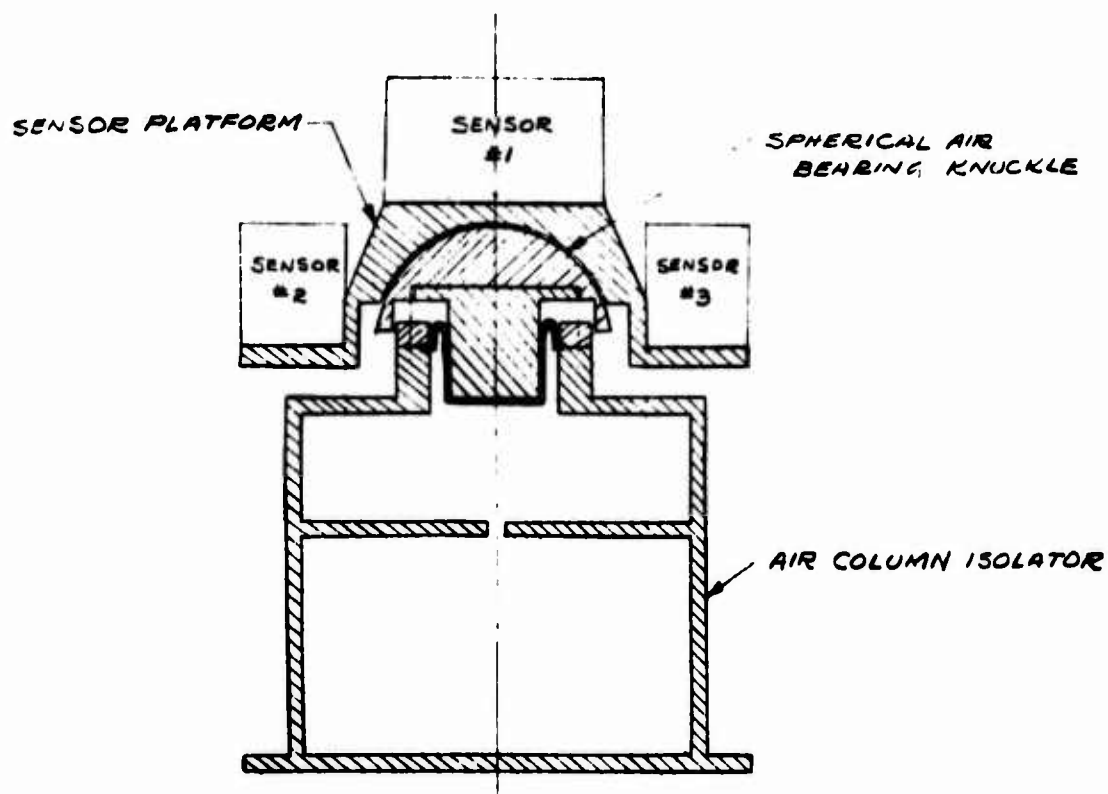


Figure A-20. Air column isolator with spherical air bearing knuckle.

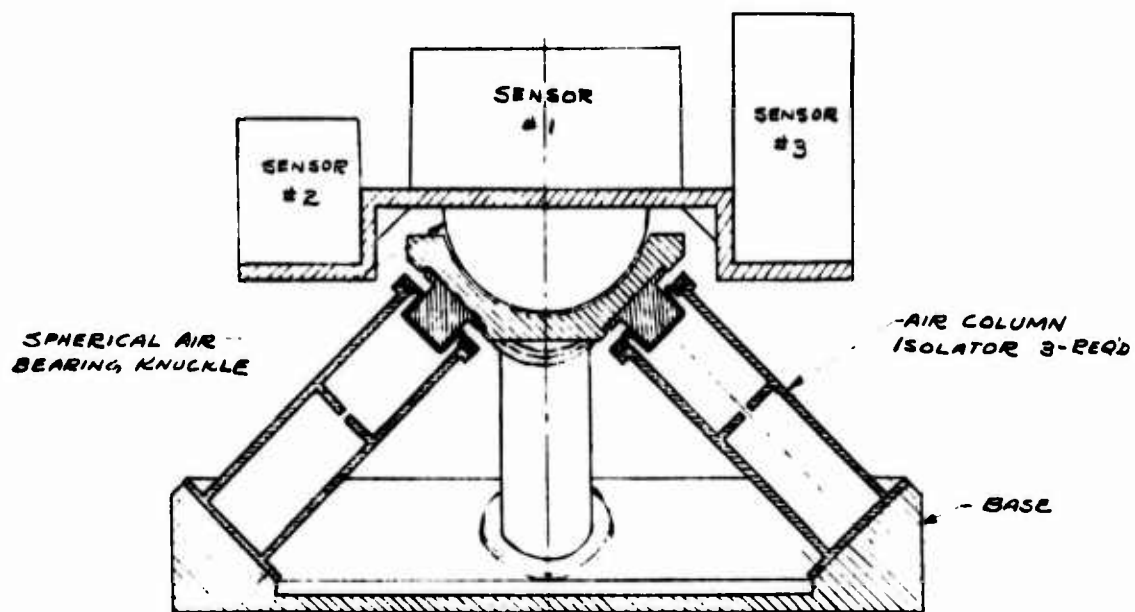


Figure A-21. 3-Point air column isolator support with spherical air.

TABLE A-3. ACCEPTANCE TEST 101 HS
SPHERICAL GAS BEARING LOAD TEST

Gas Pressure to Sphere, psi	Load Supported, pounds		Gas Flow	
	Gross	Net	MM	SCFM
5	636	236	1.2	0.022
10	795	395	1.6	0.025
15	922	522	1.8	0.030
20	1049	649	1.9	0.035
25	1240	840	2.0	0.040
30	1431	1031	2.4	0.050
35	1590	1190	3.1	0.065

Load test was terminated at 35 psi. because of range of gauge used on loading ram. At each measurement the load was increased until the caging piston was moved downward from its upper seat. The sphere was free moving throughout the test. The gross load figures include the 400 pound counterweight assembly on the ram.

FLOW METER Brooks, Serial No. 6503-78834, Tube R-2-15-C.
(Calibration certified at 50 psi. flowing pressure at 70 deg. F.)
Gas used-Dry nitrogen, Temperature 85 deg. F.

TURBINE TORQUE TEST This test showed a torque of 1 Dyne CM.

Gas bearing support surface area = 40 in^2 .

or

$$\frac{S}{V} = \frac{39.4}{ng} = 0.0729$$

The piston area and diameter will be:

$$S = \frac{W}{P} = 20 \text{ in}^2$$

$$D = 5.50 \text{ in.}$$

The air chamber volume will be:

$$V = \frac{S}{0.0729} = 275 \text{ in}^3$$

SUMMARY AND CONCLUSION

A low resonant frequency broadband isolation system can be designed and fabricated utilizing available commercial components to provide the required vibration isolation necessary for accurate gravitational gradient sensor operation aboard a moving aircraft.

Considering the typical vibration environment of a DC-3 aircraft, an evaluation of three different types of suspension systems was made in an attempt to select a system design that would best meet all of the requirements. The basic requirements upon which a design selection was made are of the following order:

1. A system design that best isolates the vibration frequencies experienced during stable flight of the aircraft stated.
2. A design that will prove highly reliable with a minimum of maintenance.
3. A design that is flexible in that it will accommodate an increase or decrease in the support mass without affecting the isolation capabilities.
4. A system that can be fabricated utilizing commercially available components.

An elastomer suspended system can be designed to provide the required 1 Hz resonant system utilizing either shock absorber "Bungee cord" or amber latex rubber tubing. Each of these elastomers have decided drift and set characteristics which would make it somewhat difficult to maintain the system orientation and resonant frequency. The fatigue life and aging properties of elastomers would normally be inadequate for this application without frequent cord or tubing replacement. Although this type of suspension may be highly suitable for laboratory applications, the elastomer material properties precludes its use for installations where long fatigue life and stability are a prime requisite.

A system consisting of helical "coil springs in conjunction with viscous dampers is a more conventional approach to vibration isolation than using an elastomer suspension. A system of this type can be designed around using conventional spring and viscous damper components with a minimum of research and development time since much information is available. A certain amount of drift and set can also be expected in coil springs and adjustment features must be designed into the system to correct for this when it tends to affect the isolation characteristics of the system

An evaluation of each of the three systems investigated indicates that an air column, spring damped system will best meet the requirements. This is based on the following results and information:

1. The air column, spring damped system will provide vibration isolation efficiency equal to that of a completely undamped isolator at the higher frequencies, while still providing near critical damping of resonant frequencies. This feature is not included in the design of the other two systems.
2. Once installed the air supported mass system should function satisfactorily for extended periods with a minimum of part replacement since there are no critical elastomeric or steel spring parts that could affect the isolation characteristics due to aging, set or drift.
3. Air column supported isolators will provide a greater degree of flexibility if a change in mass is required. This is accomplished through a servocontrolled system which controls the air pressure to suit the load support requirements and maintains the preset orientation of the mass.
4. The air column isolator can be adapted to a spherical air bearing knuckle joint to provide a system that will provide angular rate isolation as well as isolation of translational vibrations.
5. Most of the components are commercially available and are commonly used in high efficiency vibration isolation systems. These include aircraft installations for vibration isolation of highly sensitive instrumentation.
6. Engineering and technical sources specializing in design and development of components for servocontrolled air-column isolators and spherical air bearings are currently available for consultation or contracting on a job basis. Sources that have been contacted and expressed interest in developing and supplying components for an air column supported system are listed below:
 - Barry Controls - Watertown, Massachusetts:
Specializes in servocontrolled, air spring vibration isolators and design of systems for vibration isolation of highly sensitive instrumentation for aircraft environment.

- Lansing Research Corporation — Ithaca, New York: Specializes in precision measuring instruments and one Hz resonant frequency vibration isolation tables using air column servo-controlled isolators.
- Modern Optics Corporation — El Monte, California: Specializes in precision optical components and servocontrolled air column vibration isolation systems.
- Astro Space Laboratories, Inc. — Huntsville, Alabama: Specializes in research, development and manufacture of precision instruments utilizing spherical air bearings as a means of low frequency angular rate isolation.
- Team Corporation — Los Angeles, California: Specializes in high precision spherical air bearing knuckle joint design and fabrication for applications requiring high frequency translational vibration isolation and low frequency angular vibration isolation.

REFERENCES:

1. J. P. Den Hartog, "Mechanical Vibrations." McGraw-Hill, New York, N. Y.
2. S. Timoshenko, "Vibration Problems in Engineering," D. Van Nostrand Co., Princeton, N. J.
3. A. H. Church "Elementary Mechanical Vibrations." Pitman Publishing Corp., New York, N. Y.
4. SAE, J., Ride and Vibration Data Manual - 1965. Society of Automotive Engineers, Inc., New York, N. Y.
5. Hughes Aircraft Co. Report "Feasibility Study Application of Hughes Gravity Gradiometer to Airborne Geophysical Exploration, Dec. 1969.
6. Military Specification - MIL-C-5651B, 29 Dec. 1961 Cord; Elastic, Exerciser and Shock Absorber for Aeronautical Use.
7. L. R. G. Treloar, "The Physics of Rubber Elasticity - 1958, Oxford University Press.

APPENDIX B

PRELIMINARY PROCUREMENT SPECIFICATION FOR A GRAVITY GRADIOMETER THREE-AXIS MOTION ISOLATION PLATFORM

Note — This specification was written in June 1970 and submitted to potential vendors at that time. The description of payload size requirements was based on conservative projections of the then current laboratory model sensor. Its purpose was to assure an early, specific application to a special test aircraft to be used in gravity surveying. In such an application, the sensor size and weight would have been traded-off for early operational capability. No specific attempt was made to minimize sensor and support size and weight. Thus, the reader is cautioned not to draw direct inferences as to the size and weight of a productized sensor.

1.0 REQUIREMENTS OF ENTIRE MOTION ISOLATION SYSTEM

The intended application of the Hughes Gravity Gradiometer (hereinafter referred to as the sensor) requires that three sensors be mounted on an inertially stabilized platform. The basic sensor consists of a pair of rotating mass quadrupoles. A cluster of three such sensors, whose spin-axes form an orthogonal triad, are required to provide the necessary measurements of the nine-element gravity gradient tensor.

1.1 Angular Rate Sensitivity

Inherent to the basic sensor configuration, its output is sensitive to not only gravity gradients, but also to angular rates normal to its spin axis. Since it is desired to measure only the gravity gradients, the motion isolation system must limit and/or measure such angular rates. Since a cluster of three orthogonally mounted sensors will be used, angular rates about all three axes must be controlled. The output of each sensor is proportional to the square of the inertial angular rate normal to its spin axis, that is:

$$\Gamma_e = \Omega^2$$

where

Γ_e = the equivalent sensor output caused by inertial angular rate

Ω = the inertial angular rate normal to a given sensor's spin-axis

The required sensitivity of a given sensor is such that the equivalent sensor output caused by inertial angular rate normal to its spin axis, Γ_e , shall not exceed 10^{-10} (rad/sec)². Note that this requirement is independent

of disturbance frequency. For example, if the angular rate were sinusoidal at frequency β , i.e., $\Omega = \Omega_0 \sin \beta t$, the resultant equivalent gradient would be:

$$\Gamma_e = \Omega_0^2 \sin^2 \beta t = \Omega_0^2 \left[\frac{1}{2} - \frac{1}{2} \cos 2\beta t \right]$$

Hence any oscillatory angular rate disturbance produces a d.c. plus a double frequency output. Electronic filtering may be employed to attenuate the double frequency term but the d.c. term may not be "filtered." The requirement of 10^{-10} (rad/sec)² represents the total allowable one sigma error considering the total angular rate spectrum of the three-sensor cluster.

1.2 Angular Position Sensitivity

The gravity gradient data measured by the three-sensor cluster must be referenced to a geodetic base. It is planned that this reference be established, in the airborne application, through use of an inertial navigation system mechanized in a "local level," azimuth wander coordinate reference. The allowable deviation of the angular position of the three-sensor cluster from the above established geodetic vertical reference shall not exceed $\pm .005$ degree from the initially established vertical before aircraft take-off, and the allowable deviation in azimuth shall not exceed ± 0.1 degree from the initial azimuth. The allowable initial alignment uncertainty shall not exceed ± 0.1 degree from the local vertical and ± 0.2 degree from true North.

1.3 Translational Acceleration and Vibration

Ideally, the sensor is not sensitive to acceleration disturbances. However, due to inability to obtain perfect mass balance and to structural

deflections of the sensor arms, it is sensitive to accelerations. The allowable acceleration levels will be dependent upon the final flight-sensor configuration. Preliminary requirements are as follows. The vibration level (in any axis) of the three-sensor cluster shall not exceed 0.01 g rms except that at frequencies f_0 and $3f_0$ (f_0 = spin rate of sensor \approx 20 Hz), the vibration level shall not exceed 5×10^{-4} g.

1.4 Anticipated Aircraft Motion Environment

The following data presents anticipated aircraft motion expressed as power spectral densities. This data is very preliminary and should be treated only as a gross approximation to the actual power spectrum which may be encountered; e.g., the data does not contain the fine grain details such as sharp resonant peaks which would actually occur in flight. Figure 1 is the translational acceleration power spectral density assumed typical for all three axes, i.e., vertical, fore and aft, and lateral. Figure 2 is the angular rate power spectral density also assumed typical for all three rotational axes, pitch, yaw and roll.

APPROXIMATE AIRCRAFT MOTION ENVIRONMENT

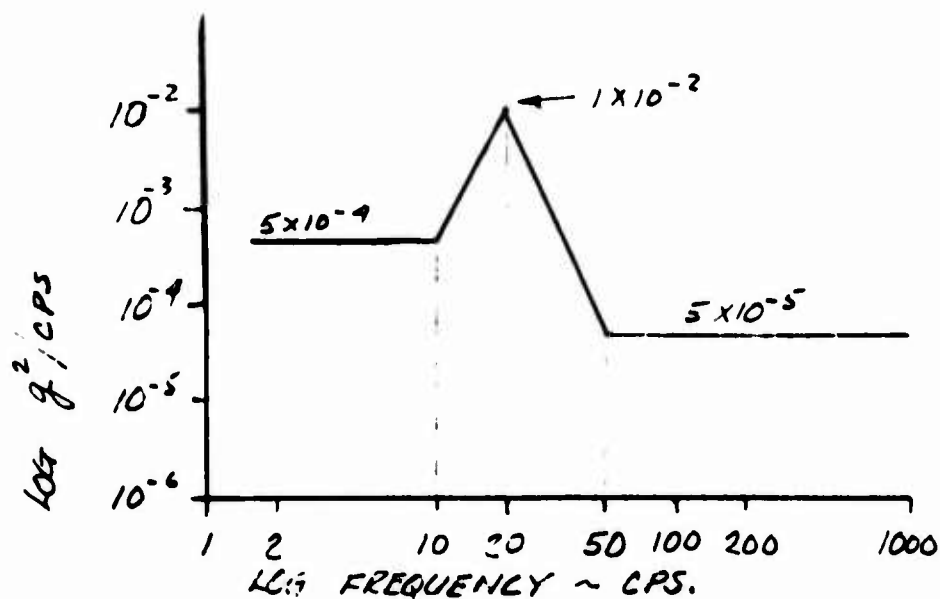


FIG. 1 - TRANSLATIONAL ACCELERATION POWER SPECTRAL DENSITY

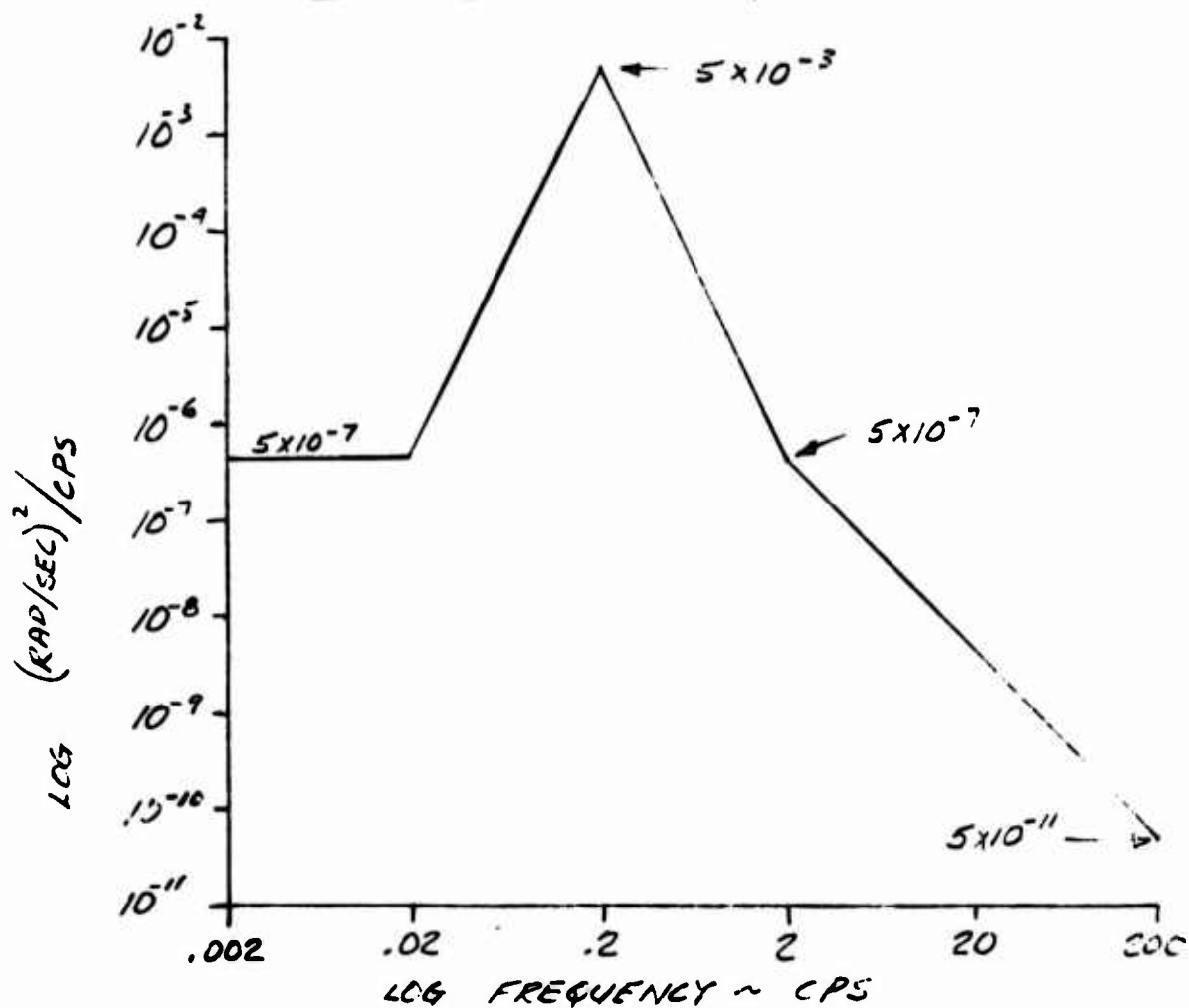


FIG. 2 - ANGULAR RATE POWER SPECTRAL DENSITY

2.0 BASELINE MOTION ISOLATION SYSTEM

The baseline motion isolation system described herein has been developed to meet the requirements delineated in section 1. The purpose of including a description of the entire motion isolation system is two-fold: first, to acquaint the vendor with the entire motion isolation system concept so as to provide an understanding of the interfaces which occur between the three-axis motion isolation platform and the balance of the motion isolation system; and second, it is desired that the vendor submit any alternate proposals for mechanization concepts differing from the herein described baseline, provided they will adequately meet the requirements of paragraphs 1.

The baseline system mechanization is best illustrated by the building block concept shown below.

Gradient Sensor(s)
High Frequency Angular Isolation System
Three-Gimbal Stable Platform
Vibration Isolation System
Airframe

The gravity gradient sensor(s) are supported by a very low friction air knuckle bearing joint which provides a small amplitude-high frequency angular motion isolation. The knuckle joint is supported by a three-gimbal platform whose inner, inertially stabilized element provides the basic

vertical and azimuth alignment reference. The knuckle platform is servo controlled to follow only the long time average orientation of the three-gimbal platform stable element. The three gimbal platform thus provides the gross, large amplitude-low frequency angular isolation and stabilization while the secondary knuckle bearing and servo provide the small amplitude-high frequency angular isolation.

The base of the three-gimbal platform is supported by a vibration isolation system which primarily provides the isolation of translational aircraft vibrations from the sensor and secondarily provides a certain degree of angular vibration isolation, depending on the specific mechanization of this subsystem.

3.0 THREE-AXIS MOTION ISOLATION PLATFORM REQUIREMENTS

This paragraph specifies the requirements for the three-axis motion isolation platform subsystem of the baseline motion isolation system. In determining these requirements, a three gimbal platform utilizing ball-type gimbal bearings has been assumed. Thus, the angular rate limits specified herein for the angular motion of the inertially stabilized element are considerably more gross than that actually required for the three-sensor cluster because of the inherent servo hang-off error associated with the coulomb friction characteristic of ball-type gimbal bearings. (Note that this inherent hang-off error characteristic is the primary reason for the use of the secondary spherical knuckle air bearing platform in the baseline system.)

3.1 Functional and Performance Requirements

3.1.1 Angular Freedom:

Pitch and Roll	± 30 degrees
Azimuth	Full Freedom

3.1.2 Gimbal Order:

Inner:	Azimuth
Middle:	Pitch
Outer:	Roll

3.1.3 Gimbal Readout: Angle transducers providing a signal proportional to gimbal angle for each of the three gimbals will be required. These transducers shall have an accuracy of at least 1 arc minute. Note that this requirement is in addition to any resolvers associated with the stabilization servo loops of the platform.

3.1.4 Initial Alignment:

Vertical: ± 0.1 degree 1σ with respect to local plumb-bob vertical.

Azimuth: ± 0.2 degree 1σ with respect to a true North reference.

3.1.5 Angular Drift: The stable element orientation shall not drift with respect to the initially established navigation reference coordinate system by more than the following amount for flight durations up to 10 hours:

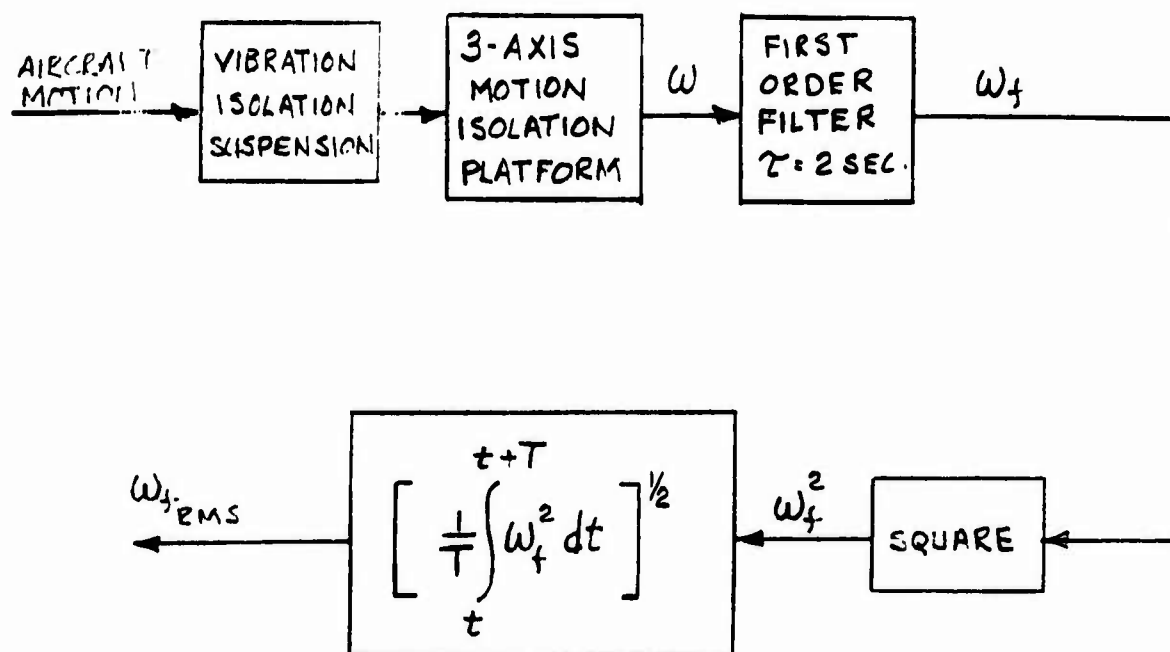
Vertical: ± 0.0025 degree, 1σ

Azimuth: ± 0.1 degree, 1σ

3.1.6 Angular Oscillations: In addition to the steady drift requirements specified in paragraph 3.1.5, the angular oscillations of the stable element of the three-axis motion isolation platform when operating in the specified aircraft motion environment shall be limited by the following criteria.

3.1.6.1 Angular Position Excursion - The amplitude of any oscillatory motion of the stable element shall not exceed ± 0.05 degree per axis.

3.1.6.2 Angular Rate - The root-mean-square value of the filtered (by a two-second time constant first order filter) inertial angular rate of the stable element shall not exceed $3^\circ/\text{hr}$ per axis for averaging times greater than 10 seconds. The following block diagram represents the above described process.



$T \triangleq$ AVERAGING TIME > 10 SEC.

$w \triangleq$ STABLE ELEMENT INERTIAL ANGULAR RATE

$w_f \triangleq$ FILTERED w

$w_{f_RMS} =$ RMS VALUE OF w_f AVERAGED OVER TIME T
SHALL NOT EXCEED 3 °/hr.

3.1.7 Navigation Coordinates/Mechanization: Schuler tuned, local level, azimuth wander.

3.1.8 Navigation Computer: A navigation computer will be required whose accuracy is compatible with meeting the angular stability requirements of paragraphs 3.1.5 and 3.1.6. This computer is needed to perform the platform management function and navigation output data will be only of secondary importance. It should be assumed that some form of an independent navigation reference will be available to provide updating of this computer. Assume navigation position update data will be accurate to ± 0.5 nautical miles per hour over a 10 hour flight or will not exceed 5 nautical miles at any time during the flight.

3.2 Environment - Operating

The sensor will be used for collection of gravity anomaly data in two types of aircraft. The aircraft will be flown in a straight and level cruise condition only during non-turbulent weather conditions. One type of airborne operation is a slow flight, at approximately 100 to 150 mph at a constant cruise altitude of between 2,000 to 4,000 feet in a piston engine aircraft such as a DC-3 or Twin Otter. The second type of airborne operation is at a high subsonic speed, approximately 500 to 600 mph at a constant cruise altitude of between 25,000 to 35,000 feet in a multi-engine jet aircraft such as the KC-135. Assume that a nominal cabin temperature will be maintained in both cases. The anticipated aircraft motion environment specified in paragraph 1.4 should be assumed applicable for both cases.

3.3 Payload Description *

The three-sensor cluster, including the associated knuckle bearing and servo, batteries, etc., are described below. The weight and size of each sensor is as follows:

Weight: 75 lbs.
Size: 12" dia. cylinder 25" long with a flange mounting ring at mid-length of cylinder.

The remaining items to be mounted on the stable element of the three-axis motion isolation platform are:

<u>ITEM</u>	<u>WT.</u>	<u>APPROX. SIZE</u>
3-sensor support structure	100 lbs.	----
Sensor electronics	20	.3 ft. ³
Sensor spin motor batteries	100	1.5 ft. ³
Counter momentum wheel	50	12" dia. x 9" long
Air knuckle bearing	30	6" dia. sphere
Servo sensors, torques & electronics	<u>50</u>	.5 ft. ³
TOTAL	350 lbs.	

The payload layout is purposefully not specified at this time to allow freedom of choice in a layout which would be advantageous to the vendor's particular mechanization approach. The only requirement which must be met is that the center of gravity of the three-sensor cluster fall at the geometrical center of the air knuckle bearing.

3.4 Interface Considerations:

3.4.1 Power and Signal Transmission: Slip rings or their equivalent will be required to transmit power to and signals to and from the three-

* See Note on cover page of Appendix B

sensor cluster as follows:

A.C. Power: 100 volt, 60 to 100 Hz, 2-phase (90° phase shift) power. 2 amps run per leg plus 2.8 amps return.

28 volt, 400 Hz, 3-phase - 100 watts.

D.C. Power: 2 amps at 28 volts d.c.

Signal: Provision for approximately 32 signal channels.

3.4.2 Mechanical Impedances:

3.4.2.1 Vibration Isolation Mount: The three-axis motion isolation platform will be mounted on a vibration isolation suspension. This suspension will provide for the isolation of both translational and angular vibrations. Its characteristic transmissibility (assuming the three-axis motion isolation platform to be a dead weight) can be approximated by a resonant frequency of 1 Hz with a damping ratio of 0.1. These characteristics are only approximate since a detailed design is not yet available. The suspension may be mechanized using pneumatic piston/bellows or conventional springs with parallel dashpots as the basic suspension element. Several such elements would be utilized to provide both translational as well as rotational support. Note that if the pneumatic piston/bellows are used, the transmissibility characteristics above are only approximate, i.e., such a system would have non-linear characteristics.

3.4.2.2 Reaction Torques: The knuckle bearing servo system will exert reaction torques on the stabilized element of the three-axis

motion isolation platform. These torques will be from the following sources:

1. Viscous air drag.
2. Flex lead spring restraint.
3. Mass unbalance, i.e., reaction torques resulting from the servo system responding to torques caused by aircraft translational acceleration acting on the mass unbalance of the three-sensor cluster payload.

Estimates of the magnitude of these torques are not available; however, it is assumed that these torques will be extremely small in comparison to other disturbance torques acting on the stable element of the three-axis isolation platform.

3.5 Acceptance Test Criteria

Due to the preliminary nature of this specification, no detailed acceptance test criteria is included herein. Because one of the intended applications of this system is for military purposes, appropriate military specifications will be applicable.

4.0 ALTERNATIVE CONFIGURATIONS

The above described baseline system was chosen because it appeared to be feasible, cost effective (based on the assumption of a limited production quantity), and relatively quickly available. However, it is recognized that alternatives to this baseline system are possible, and any reasonable alternative system will be given full consideration providing it is capable of meeting the functional and performance requirements set forth herein.

UNCLASSIFIED
Security Classification

DOCUMENT CONTROL DATA - R&D		
(Security classification of title, body of abstract and indexing annotation must be entered when the overall report is classified)		
1. ORIGINATING ACTIVITY (Corporate author) Hughes Research Laboratories 3011 Malibu Canyon Road Malibu, California 90265		2a. REPORT SECURITY CLASSIFICATION Unclassified
		2b. GROUP —
3. REPORT TITLE DEVELOPMENT OF A GRADIOMETER FOR MEASURING GRAVITY GRADIENTS UNDER DYNAMIC CONDITIONS.		
4. DESCRIPTIVE NOTES (Type of report and inclusive dates) Scientific Final Report. 15 April 1969 - 14 August 1970		Approved 20 Jan 1971.
5. AUTHOR(S) (First name, middle initial, last name) Curtis C. Bell David W. Rouse Robert L. Forward Glenn F. Kloiber Robert W. Peterson Charles B. Ames		
6. REPORT DATE November 1970	7a. TOTAL NO. OF PAGES 162	7b. NO. OF REFS 7
8a. CONTRACT OR GRANT NO. F19628-69-C-0219		9a. ORIGINATOR'S REPORT NUMBER(S)
b. PROJECT, TASK, WORK UNIT NOS. 7600-07-01, 8607-03-01		
c. DOD ELEMENT 62101F, 61102F		9b. OTHER REPORT NO(S) (Any other numbers that may be assigned this report)
d. DOD SUBELEMENT 681000, 681309		AFCRL-71-0003
10. DISTRIBUTION STATEMENT This document has been approved for public release and sale; its distribution is unlimited.		
11. SUPPLEMENTARY NOTES TECH, OTHER		12. SPONSORING MILITARY ACTIVITY Air Force Cambridge Research Laboratories (LW) L. G. Hanscom Field Bedford, MA 01730
13. ABSTRACT <p>Design and development of a portable rotating gravitational gradiometer has been continued. A breadboard laboratory model of the gradiometer was constructed and tested. Testing has indicated that angular rate isolation and spin speed control represent major factors in maintaining noise free sensor operation.</p> <p>Analysis has been performed on the sensor's susceptibility to angular rate and a feasible rate isolation method is outlined.</p> <p>Preliminary design studies for an isoelastic servo-balanced arm have been completed and are discussed.</p> <p>A preliminary design specification for an appropriate inertial platform for use in an airborne application was generated, and vendor liaison was established to obtain initial response to this specification.</p> <p>Studies were also performed on sensor angular position errors, noise and clutter due to proximate masses, and first stage vibration isolation methods.</p>		

DD FORM 1473
1 NOV 65

UNCLASSIFIED
Security Classification

UNCLASSIFIED
Security Classification

14. KEY WORDS	LINK A		LINK B		LINK C	
	ROLE	WT	ROLE	WT	ROLE	WT
gravity gradiometer gradiometry inertial guidance airborne - gravimetry gravimetry						

UNCLASSIFIED
Security Classification